UNIVERSITAT POLITÈCNICA DE VALÈNCIA

INSTITUTO INTERUNIVERSITARIO DE INVESTIGACIÓN DE RECONOCIMIENTO MOLECULAR Y DESARROLLO TECNOLÓGICO

Smart drug delivery systems designed to improve Inflammatory Bowel Disease therapy

PhD. THESIS

Submitted by

Adrián Hernández Teruel

PhD. Supervisors:

Prof. Ramón Martínez Máñez
Prof. Virginia Merino Sanjuán
Dr. Marta González Álvarez

Valencia, July 2019

RAMÓN MARTÍNEZ MÁÑEZ, PhD in Chemistry and Professor at the *Universitat Politècnica de València*, VIRGINIA MERINO SANJUÁN, PhD in Pharmacy and Professor at the *Universitat de València* and MARTA GONZÁLEZ ÁLVAREZ, PhD in Pharmacy and Lecturer at the *Universidad Miguel Hernández de Elche*.

CERTIFY:

That the work *"**Smart drug delivery systems designed to improve Inflammatory Bowel Disease therapy**"* has been developed by Adrián Hernández Teruel under their supervision in the Instituto Interuniversitario de Investigación de Reconocimiento Molecular y Desarrollo Tecnológico (IDM) of the *Universitat Politècnica de València*, as a Thesis Project in order to obtain the degree of PhD in Chemistry at the *Universitat Politècnica de València.*

Valencia, July 2019.

Prof. Ramón Martínez Máñez	Prof. Virginia Merino Sanjuán	Dr. Marta González Álvarez

A mi familia,
porque lo sois TODO para mi

“The electric light did not come from the continuous improvement of candles.”

Oren Harari

“Stay hungry. Stay foolish.”

“I'm convinced that about half of what separates successful entrepreneurs from the nonsuccessful ones is pure perseverance.”

Steve Jobs

“Innovation is taking two things that already exist and putting them together in a new way.”

Tom Freston

Acknowledgements
Agradecimientos

En primer lugar, quiero agradecer a mis 3 directores Ramón, Vir y Marta que me hayan acompañado y apoyado durante este trabajo que comenzó hace 4 años. Os agradezco tanto la aceptación en vuestras correspondientes familias científicas, como vuestro tiempo dedicado y la buena relación creada. Me satisface además, que esta relación haya desembocado en nuevos proyectos que nos hagan seguir trabajando juntos.

Agradezco el apoyo y sobre todo la calidad humana de Isa y de Félix, que también os considero mis co-directores, ya que habéis estado siempre disponibles cuando lo he necesitado. A los dos, gracias de verdad!! Tanto en lo profesional como en lo personal sois inmejorables.

A Carmen Coll le quiero agradecer el haberme acogido al llegar a la familia IDM y que me hiciese sentir que estaba en el lugar correcto para aprovechar al máximo esta aventura y aprendizaje que es hacer una tesis doctoral. Cuando nos abandonó para irse a Dublín, la echamos mucho de menos (ya lo sabes Carmen), pero a la vez nos alegramos por ella, porque se fue para seguir creciendo profesionalmente y demostrar una vez más su valía.

A mis compañeros y amigos del IDM quiero deciros que me ha encantado estar rodeado de gente tan capaz a todos los niveles. Sin duda, he sentido vuestro apoyo y recibido vuestra ayuda siempre que la he necesitado. Espero que hayáis sentido lo mismo, y espero haber respondido igual de bien cuando me haya tocado. Y por supuesto… siempre tendré un recuerdo muy especial, de aquel momento

despedida-sorpresa antes de irme a USA, no pudo sorprenderme y gustarme más.

I would like to thanks Mike (Professor Michael J. Sailor in the University of California San Diego) to grant me with the opportunity to perform my international PhD stage in his team/family, one of the world leading research groups in the porous silicon and drug delivery field. That experience was really amazing, I will never forget it. I would like to highlight Mike's kindness and empathy. Inside and outside the lab… your dedication, with your guests, students and workers is outstanding. We (guest researchers and students) felt like real members of your team/family. Mike, you are a genuine leader to follow.

Empezar una tesis doctoral motivado es necesario, pero el período pre-doctoral es un período con muchos alti-bajos, como la vida, pero intensificado muchas veces por la frustración innata del trabajo de investigador. En mi caso lo he llevado siempre bastante bien, incluso cuando las cosas salían peor en el "lab", porque en mi vida, en general, seguía siendo FELIZ. Aunque la preocupación por los resultados y avances en el lab, no desaparecía, ni mucho menos… luego llegábamos juntos a casa, o llegaba y estabas en casa, o al contrario, da igual… lo importante, Eva, es que me hicieses llamarlo por primera vez casa, y que seas en gran parte responsable de mi FELICIDAD en el día a día, independientemente de como vayan las cosas.

Y por su puesto agradecer el cariño, amor y apoyo incondicional y constante de las 2 personas a las que SIEMPRE y desde SIEMPRE tengo TODO que agradecer, mis padres. A todos los niveles los mejores padres que se puede tener y que les desearía a todos, pero me han tocado a mí, y no puedo ser más FELIZ por ello.

Resumen

La presente tesis doctoral titulada “Sistemas de liberación controlada de fármacos diseñados para mejorar el tratamiento de Enfermedad Inflamatoria Intestinal” se centra en el diseño, preparación, caracterización y evaluación *in vivo* de distintos sistemas de liberación controlada de fármacos en colon (CDDS, por sus siglas en inglés) utilizando como soporte micropartículas de sílice mesoporosa, funcionalizadas con puertas moleculares.

En el primer capítulo se describe qué es la Enfermedad Inflamatoria Intestinal (EII), sus principales características y la problemática a nivel global que representan la enfermedad de Crohn y la colitis ulcerosa (enfermedades que engloba la EII). A continuación, se discuten los tratamientos clínicos disponibles en la actualidad para el tratamiento de EII, así como algunos de los avances más recientes con la misma finalidad. Para completar este primer capítulo introductorio, se describe en qué consisten los materiales mesoporosos y el concepto de puerta molecular aplicado a la detección de diferentes moléculas (sensing) y a la liberación de fármacos (drug delivery).

En el segundo capítulo se presentan los objetivos generales que son abordados en los siguientes capítulos experimentales.

En el tercer capítulo se presenta un CDDS que libera su carga en respuesta a agentes reductores y en cierta medida a pH ácido. En concreto, se desarrollaron micropartículas de sílice mesoporosa con nanopartículas de magnetita en su interior para dotar de propiedades magnéticas a estos CDDS. Estos soportes magnéticos se cargaron con el colorante safranina O y sus poros se taparon con una molécula orgánica que contiene un enlace azo y un grupo carbamato, para impedir la liberación del colorante. Los estudios de liberación de la carga se llevaron a cabo en disoluciones acuosas a diferentes pH y también en fluidos gastrointestinales simulados. Los estudios mostraron que la liberación

específica de la carga se puede inducir selectivamente en un medio reductor (tal y como ocurre en colon), simulado en el trabajo mediante la adición de ditionito de sodio (agente reductor). Esto induce la ruptura de los enlaces azo y la liberación del colorante. A su vez, se observó una liberación parcial de la carga en medios a pH ácido, probablemente debido a la hidrólisis parcial del grupo carbamato. En este capítulo también se estudiaron las propiedades magnéticas del sistema.

En el cuarto capítulo se presenta otro CDDS que responde en presencia de agentes reductores, liberando su carga. En concreto, se prepararon micropartículas de sílice mesoporosa incluyendo nanopartículas de magnetita siguiendo el mismo protocolo descrito en el tercer capítulo. Estos soportes se cargaron con el colorante safranina O (S1) o con el fármaco hidrocortisona (S2), y ambos sistemas se funcionalizaron con un derivado del colorante rojo Congo, que incluye un enlace azo y un grupo urea. Los estudios de liberación de la carga llevados a cabo con S1 en disoluciones acuosas a diferentes pH y también en fluidos gastrointestinales simulados, mostraron que una pequeña parte de la carga se libera en el medio a pH ácido, pero que la liberación del colorante safranina O se produce, mayoritariamente, en presencia del agente reductor ditionito de sodio. La eficacia de los CDDS desarrollados en este capítulo se evaluó mediante estudios *in vivo* en un modelo de colitis ulcerosa inducida en ratas Wistar. Los resultados *in vivo* mostraron una mejora general en los sujetos tratados con S2 en comparación con los sujetos que recibieron una disolución de hidrocortisona. Cuando el tratamiento con S2 es combinado con la aplicación externa de un campo magnético para retener las partículas en la zona del colon, los resultados clínicos parecen mejorar en estos sujetos.

El quinto capítulo muestra un nuevo CDDS con doble acción terapéutica. Para la obtención de este último CDDS, se prepararon micropartículas de sílice mesoporosa, cargadas con el colorante rodamina B (S1) o el fármaco hidrocortisona (S2) y ambos sistemas se funcionalizaron con un derivado del profármaco olsalazina, que incluye un

enlace azo y un grupo amida. Los estudios de liberación de la carga, llevados a cabo con S1 en disoluciones acuosas a diferentes pH y también en fluidos gastrointestinales simulados, mostraron que la liberación del colorante rodamina B se produce en presencia del agente reductor ditionito de sodio, y no se observó liberación de la carga a pH ácido. La eficacia de los CDDS preparados en este quinto capítulo se evaluó mediante estudios *in vivo* siguiendo los mismos protocolos y mismo modelo utilizados en el cuarto capítulo. Los resultados de los estudios *in vivo* mostraron que los sujetos que reciben la formulación S2 presentan una disminución en el índice de actividad de colitis ulcerosa, y una mayor regeneración de los tejidos afectados. La mejoría observada en los sujetos que recibieron S2 es atribuida al tratamiento combinado de la hidrocortisona (liberada desde el interior de los poros) y el 5-ASA (liberado al reducirse el derivado de olsalazina utilizado como puerta molecular).

En conclusión, los estudios realizados demuestran que los materiales de sílice mesoporosa, en combinación con puertas moleculares sensibles a estímulos específicos, tienen un gran potencial para el desarrollo de nuevos sistemas de liberación controlada de fármacos en el colon, dirigidos a mejorar el arsenal terapéutico disponible para el tratamiento de EII. La posibilidad de adaptar o personalizar la carga y las puertas moleculares hace que estos soportes de sílice mesoporosa sean una opción interesante para el desarrollo de nuevos sistemas de liberación controlada de fármacos en diferentes aplicaciones biomédicas. Finalmente, esperamos que los resultados obtenidos en esta tesis doctoral sirvan de inspiración para el desarrollo de sistemas de liberación controlada de fármacos innovadores y cada vez más inteligentes, para su aplicación tanto en medicina como en otras áreas.

Resum

La present tesi doctoral titulada “Sistemes d'alliberament controlat de fàrmacs dissenyats per a millorar el tractament de Malaltia Inflamatòria Intestinal” se centra en el disseny, preparació, caracterització i avaluació *in vivo* de diferents sistemes d'alliberament controlat de fàrmacs en còlon (*CDDS, per les seues sigles en anglès) utilitzant com a suport micropartícules de sílice mesoporosa, funcionalitzades amb portes moleculars.

En el primer capítol es descriu què és la Malaltia Inflamatòria Intestinal (MII), les seues principals característiques i la problemàtica a nivell global que representen la malaltia de Crohn i la colitis ulcerosa (malalties que engloba la MII). A continuació, es discuteixen els tractaments clínics disponibles en l'actualitat per al tractament de MII, així com alguns dels avanços més recents amb la mateixa finalitat. Per a completar aquest primer capítol introductori, es descriu en què consisteixen els materials mesoporosos i el concepte de porta molecular aplicat a la detecció de diferents molècules (sensing) i a l'alliberament de fàrmacs (drug delivery).

En el segon capítol es presenten els objectius generals que són abordats en els següents capítols experimentals.

En el tercer capítol es presenta un CDDS que allibera la seua càrrega en resposta a agents reductors i en certa mesura a pH àcid. En concret, es tracta de micropartícules de sílice mesoporosa que contenen nanopartícules de magnetita per a dotar de propietats magnètiques a aquests CDDS. Aquests suports magnètics es van carregar amb el colorant safranina O i els seus porus es van tapar amb una molècula orgànica que conté un enllaç azo i un grup carbamat, per a impedir l'alliberament del colorant. Els estudis d'alliberament de la càrrega es van dur a terme en dissolucions aquoses a diferents pH i també en fluids gastrointestinals simulats. Els estudis van mostrar l’alliberament específic de la càrrega, és a dir, es pot induir selectivament en un medi reductor (tal i

com ocorre al colon) simulat en el treball mitjançant l'adició de ditionit de sodi (agent reductor). Açò indueix la ruptura dels enllaços azo i l'alliberament del colorant. A més, es va observar un alliberament parcial de la càrrega en medis a pH àcid, probablement a causa de la hidròlisi parcial del grup carbamat. En aquest capítol també es van estudiar les propietats magnètiques del sistema.

En el quart capítol es presenta un altre CDDS que respon en presència d'agents reductors, alliberant la seua càrrega. En concret, es preparen micropartícules de sílice mesoporosa que inclouen nanopartícules de magnetita seguint el mateix protocol descrit en el tercer capítol. Aquests suports es van carregar amb el colorant safranina O (S1) o amb el fàrmac hidrocortisona (S2), i tots dos sistemes es van funcionalitzar amb un derivat del colorant roig Congo, que inclou un enllaç azo i un grup urea. Els estudis d'alliberament de la càrrega duts a terme amb S1 en dissolucions aquoses a diferents pH i també en fluids gastrointestinals simulats, mostren que una xicoteta part de la càrrega s'allibera en el medi a pH àcid, però que l'alliberament del colorant safranina O es produeix, majoritàriament, en presència de l'agent reductor ditionit de sodi. L'eficàcia dels CDDS desenvolupats en aquest capítol es va avaluar mitjançant estudis *in vivo* en un model de colitis ulcerosa induïda en rates Wistar. Els resultats *in vivo* van mostrar una millora general en els subjectes tractats amb S2 en comparació amb aquells que van rebre una dissolució de hidrocortisona. Quan el tractament amb S2 és combinat amb l'aplicació externa d'un camp magnètic per a retindre les partícules en la zona del còlon, els resultats clínics semblen millorar en aquests subjectes.

El cinqué capítol mostra un CDDS amb doble acció terapéutica. Per a l'obtenció d'aquest últim CDDS, es van preparar micropartícules de sílice mesoporosa, carregades amb el colorant rodamina B o el fàrmac hidrocrotisona i tots dos sistemes es van funcionalitzar amb un derivat del profàrmac olsalazina, que inclou un enllaç azo i un grup amida. Els estudis d'alliberament de la càrrega duts a terme amb S1 en dissolucions aquoses a diferents pH i també en fluids gastrointestinals simulats, van mostrar que

l'alliberament del colorant rodamina B es produeix en presència de l'agent reductor ditionit de sodi, i no es va observar alliberament de la càrrega a pH àcid. L'eficàcia dels CDDS preparats en aquest cinquè capítol es va avaluar mitjançant estudis *in vivo* seguint els mateixos protocols i mateix model utilitzats en el quart capítol. Els resultats dels estudis *in vivo* van mostrar que els subjectes que reben la formulació S2 presenten una disminució en l'índex d'activitat de colitis ulcerosa, i una major regeneració dels teixits afectats. La millora observada en els subjectes que reben S2 s'atribueix al tractament combinat de la hidrocortisona (alliberada des de l'interior dels porus) i el 5-ASA (alliberat en reduir-se el derivat d'olsalazina utilitzat com a porta molecular).

En conclusió, els estudis realitzats demostren que els materials de sílice mesoporosa, en combinació amb portes moleculars sensibles a estímuls específics, tenen un gran potencial per al desenvolupament de nous sistemes d'alliberament controlat de fàrmacs en el còlon, dirigits a millorar l'arsenal terapèutic disponible per al tractament de MII. La possibilitat d'adaptar o personalitzar la càrrega i les portes moleculars, fa que aquests suports de sílice mesoporosa siguen una opció interessant per al desenvolupament de nous sistemes d'alliberació controlada de fàrmacs en diferents aplicacions biomèdiques. Finalment, esperem que els resultats obtinguts en aquesta tesi doctoral servisquen d'inspiració per al desenvolupament de sistemes d'alliberament controlat de fàrmacs innovadors i cada vegada més intel·ligents, per a la seua aplicació tant en medicina com en altres àrees.

Abstract

This PhD thesis entitled “Smart drug delivery systems designed to improve Inflammatory Bowel Disease therapy” is focused on the design, synthesis, characterization and *in vivo* evaluation of several Colon Drug Delivery Systems (CDDS) using hybrid mesoporous silica microparticles as scaffolds containing molecular gates.

The first chapter describes Inflammatory Bowel Disease (IBD) features and gives an overview about the global problematic of the Crohn’s disease and ulcerative colitis. Current clinical treatments as well as some recent advances carried out in research to treat IBD are also discussed. The introduction also describes mesoporous materials and the concept of molecular gates applied to sensing and drug delivery.

In the second chapter there is the presentation of the general objectives that are addressed in the following chapters.

The third chapter describes the development of a CDDS responsive to reducing agents and to some extent to acidic pH. Mesoporous silica microparticles containing magnetite nanoparticles to endow with magnetic properties the CDDS are prepared. The magnetic scaffold is loaded with the dye safranin O and capped with an organic molecule including an azo bond and a carbamate group. Cargo release studies are carried out in solutions at different pHs and in simulated GIT (gastrointestinal tract) fluids. The magnetic properties of the nanoparticles are also studied. A selective cargo release in response to the reducing agent sodium dithionite in simulated colon fluid is produced due to the reduction of the azo bonds. A partial delivery of the cargo is also observed at acidic pH most likely because of the partial hydrolysis of the carbamate group.

The fourth chapter presents another CDDS responsive to reducing agents. Mesoporous silica microparticles including magnetite nanoparticles are prepared following a similar procedure to that reported in chapter three.

The scaffold is loaded with safranin O dye (S1) or with hydrocortisone (S2) and both systems capped with a Congo red dye derivative that includes an azo bond and a urea moiety. Cargo release studies are carried out with S1 in water solutions at different pHs and in simulated GIT fluids. A low release is detected at acidic pH, while safranin O dye voids out of the pores in the presence of the reducing agent, sodium dithionite. The efficacy of the CDDS developed in this chapter is evaluated *in vivo* in an induced-colitis model in Wistar rat. *In vivo* results showed an overall improvement in subjects orally treated with S2 compared with those receiving a hydrocortisone solution. When the treatment with S2 is combined with an external magnetic field to retain the particles in the colon area, the clinical outcome for these subjects seems to further ameliorate.

The fifth chapter shows a new CDDS with double therapeutic effect. Mesoporous silica microparticles are loaded with rhodamine B dye (S1) or with hydrocortisone (S2) and both systems capped with an olsalazine derivative that includes an azo bond and an amide group. Cargo release studies with S1 were carried out in water at different pHs as well as in simulated GIT fluid. The particles do not deliver the payload at acidic pH, whereas a clear release was observed in the presence of the reducing agent, sodium dithionite. The efficacy of this CDDS is evaluated *in vivo* in the same induced-colitis model (Wistar rat) used in chapter four. *In vivo* results showed a decrease in the activity score of ulcerative colitis and a major healing of tissues observed by histology, in subjects receiving S2. The improvement in subjects treated with S2 is attributed to the hydrocortisone released from the pores and 5-ASA released from the reduction of the olsalazine derivative used as molecular gate.

In conclusion, the studies shown in this Thesis demonstrate that mesoporous silica materials in combination with responsive molecular gates have great potential in the design and preparation of new CDDS to improve the therapeutic options available for IBD. The possibility to adapt the cargo and the molecular gate makes mesoporous silica support especially appealing for similar controlled drug delivery applications in the

biomedical field. We hope that the obtained results could inspire the development of new innovative smart drug delivery systems in this or other fields.

Publications & Patents

Results of this PhD Thesis have resulted in the following scientific publications and in a patent:

- **H Teruel, A.**; Coll, C.; Costero, A.; Ferri, D.; Parra, M.; Gaviña, P.; González-Álvarez, M.; Merino, V.; Marcos, M.; Martínez-Máñez, R.; et al. Functional Magnetic Mesoporous Silica Microparticles Capped with an Azo-Derivative: A Promising Colon Drug Delivery Device. *Molecules* **2018**, *23* (2), 375.

- **H Teruel, A**.; Pérez-Esteve, É.; González-Álvarez, I.; González-Álvarez, M.; Costero, A. M.; Ferri, D.; Parra, M.; Gaviña, P.; Merino, V.; Martínez-Mañez, R.; et al. Smart Gated Magnetic Silica Mesoporous Particles for Targeted Colon Drug Delivery: New Approaches for Inflammatory Bowel Diseases Treatment. *J. Control. Release* **2018**, *281*, 58–69.

- **Teruel, A. H.**; Pérez-Esteve, É.; González-Álvarez, I.; González-Álvarez, M.; Costero, A. M.; Ferri, D.; Gaviña, P.; Merino, V.; Martínez-Máñez, R.; Sancenón, F. Double Drug Delivery Using Capped Mesoporous Silica Microparticles for the Effective Treatment of Inflammatory Bowel Disease. *Mol. Pharm.* **2019**, 16 (6), 2418–2429.

- **Hernández Teruel, A**, González Álvarez M, González Álvarez M, Bermejo Sanz M, Merino Sanjuán V, Sancenón Galarza F et al. SISTEMA DE LIBERACIÓN CONTROLADA Y MÉTODO DE PREPARACIÓN DEL MISMO. Spain; ES 2 692 165 B2, 2019.

Additionally, contributions with other authors have resulted in these publications, not included in this PhD Thesis:

- Daniel, F.; Pablo, G.; Margarita, P.; Ana M., C.; Jamal, E. H.; Pedro, A.; Virginia, M.; **Adrián, H. T.**; Félix, S.; Ramón, M.-M. Mesoporous Silica Microparticles Gated with a Bulky Azo Derivative for the Controlled Release of Dyes/Drugs in Colon. *R. Soc. Open Sci.* **2018**, *5* (8), 180873.

- Ferri, D.; Costero, A. M.; Gaviña, P.; Parra, M.; Merino, V.; **H Teruel, A**.; Sancenón, F.; Martínez-Máñez, R. Efficacy of Budesonide-Loaded Mesoporous Silica Microparticles Capped with a Bulky Azo Derivative in Rats with TNBS-Induced Colitis. *Int. J. Pharm.* **2019**, *561*, 93–101.

Abbreviations and Acronyms

5-ASA	5-aminosalicylic acid
APTES	(3-aminopropyl) triethoxysilane
BET	Brunauer-Emmet-Teller
BJH	Barret-Joyner-Halenda
CD	Crohn's Disease
CDDS	Colon Drug Delivery System
CTABr = HTAB	Cetyltrimethylamonium bromide
^{13}C-NMR	Carbon-13 nuclear magnetic resonance
DCU	Dicyclohexylurea
DDC	N,N′-dicyclohexylcarbodiimide
DMF	N,N-Dimethylformamide
DMSO	Dimethyl sulfoxide
EA	Elemental analysis
FDA	Food and Drug Administration
FT-IR	Fourier-transform infrared spectroscopy
GIT	Gastrointestinal tract
IBD	Inflammatory Bowel Disease
ICPT	(3-isocyanatopropyl) triethoxysilane
IR	Infrared
IUPAC	International Union of Pure and Applied Chemistry
HC	Hydrocortisone
HPLC	High-performance liquid chromatography
HRMS	High Resolution Mass Spectrometry
HTAB = CTABr	Hexadecyltrimethylammonium bromide
MCM	Mobile Composition of Matter
MNPs	Magnetic Nanoparticles
MSNs	Mesoporous silica nanoparticles
MSPs	Mesoporous silica particles
NHS	N-hydroxysuccinimide

NMR	Nuclear magnetic resonance
PBS	Phosphate buffer saline
PXRD	Powder X-ray diffraction
SEM	Scanning electron microscopy
STEM	Scanning transmission electron microscopy
$TEAH_3$	Triethanolamine
TEM	Transmission electron microscopy
TEOS	Tetraethyl orthosilicate
TGA	Thermogravimetric analysis
TMB	3,3',5,5'-Tetramethylbenzidine
TNBS	2,4,6-trinitrobenzenesulfonic acid
TNF	Tumor necrosis factor
UC	Ulcerative colitis
UV	Ultraviolet spectroscopy

Table of Contents

Chapter 1

General Introduction

1.0 Oral Colon Drug Delivery Systems for IBD therapy

The development of new Colon Drug Delivery Systems (CDDS) has gained interest in the last decades since the colon has several advantages as a local target to improve the outcomes for different drugs and pathologies. There are some situations in which CDDS are especially advantageous:

(1) To achieve stable plasma levels from controlled release formulations. Adsorption in colon is very important due to the high residence time that allows a low and prolonged absorption of drugs (20-22h),

(2) To deliver therapeutic molecules as protein and peptides based drugs (e.g., insulin, calcitonin, and vasopressin), that should be protected from proteolytic enzyme activity present along the gastrointestinal tract (GIT) to found in the colon a suitable environment that enhance their absorption and

(3) To target disorders or diseases in the colon that require local treatment in order to improve efficacy and reduce systemic adverse effects

(e.g., irritable bowel syndrome, inflammatory bowel diseases (IBD), colorectal cancer, etc.) [1,2].

In these cases, decreased systemic absorption of active agents would imply smaller amounts to be administrated to reach desirable therapeutic effects since high local concentrations in targeted tissues will be attained. Finally, the use of oral dosage forms will count with major compliance of patients because of the comfort of the oral route and the reduced frequency of drug administration.[3,4]

This introduction focuses in the use of colon delivery systems to improve the effectiveness of the treatments of inflammatory bowel disease (IBD). First, the current context around inflammatory bowel disease (IBD) will be introduced, then, we will focus on last Colon Drug Delivery Systems designed to improve the outcome of IBD, and finally, gated mesoporous silica particles are introduced as suitable supports. Those materials are the framework of the novel CDDS developed in this Thesis work.

1.1 Inflammatory Bowel Disease: Ulcerative colitis and Crohn's Disease

1.1.1. Pathology outlines

Inflammatory bowel disease (IBD) includes autoimmune, chronic relapsing inflammatory diseases affecting the gastrointestinal tract (GIT) and causing epithelial injuries. Because of an overreaction of the immunity system, GIT cells are attacked by the immunity system resulting in chronic inflammation and several damages. Alterations in epithelial barrier allow the translocation of luminal antigens (for example, bacterial antigens from the commensal microbiota) into the bowel wall, which exacerbates the damage and inflammation response. The most frequent phenotypes of this disease are ulcerative colitis (UC) and Crohn's disease (CD). Huge breakthroughs

have been made in the understanding of IBD genetics thanks to the advances in genotyping and sequencing technology but an accurate pathogenic mechanism remains still unclear. Clear defined etiology is still unknown. Many evidences lead to the conclusion that the IBD etiology results from the complex interaction among genetic predisposition, environmental factors, immune dysfunction (overreaction, continued activation of T lymphocytes) and dysbiosis in gut microbiota.[5-7] No factor in itself is sufficient for the development of the disease.

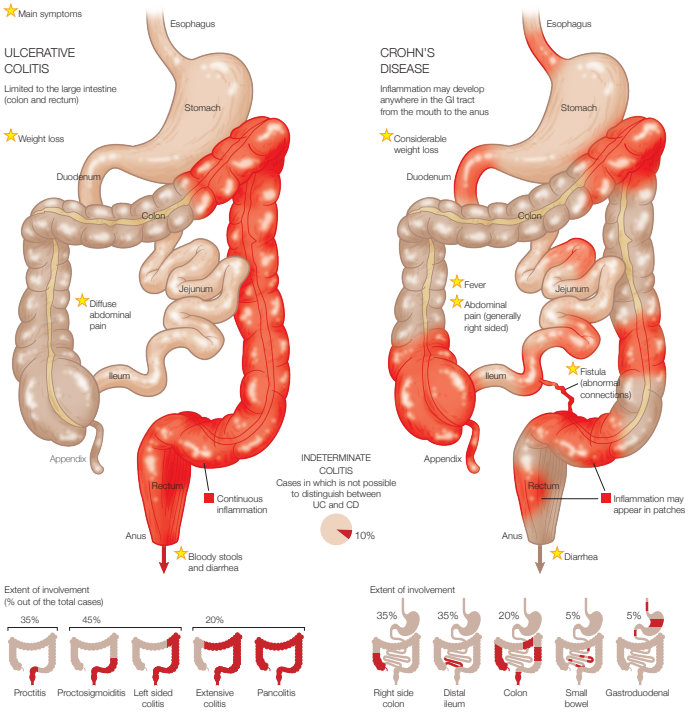

Figure 1. Gastrointestinal tract (GIT) affected by Inflammatory Bowel Disease. Left: GIT showing ulcerative colitis. Right: GIT showing Chron's disease. *Adapted with permission from Clínica Universidad de Navarra (CUN). Copyright © 2011 CUN.*

It is hard to classify IBD as either UC or CD since they have some overlapping clinical (bloody diarrhea, abdominal cramps and pain, weight loss, lethargy, etc) and pathologic (tissue inflammation, fissures, ulcers,

etc.) features. Even though there are still important clinical and pathological properties allowing the differentiation of UC and CD as two independent clinical entities (see Figure 1 and Table 1).[8-10]

Ulcerative colitis was primarily referred to by name in 1859 by Sir Samuel Wilkes who differentiated it from bacterial dysentery. His work was confirmed by Sir Arthur Hirst 1931.[11,12] Currently the best known hallmark that distinguish UC from CD is the homogenous and uniform localization in the colorectal mucosa in UC that does not penetrate to other intestinal layers nor spread out of the large intestine along the GIT.

Crohn's disease was named in 1932 by the gastroenterologist Burrill Bernard Crohn who described a series of patients with inflammation of the terminal ileum of the small intestine, the area most commonly affected by the illness, together with two other colleagues at Mount Sinai Hospital in New York.[11,13] CD is pathologically characterized for skip lesions (inflamed areas admixed with healthy areas) which may penetrate any layer in the intestinal tube (transmural). This may occur all along the GIT, although it usually involves ileum and colon.

UC and CD are both associated with high morbidity having a detrimental impact on individual's quality of life.

Table 1. Key features of UC and CD

	Ulcerative colitis
Incidence	2.2 to 19.2 cases per 100,000 individuals per year.
Onset of disease	Usually between 15 and 40 years.
Location	Inflammation **affects only the colon**: distal colitis or proctitis (55%), left-sided colitis (25%) and extensive pancolitis (20%).
Pathology	**Continuous inflammation** with crypt abscesses and polymorphonuclear leukocyte infiltration from the rectum to proximal segments of the colon.
Histology	**Superficial inflammation** (mucosa and submucosa layers).
Symptoms	Diarrhea (bloody), abdominal cramping, anaemia, weight loss and fatigue.
Clinical presentation	Severe bleeding, toxic megacolon, rupture of the bowel and colon cancer.
Extra-intestinal inflammatory manifestations	Various organs and systems are affected. E.g. Joints, skin, liver, eye, mouth and coagulation issues.
Diagnosis	Blood in the stool, continuous diarrhea, urgency and incontinence, mucus discharge in stool, nocturnal defecations, and crampy abdominal discomfort. The gold-standard in UC diagnostic is based on colonoscopy and histological findings.
Management	The goal of ulcerative colitis treatment is to induce and maintain both clinical (symptoms) and endoscopic remission (mucosa healing). In mild to moderate disease, topical and oral 5-aminosalicylic acid formulations are the mainstay of treatment. Patients with flares or moderate to severe symptoms often need systemic steroids, such as prednisone, although steroids with less systemic absorption, such as budesonide and beclomethasone, are becoming favoured alternatives. To limit steroid exposure, patients with moderate to severe disease should be treated with immunosuppressants (azathioprine or 6-mercaptopurine) or biologics, such as anti-TNF drugs (such as infliximab, adalimumab, or golimumab) or anti-integrins (such as vedolizumab), or both. **Patients who are refractory to all treatments might require colectomy with restorative proctocolectomy with ileal pouch-anal anastomosis**. Management of patients with UC includes regular surveillance colonoscopies (high risk of colorectal cancer); and close monitoring.

Table 1. Key features of UC and CD (continue)

	Crohn's disease
Incidence	3.1 to 20.2 cases per 100,000 individuals per year
Onset of disease	Usually between 15 and 40 years.
Location	Inflammation **frequently affects distal ileum and colon**.
Pathology	**Discontinuous and asymmetric gut inflammation**, intercalating granuloma, focal lymphoid hyperplasia and fibrotic patches with skipped lesion areas.
Histology	**Transmural inflammation** (all layers of the bowel wall, from mucosa to muscular layer).
Symptoms	Abdominal cramping and pain, diarrhea, fever, weight loss and fatigue.
Clinical presentation	From benign perianal fissures to highly debilitating complex stenosis, fistulas or even colon cancer development.
Extra-intestinal inflammatory manifestations	Various organs and systems are affected. E.g. Erythema nodosum, arthritis.
Diagnosis	Thrombocytosis, anaemia and elevated concentrations of C-reactive protein and faecal calprotectin. Hypoalbuminaemia and vitamin deficiencies might also exist. Ileocolonoscopy with biopsies remains the gold-standard for diagnosis.
Management	Starting therapy for mild cases comprises, aminosalicylates, steroids, or thiopurines, with escalation to anti-TNF agents therapy for medium and severe cases. This strategy has shown to be unsatisfactory, and unfortunately **surgery is not curative, recurrence will occur in up to 80% of patients 1 year postoperative**. Thus, early biological therapy has been adopted. Management of patients with CD is complex and tight monitoring is always required to improve the patient outcome.

1.1.2. IBD impact. A global epidemia

IBD (UC and CD together) affects over 2 million and 1.5 million people, just in Europe and North America, respectively.[14] Moreover, since the last decade IBD has become a global health burden with an exponential rise incidence in developing countries of Asia, South America and Africa, which are being socially westernized, thus, changing the trend from the 20th century when IBD was mainly affecting developed or westernized countries (Europe, North America, and Oceania). Besides, unlike the incidence seems to be stabilizing in the western world, the prevalence is rising exponentially in those countries, as a consequence of the high number of cases diagnosticated and the lower mortality rates. (See graph 1 and graph 2)

This increasing global health problem represents an important challenge to health-care systems around the world as IBD is a complex, chronic and costly disease.

Graph 1. Incidence of IBD since 1990 to 2016.

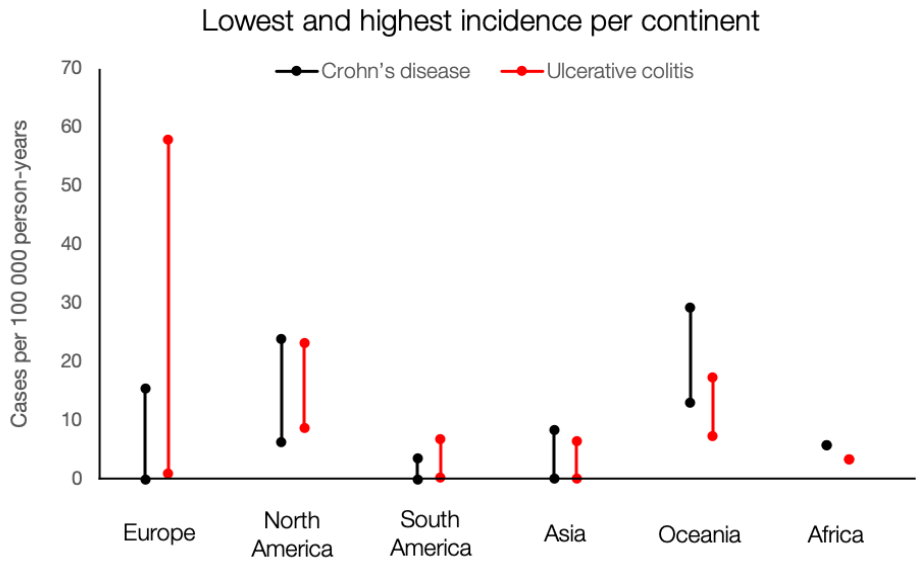

Graph 2. Prevalence of IBD since 1990 to 2016.

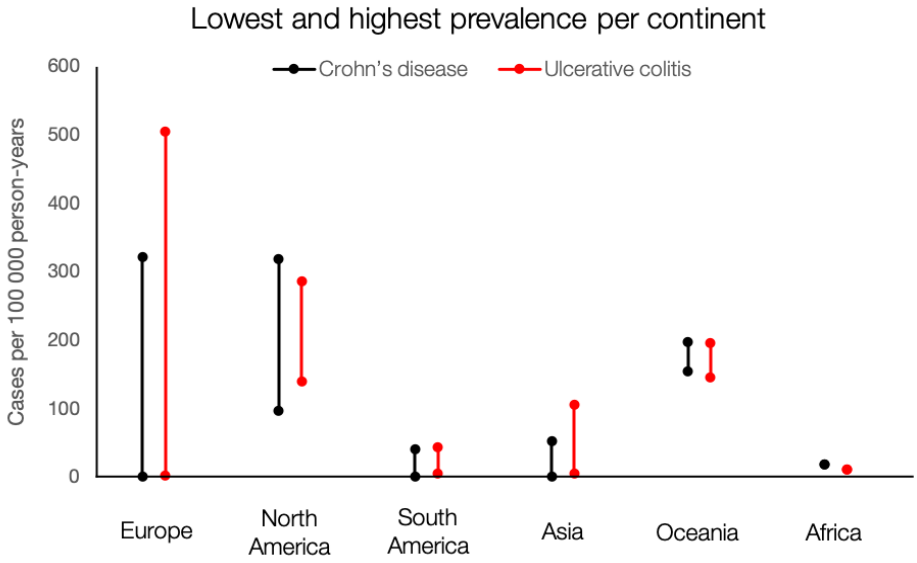

Data showed in **graphs 1 and 2** were extracted from the systematic review of population-based studies, published in The Lancet in 2017 by Siew C Ng et al. The authors gathered epidemiology studies from 1990 to 2016.[14]

1.1.3. IBD treatments

Most available remedies for IBD are focused on the remission of symptoms and the selected drugs to treat IBD depend on the phenotype and severity of the disease. Mild to moderately active UC and CD are mainly addressed with 5-ASA (also known as mesalazine or mesalamine) or other 5-ASA-containing aminosalicylates, e.g. sulfasalazine, olsalazine and balsalazide (see figure 2). Oral administration of 5-ASA in a rapid release dosage form is not a good option because it is absorbed in proximal small intestine being metabolized without reaching the therapeutic levels on inflamed tissues. 5-ASA plasma levels have no therapeutic effects as it only acts as local agent. One of the first options developed to treat IBD more efficiently than using 5-ASA was sulfasalazine. This drug combines 5-ASA and sulfapyridine, bound by an azo link. Orally administered sulfasalazine is 10% taken up by the small intestine and the rest reach intact the colon. Once there, anaerobic microbiota split it into sulfapyridine and 5-ASA (active compound) by means of azoreductase enzymes. When sulfapyridine is absorbed it is carried to the liver where is acetylated, hydroxylated and conjugated with glucuronic acid to be removed by the kidneys. Sulfapyridine does not produce therapeutic effects, instead it is the responsible of most of sulfasalazine adverse effects. Meanwhile 5-ASA molecule is partially absorbed, most of it excreted in feces and in a lesser extent in urine in its acetylated form. Therefore, the administration of sulfasalazine allows 5-ASA reaching necessary concentration in the inflamed tissue, matching its therapeutic effect.

The mechanism of action of these drugs stays still unknown. It has been suggested that 5-ASA has effect over prostaglandins and leukotrienes syntheses, inhibition of leukocytes migration to the intestinal mucosa and antioxidant action acting as free radical scavenger or inhibiting its production, [15,16] all this improving tissue restoration.

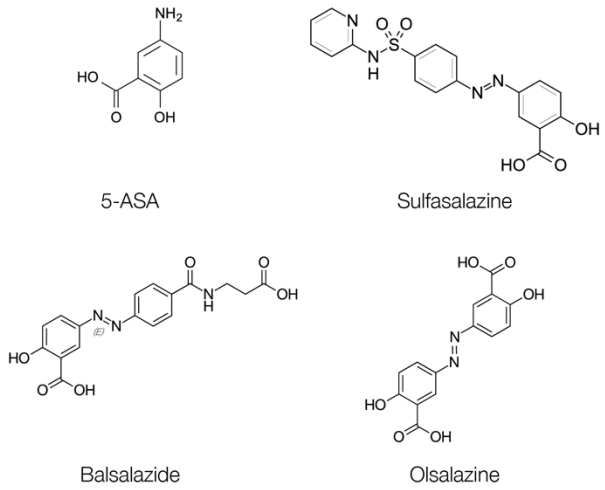

Figure 2. Chemical structures of the main aminosalicylate drugs: 5-ASA, sulfasalazine, balsalazide and olsalazine.

Corticosteroids, like prednisolone, hydrocortisone, budesonide and beclomethasone dipropionate are used for moderate to severe cases or when there is some contraindication with aminosalicylates. Corticosteroids are formulated for this purpose as rectal foam, suppository or enema when the problem is in distal colon. These forms increase the therapeutic effects with less adverse effects than oral forms. As limitations, rectal foam, suppository or enema may distribute non homogeneously the drug [17,18] and are limited to the distal part in the colon [3,19]. Moreover, certain patients are reluctant to this route of administration. Oral dosage forms of corticosteroids work out these last disadvantages, nevertheless non-specific drug release and subsequent systemic absorption causes important undesirable effects such as disruption of metabolic activity, adenosuppression, immunosuppressive effects, cushinoid symptoms, osteoporosis, etc.

When severe disease stages must to be faced, intravenous corticosteroids or immunosuppressive agents, like azathioprine, 6-mercaptopurine, methotrexate, tacrolimus, cyclosporine, calcineurin

inhibitors and anti-TNF-α-antibodies, such as infliximab and adalimumab are chosen.

Some authors [20] have classified the drugs mentioned (i.e. aminosalicylates, corticosteroids and immunosuppressive agents), as pre-biologic era symptom-focused therapeutic options, which do not address the chronic inflammation and can lead to structural damage over time. On the contrary, there are biologic-era therapies including anti-TNF (infliximab, adalimumab, golimumab, and certolizumab) and other biological agents as anti-integrin agents (natalizumab and vedolizumab), which are able to induce mucosal healing and recovery of the structural damage due to chronic inflammation. The goals of biologic therapies focus on maintenance of steroid-free remission, improvement in quality of life, induction of mucosal healing, and reduced need for surgery and hospitalization.

If pharmacological therapy is not enough or fulminate disease stages appear, IBD patients may require surgery [4,21]. In CD cases the disease may reemerge but not in UC patients. Nonetheless this surgery (colectomy) bring a decrease in the wellbeing of patients.

1.1.4. CDDS strategies depending on GIT physiology and microbiota

The inter- and intra-variability in the physiology of the GIT while active IBD is even more significant than that observed in healthy subjects and most of the times this variability is not considered when designing new CDDS for IBD therapy.

Gastrointestinal transit varies depending on several factors: (1) stomach transit time varies between less than 1h when fasting to more than 3h in non-fasting conditions, (2) small intestinal transit time generally vary between 2 to 6 hours in healthy subjects but this time is delayed (≈30%) in IBD patients.[22-25] On the contrary, colonic transit time, which ranges from 6 to 70 hours in healthy patients, is significantly faster in IBD patients, likely because of diarrhea, which is a hallmark of these diseases.[22,26-29]

The pH value is another changing factor along the GIT. In healthy individuals the mean value of pH in the stomach is acidic, ranging between 1 and 5 depending on the absence or presence of food. pH rises to approximately 6 when arriving in the duodenum, and increases along the small intestine until pH≈7.4 at the terminal ileum. Then, pH decreases in the cecum to pH≈5.5-6, finally it rises again (pH≈6.7) at the rectum. Nevertheless, pH ranges can vary intra or interindividually depending on factors such as water or food intake, microbial metabolism, but especially due to the presence of active IBD [18]. It has been reported important pH decreases affecting the colon in both UC and CD, that lead pHs of 2.3-5.5.[22,30-34] Many controlled delivery systems relies on pH changes along the GIT, to allow the release of their cargo in a specific GIT region. Some CDDS use that approach to target the colon, as we will detail below.

Enzymes produced by colon microbiota have also been exploited to deliver drugs specifically in the colon. Microbiota of the stomach and the small intestine mainly consists on gram-positive facultative bacteria (10^3–10^4 CFU/ml).[35-37] On the contrary, local colon microbiota is mainly composed for anaerobic bacteria (e.g. Bacteroides, Bifidobacteria, Eubacteria, Clostridia, Enterococci, Enterobacteria, etc.) and it is many times greater (10^{11}–10^{12} CFU/mL).[38] This microflora fulfills its energy needs by fermenting various types of substrates that have been left undigested in the small bowel (e.g. di- and polysaccharides, mucopolysaccharides, etc.).[39] To do that these microorganisms produce an extensive number of enzymes such as azoreductase, ß-galactosidase, ß-xylosidase, nitroreductase, glycosidase deaminase, etc.[40,41] For the treatment of IBD these enzymes are profited as triggers for releasing drug molecules from various undigested drug carrier systems. For instance, enzyme-responsive prodrugs (e.g. olsalazine or balsalazide), or drugs coated with enzyme-sensitive polymers (e.g. resistant starch), exploit this approach.[42] In these systems, increasing the residence time of the formulation in the expected colon areas where drug has to release is advantageous, considering that these enzymes need enough time to cleave the corresponding bounds.[43] Nevertheless, some changes in microbiota

composition (intestinal dysbiosis) are common on GI diseases like IBD, due to alterations in physiology, inflammatory state or as a result of treatment regimens. Moreover, the bacterial enzymatic metabolism may also be affected by changes in colonic luminal pH as well.[22,44,45] Thus, dysbiosis could impact in the efficacy of some drug delivery systems relying on the enzyme responsive approach.

Another important aspect to reach the colon epithelium is the proper particle size of drugs or their carriers. Particles with diameter higher than 200μm have low GIT transit times because of the physiological conditions in the injured intestine. Micro and nanoparticles introduce some advantages in targeting the inflamed areas in colon. Because of their smaller particle size, they can pass through the GIT easier than classical single unit dosage forms.[41,46] Nanoparticles have unique physicochemical properties which are distinct from those of the same material with larger macroscopic or microscopic sizes. A genuine feature of nanoparticles is its epithelial enhanced permeability and retention (eEPR) effect, that allows the preferential uptake of nano-sized particles by immune cells which are highly increased in number at the inflamed regions.[22,34,47,48] By reducing the diameter of the particles, it is also possible to avoid rapid carrier elimination by diarrhea, which is a common symptom in IBD.[49] All these features would point out to nano-sized particles as the best option to IBD treatment, as they seem to easily reach the colon and they are preferentially retained in inflamed tissues intrinsically. Nevertheless, it has to be taken into account that nanoparticles show significantly greater tissue uptake, which will lead to greater systemic absorption through different paths.[50] Some studies have shown the potential of nano- and microparticle uptake into the rectal mucosa of human IBD patients and found an obvious accumulation of microparticles in active IBD, whereas nanoparticles were detectable only in traces in the mucosa of these patients.[22,51] These studies demonstrated that microparticles exhibited accumulation and bioadhesion to the inflamed mucosal wall, but no absorption of these particles across the epithelial barrier was detected. Conversely, nanoparticles were translocated to the serosal compartment of IBD patients, this effect is

undesirable because it prohibits the formation of local drug depots at the site of inflammation and increases the risk of systemic adverse effects. Furthermore, particles in systemic circulation are likely to be recognized by the mononuclear phagocyte system and deposited in liver and spleen, reducing the efficacy to safety profile of the formulation based on nanoparticles. Considering the differences in the transport across inflamed intestinal mucosa for the different sized particles, nanoparticles reach the deeper layers of the mucosa while microparticles are retained in the more superficial layers.[51,52] Thus, microparticles could be useful in the cure of IBD disease where the mechanism of persorption permits the passage of the larger particles, whereas nanoparticles could be more effective under conditions of remission or minor inflammation where the mucosal barrier is less permeable and absorption through epithelial cells prevails with respect to persorption.

As we will detail below, a continuous effort is being made to get targeted drug delivery systems to prevent or treat IBD. The longer lasting permanence of the drug locally within the affected epithelium in colon will allow the reduction in drug amounts necessary and frequency of intakes, thereby improving adherence to treatment. The final aim of these drug delivery systems is to increase the desired therapeutic effects of existing or novel drugs, decreasing the adverse effects as much as possible.

1.2 Oral CDDS for IBD management. Advances in the last few years

From several decades different approaches have been used to target the colon, such as biodegradable polymers which respond to changes in pH, the use of time-dependent formulations, pressure-controlled and osmotic-controlled systems, bioadhesive formulations, systems targeting inflammation, microbiota and enzyme responsive prodrugs or drugs coated with enzyme-sensitive polymers. These strategies are described in many

articles and reviews.[53-56] Some examples found in last five years on oral CDDS for IBD therapy are shown below.

1.2.1. Oral CDDS following pH-sensitive approach

The use of pH-sensitive delivery systems is still the most popular approach to develop oral CDDS to treat IBD. The reason behind is most likely related to the availability in the market of many biocompatible or GRAS (Generally Recognized as Safe) polymers that are able to degrade or change its conformation depending on the pH such as the well-known acrylic family polymers marketed under the trade mark Eudragit™ by Evonik. For instance, Naeem, M et al. prepared cyclosporine A-loaded Eudragit FS30D nanoparticles (ENPs), PLGA nanoparticles (PNPs), and Eudragit FS30D/PLGA nanoparticles (E/PNPs) using the oil-in-water emulsion method. The dual-functional E/PNPs minimized burst drug release (only 18%) at pH 1.2 and 6.8, and generated a sustained release at pH 7.4. E/PNPs significantly improved cyclosporine A distribution to the colon compared with PNPs or ENPs. In a mouse model of colitis, E/PNP treatment improved weight loss and colon length, and decreased rectal bleeding, spleen weight, histological scoring, myeloperoxidase activity, macrophage infiltration and expression of proinflammatory cytokines compared with PNPs or ENPs.[57] Natural derived polymers such as alginates are also widely used in this field, as it could be seen in the next examples. Oshi, M. A. and others developed colon-targeted dexamethasone microcrystals (DXMCs) coated with multilayers of chitosan oligosaccharide (CH), alginate (AG) and finally Eudragit S 100 (ES) using a layer-by-layer (LBL) coating technique. This formulation demonstrated pH-dependent dexamethasone release, avoiding initial burst drug release in acidic pH conditions of the stomach and small intestine, and providing subsequent sustained drug release in the colonic pH. It exhibited a significant therapeutic activity in a mouse model of colitis compared to other DXMCs.[58]

Cong, Z. et al. obtained a pH-sensitive drug delivery system based on a matrix composed by an alginate hydrogel and chitosan micelles. The hydrogel/micelle (1:1) exhibited a sustained-release profile, while hydrogel/micelle (3:1) exhibited a colon-specific profile. Their corresponding release mechanisms, proved in simulated GIT fluids, revealed that the release of drug (emodin) from these two formulations followed a complex process, in which several mechanisms were involved or occurred simultaneously.

pH-sensitive systems are very useful and work well but generally the release occurs quickly when the pH change occurs. A limitation of the pH-sensitive approach is, as commented before, the changes in the pH of the GIT in a non-defined and unexpected way in IBD patients as well as the inter- and intravariability in patients and the fast or fed condition of subjects.[22,30-34]

1.2.2. Oral CDDS following enzyme-sensitive approach

Many enzyme-sensitive CDDS for IBD treatment have been developed in the last years. In addition to enzyme-responsive biocompatible polymers available in the market, as it occurs with pH-sensitive systems, there are other more sophisticated CDDS for instance based on prodrugs that allow the release of the drug just in the presence of the enzymes specifically produced by colon microbiota. The mechanism is based on the enzymatic cut or splitting of polymers or other molecules into small pieces allowing drug release. As an example, this is the case for resistant starch not hydrolyzed in the small intestine that can only be fermented to short-chain fatty acid (SCFA) by anaerobic microbiota found in colon, thus it can be used as coating or capsule to develop CDDS. For instance, Chen, J. et al. developed an oral colon-specific controlled-release system in the form of 5-ASA-loaded microparticle cores (MP) containing microcrystalline cellulose and medicinal starch in the ratio of 3:1 and the 5-ASA in the content of 16%, w/w. The particles were obtained via extrusion–spheronization. MPs were coated with a resistant starch film (23.4% of RS2 and 76.6% of RS3)

through an aqueous suspension coating process, obtaining RS@MPs. RS2 was chosen from a high-amylose cornstarch with 88.5% digestion resistibility. RS3 was prepared by a high-temperature/pressure (HTP) treatment, with the following of enzymatic debranching, and retrogradation, resulting in a dramatic increase in enzymatic resistance. RS@MPs showed 40.7% of 5-aminosalicylic acid release within 8 h. *In vivo* studies with fluorescein-loaded RS@MPs indicated the high acidic and enzymatic resistibility of RS@MPs and a restrained release in the upper GIT.[42]

Pectin derived particles are another example of a natural derived polymer that can be gradually degraded by pectinase found in colon. In the work carried out by Günter, E. A. et al. the authors obtained low methyl-esterified pectins from the cell walls of the campion or S. vulgaris (SV, SV>300, tansy or T. vulgare (TV, TV > 300) and duckweed or L. minor (LM, LM > 300) callus cultures and apple pectin (AP, Classic AU 701). Those pectins were used to develop prednisolone-loaded calcium pectinate gel beads. Release aspects of prednisolone (drug) in simulated gastric (pH 1.25), intestinal (pH 7.0) and colonic (pH 7.0 + pectinase) media were investigated. Prednisolone release occurred in a larger extent in colonic medium due to the enzymatic erosion of the beads suggesting that the calcium pectinate gel beads developed can be used as potential systems for colon-targeted drug delivery.[59]

Dextran, ß-galactose or molecules containing disulfide bonds are other alternatives following the enzyme-sensitive approach for oral CDDS for IBD treatment.[60] Qiao, H. et al. obtained an amphiphilic curcumin-containing polymer (PCur) composed of hydrophilic poly(ethylene glycol) (PEG) and hydrophobic curcumin (Cur) linked by disulfide bonds. PCur showed limited drug release and enhanced robustness under the physiological pH of the gastrointestinal tract (GIT), and a significantly release was observed in the colon. *In vivo* studies with a DSS-induced (Dextran Sulphate Sodium) murine model of IBD were carried out. The authors reported a similar amelioration in the inflammatory progression when PCur or sulfasalazine was orally administered.[61]

The use of azo bond is also a popular approach that has already been used in marketed IBD drugs, such as sulfasalazine (as explained above), olsalazine or balsalazide. Many systems have also been developed under this strategy for instance using polymers and hydrogels containing azo crosslinks, allowing the release of drugs encapsulated by azoreductase activity. Naeem, M. et al. used a polymeric mixture of enzyme-sensitive azo-polyurethane to develop their enzyme/pH dual sensitive nanoparticles (*vide infra*).[62] One advantage of using azo responsive systems lays on the knowledge that at least 10 strains of anaerobic bacteria, isolated from human feces, are capable of reducing azo dyes (*Eubacterium hadrum* (2 strains), *Eubacterium spp.* (2 species), *Clostridium clostridiiforme*, a *Butyrivibrio sp.*, a *Bacteroides sp.*, *Clostridium paraputrificum*, *Clostridium nexile*, and a *Clostridium sp.*).[63] Furthermore, it looks like those species are not usually affected under common GI diseases like IBD, and other inflammatory states.[22,44,45] Thus, oral CDDS with azo bonds will be still reduced by azoreductases even in subjects suffering some of these pathophysiological states.

The main limitations of enzyme-sensitive approach are: (1) systems have certain non specific release due to intestinal enzymes or pH of GIT areas before reaching the colon, (2) the increased intestinal motility attributable to IBD decrease the residence time of CDDS in the colon area and the reactions required for the release of the drugs are not completed.[64]

1.2.3. Oral CDDS following inflammation targeting or ROS-responsive approach

As stated before nanoparticles seem to have intrinsic properties allowing them to accumulate in inflamed tissues. Furthermore, it has been demonstrated that inflamed areas present an oxidative environment rich in reactive oxygen species (ROS) and other oxidative molecules that promote the synthesis of pro-inflammatory mediators.

It is known the need of low levels of endogenously produced ROS to maintain normal cell functions and cellular signaling, but their overproduction is intimately related to the pathogenesis, development and aggravation of inflammatory diseases. Superoxide, peroxide, and hydroxyl radical are among the major components of ROS. Experimental and clinical studies, have shown that this ROS overproduction may amplify the inflammatory response in the intestinal mucosa, triggers mucosal injury, and accelerates mucosal ulceration in the pathogenesis of IBD.[65-68] Mucosal ROS has been found to reach 10 to 100 times higher concentrations in IBD patients.[68-70] In fact, there are some reported studies aiming to know the efficacy of palliative treatments including either antioxidants or free radical scavengers in subjects suffering Crohn's and ulcerative colitis diseases.[68,71-73] Some CDDS have been developed taking advantage of that property. Zhang Q. et al. designed a nanosystem (Tpl/OxbCD) based on the drug tempol (Tpl) and a biocompatible ß-cyclodextrin-derivative. The payload Tpl serves as a superoxide dismutase mimetic (SOD-mimetic),[74] while the nanocontainer was mainly composed of a hydrogen peroxide-eliminating material (i.e. OxbCD) that functions as a catalase-mimicker. In the presence of hydrogen peroxide, OxbCD is hydrolyzed into water soluble products including ß-cyclodextrin, pinacol borate, and p-hydroxylmethylphenol, thereby leading to elimination of hydrogen peroxide, and release of Tpl molecules. This SOD/catalase mimetic nanotherapy was found to effectively scavenge multiple components of ROS such as superoxide, hydroxyl radical and hydrogen peroxide. OxbCD nanoparticles showed enhancing accumulation in inflamed colon in mice. Upon triggered by abnormally elevated ROS levels, this SOD/catalase mimetic nanomedicine selectively released Tpl molecules in inflamed intestinal tissues. *In vivo* studies showed that Tpl/OxbCD nanoparticles exhibited robust therapeutic benefits and good safety profiles in mice with acute or chronic colitis induced by either dextran sodium sulfate (DSS) or 2,4,6-trinitro benzene sulfonic acid (TNBS).[68] Another pathway targeting inflamed tissues in IBD improving ulcerative colitis was described by Xiao, B. et al. The authors developed CD98 siRNA/curcumin-loaded polymeric (PLGA/PVA/chitosan combination)

nanoparticles functionalized with hyaluronic acid (HA-siCD98/CUR-NPs). The same authors had been demonstrated in a previous work that CD98 siRNA (siCD98) mediated down-regulation of colonic CD98 expression could decrease the severity of experimentally induced UC in mice.[75] Hyaluronic acid (HA) was used to functionalize the surface of the nanoparticles as it can specifically bind to glycoprotein CD44, which is over-expressed on the surface of colonic epithelial cells and macrophages in UC tissues.[76,77] Compared to either curcumin (a potent anti-inflammatory agent) or siCD98-based monotherapy, co-delivery of siCD98 and curcumin by the HA-functionalized nanoparticles exert combinational effects against ulcerative colitis by protecting the mucosal layer and alleviating inflammation both *in vitro* and *in vivo*.[78]

1.2.4. Oral CDDS following dual or combined approach

Since none of the strategies described above are 100% reliable, especially because of the inter- and intraindividual variations, some authors have attempted to improve IBD therapy by combining different approaches. The most popular combinations are (i) pH-/time-sensitive dual systems that depend not only on pH changes along the GIT but also on the different transit times and (ii) pH-/enzyme-sensitive dual systems.

pH-/time-sensitive dual systems usually rely on a combination of a double layered coating that protects the trigger of the load release in gastric conditions (acidic pH), avoids a burst release when reaching intestinal conditions pH≈6.8-7.4 and allows a sustained release in the colon. This can be achieved using combinations of the Eudragit™ polymers described above. As an example, Naeem, M. et al. developed pH-/time-sensitive nanoparticles using Eudragit® FS30D as a pH-dependent polymer, and Eudragit® RS100 as a time-dependent controlled release polymer. *In vitro* studies showed sustained release at a colonic pH preventing the burst release at acidic conditions. *In vivo* evaluation revealed that the dual pH/time-dependent nanoparticles improved the specific delivery of drugs to the inflamed colonic region, thus, enhancing the efficacy of treatment.[79]

pH-/enzyme-sensitive dual systems works in a similar way, the pH-sensitive element is intended to protect the enzyme-responsive mechanism from the acidic conditions found in the gastric area. Thus, once the gastric phase is overcome, the pH layer starts its disintegration, releasing the enzyme-responsive drug release systems. As an example, Naeem, M. et al. developed enzyme/pH dual sensitive nanoparticles using a polymeric mixture of enzyme-sensitive azo-polyurethane (Azo.pu) and pH-sensitive Eudragit S100 (ES) (ES-Azo.pu) for specific colon drug delivery.[62] ES-Azo.pu nanoparticles were loaded with coumarin-6 (C-6) as a model drug. *In vitro* release studies showed that ES-Azo.pu nanoparticles prevented drug release at acidic conditions, but present sustained release at a physiological pH and in the presence of rat cecal contents obtained from a rat model of colitis (due to the presence of azoreductase enzyme released by the colon microbiota). The authors performed an *in vivo* localization study in rat gastrointestinal tract demonstrating that ES-Azo.pu nanoparticles were selectively distributed, showing 5.5-fold higher levels of C-6 in the inflamed colon than ES nanoparticles. The authors concluded suggesting that the enzyme/pH dual sensitive nanoparticles presented in this study can serve as a promising strategy for colon-specific drug delivery against inflammatory bowel disease and other colon disorders.

Aina L.A. Cesar et al reported another example of pH-/enzyme-sensitive dual system.[80] In this case the CDDS relies on the release of 5-ASA from a prodrug consisting of chondroitin sulfate linked to 5-ASA, synthesized using a carbodiimide as conjugating agent (CS-5-ASA). The analysis of release profile showed that the covalent linkages formed between the drug (5-ASA) and the polymer (chondroitin sulfate) are more stable in acid medium as opposed to that seen at basic mediums. The authors explain that this may be indicative of the formation of the ester linkage between the drug and the polymer, suggesting that the conjugate will pass intact through the small intestine, which agrees with the system's objective. Additionally, the authors found that it requires enzymes, such as esterases, present in the intestinal environment, to complete the reaction that triggers the 5-ASA release. The biodistribution study performed,

showed that the conjugate had reached the lower GIT after 6 h of administration and remained in place for up to 8 h, suggesting a potential mucoadhesive profile. The authors concluded that, after additional *in vivo* studies, the CS-5-ASA conjugate could be considered an alternative treatment for ulcerative colitis.

1.3 Mesoporous silica materials & smart molecular gates

The CDDS developed in this Thesis work are based on mesoporous silica microparticles loaded with a certain molecule of interest (a dye or a drug) and functionalized with molecular gates that endow the system with controlled release features.

1.3.1. Mesoporous silica material

The IUPAC (International Union of Pure and Applied Chemistry) classifies porous materials according to their pore diameter in microporous (< 2 nm), mesoporous (2-50 nm) and macroporous (> 50 nm) materials.[81,82] Due to the possibility of tailoring the pore structure, framework composition, morphologies over a wide range and their large specific surface area, porous materials have gained interest for several applications such as catalysis,[83] adsorption of gasses and chemicals,[84] filtration and separation,[85] enzyme immobilization,[86] tissue regeneration,[87] sensor technology[88] and drug delivery.[89]

Zeolites (a well-known example of porous materials) are microporous aluminosilicates acting as molecular “sieves” adsorbing molecules with certain dimensions able to enter the pores, then favoring formation of specific products with high yields and minimum waste. However, the need of finding porous materials with larger pore sizes promoted the research in this field. In 1992 researchers from Mobil oil company developed, patented

and reported the synthesis of a family of mesoporous silica materials known as the M41S phases.[90] There are three main structure types (Figure 3): MCM-41 (with a hexagonal arrangement of mesopores, like a honeycomb), MCM-48 (with a cubic arrangement of mesopores) and MCM-50 (with a lamellar structure).[91] These materials usually exhibit a pore diameter between 2 to 5 nm, although it can be further expanded using different strategies. MCM-41 is the most studied and used, among these phases, due to the relative simplicity of its synthesis and its particular honeycomb-like structure. Later, in 1998 researchers from Santa Barbara University in California reported the so-called SBA-15 which have a hexagonal arrangement of pores with a tunable size from 5-30 nm.[92]

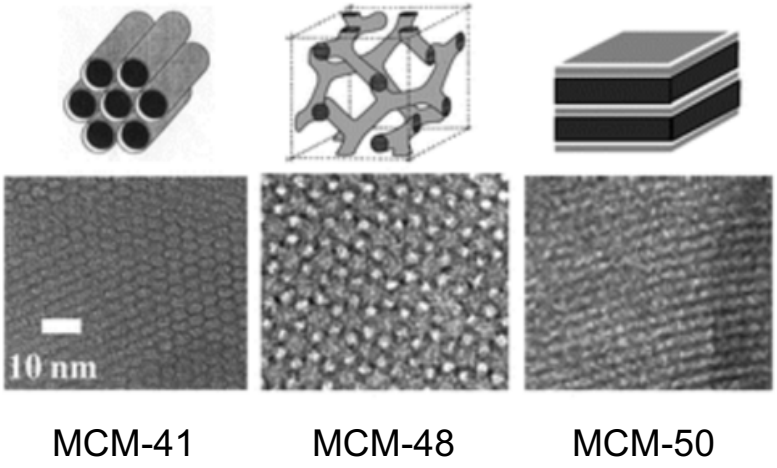

Figure 3. Mesoporous silica materials (M41S family). Top: Schematic 3-D structures. Bottom: Corresponding TEM images of the pore network. *Reprinted with permission from Chem. Soc. Rev. 2013, 42, 3663. Copyright © 2013 The Royal Society of Chemistry.*

Mesoporous silica materials have outstanding features that make these materials highly suitable in many fields of application.

The main appealing features of mesoporous silica materials are:

- Large specific surface area (500-1000 m^2/g).
- High specific pore volume and loading capacity.
- Ordered and uniform pore distribution.
- Tunable pore size from 2-30 nm.
- Preparation in the form of micrometric particles or nanoparticles with tunable size depending on the synthetic parameters.
- Their synthesis requires inexpensive and non-hazardous chemicals and can be produced in large scales.
- Thermal stability, chemical inertness and easy handling.
- Easy functionalization with trialcoxysilane derivatives (a well-known silicon oxide functionalization chemistry).
- Biocompatibility.[93]

1.3.2. Synthesis of mesoporous silica materials

To accomplish the synthesis of a high ordered porous structure with homogenous pore dimensions two basic components are necessary:

1. A **template** (for instance a cationic surfactants) able to form self-assemblies of individual micelles (supermicelles), which acts as a structure-directing agent of the high ordered porous net.[94]
2. A **silica precursor** (for instance tetraethyl orthosilicate, sodium silicate or tetramethylammonium silicate) that self-organize around the template, condensing and forming the final rigid structure by means of a polymerization reaction.

This synthesis is considered a sol-gel process involving the conversion of monomers in solution (sol) into an integrated solid network (gel). The structure of the template depends on the selected conditions such as temperature, pH, ionic force and surfactant nature and concentration. Once the supermicelles are formed, the silica precursor is added. In this step, the molecules of the silica precursor are hydrolyzed and form silanol groups (Si-OH) which polymerize by condensation creating a network of siloxane

bonds (Si-O-Si) as shown in Figure 4. At this point, the presence of the supermicelles is crucial to produce the assembly of the silica on its surroundings and the formation of the pores. The structure of the pores in the final material (hexagonal in the case of MCM-41) is the result of the arrangement of the surfactant's micelles. The progressive formation of the silica material can be observed with the naked eyed by the appearance of a white turbidity. Finally, the surfactant can be removed by an extraction process under reflux in acidic media or by calcination (heating of the solid in a muffle furnace at high temperatures for several hours).

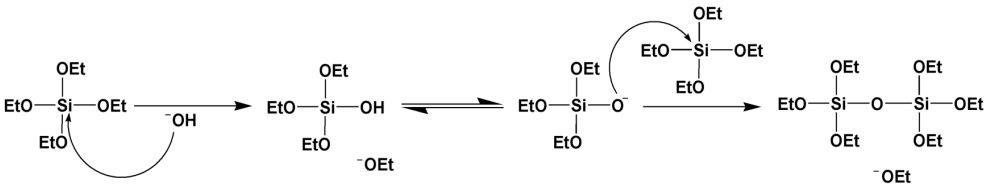

Figure 4. Mechanism of TEOS hydrolysis and condensation.

The size, shape and regularity of the resulting particles depends on different parameters such as temperature, time, amount/proportion and nature of reagents added. For 100 nm MCM-41 mesoporous silica nanoparticles (the most used type), a typical synthetic procedure involves the addition of tetraethyl orthosilicate (TEOS) as silica precursor, over a cetyltrimethylamonium bromide (CTAB) micellar solution at 80 °C and basic pH (adjusted with NaOH) (Figure 5). The mixture is stirred during 2 hours and then the solid is collected by centrifugation or filtration. Other conditions can be used for obtaining microparticles or nanoparticles with larger or smaller size. Typically, the final MCM-41 mesoporous scaffold presents cylindrical unidirectional channels of pores with a diameter of ca. 2-3 nm. As commented above, the pore size can also be modulated, using suitable swelling organic molecules, by post-synthesis treatment or by adjusting the reaction parameters.

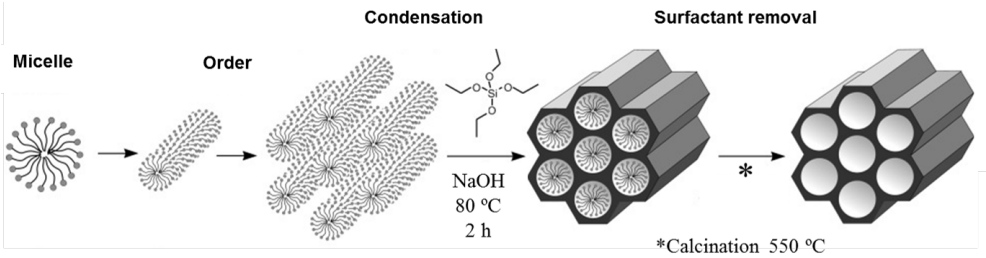

Figure 5. Synthetic procedure for preparing MCM-41-type mesoporous silica nanoparticles. *Adapted from Angew. Chem. Int. Ed. 2006, 45, 3216. Copyright © 2006 Wiley-VCH.*

1.3.3. Functionalization of mesoporous silica materials

Functionalization is the term used by researchers working in this field which refers to the incorporation of organic groups on the surface of inorganic materials. Functionalization of inorganic materials with organic molecules leads to the production of hybrid organic-inorganic materials. Those hybrid materials have a large number of interesting and promising applications, because of the synergy created between the inorganic scaffold and the functional (bio)organic moieties.

Two main strategies are used for the functionalization of porous hybrid materials:

1. Grafting. Post-synthetic modification of the surface of an inorganic silica material.
2. Co-condensation or simultaneous condensation of silica and organosilica precursors.[95]

The incorporated (bio)organic groups can have a self-function (e.g. increasing surface hydrophobicity or hydrophilicity, stabilization, fluorescence, etc.) or be used as intermediate (anchoring) groups reacting with other molecules by means of covalent bonds or by electrostatic or supramolecular interactions.

1.3.4. Grafting procedure

This is a post-synthetic functionalization method taking advantage of the high concentration of silanol groups (Si-OH) in the surface of silica materials. Silanol groups act as a reactive point to anchor organosilanes containing the desired organic moiety. There are a wide range of commercially available organosilanes, being trialkoxysilanes with structures $(R'O)_3$-Si-R (where R is an organic group) the most common and widely used. Silazanes $HN(SiR_3)_2$ and chlorosilanes $ClSiR_3$ are also available, but both of them are less frequently used. The reaction of silanol groups in the surface of silica materials with trialkoxysilanes is considered a simple condensation reaction or nucleophilic substitution (Figure 6).

The distribution of the organic molecules on the solid after the grafting may be determined by factors such as diffusion processes and steric hindrance around the silanols. If the grafting process is carried out before the removal of the surfactant, as the inner surface is occupied by the inert template, the modification takes place essentially in the external surface. On the other hand, if the template is removed before the grafting, the organosilanes react preferentially at the pore openings due to steric hindrance. Thus, although the silica mesoporous material can present some organic groups covalently bonded into their inner surface, grafting processes occur mainly in the external surface of the inorganic scaffolds.[96,97]

Polycondensation rate of the organosilane precursor (the reaction with itself rather than with the surface silanol) must be considered as well. This condensation may lead to the formation of oligomers of the organosilane, which may block the pore outlets without getting anchored to the material surface. Competition between the condensation and the grafting process itself is influenced by some parameters such as type of organosilane and solvent, temperature reaction and amount of water adsorbed on the surface.

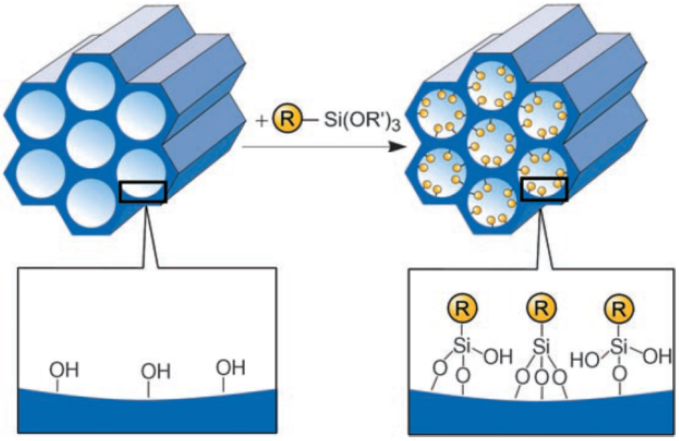

Figure 6. Schematic of the grafting procedure for functionalization of mesoporous pure silica materials with organotryalkoxysilanes of the type $(R'O)_3$-Si-R where R represents an organic functional group. *Adapted from Angew. Chem. Int. Ed. 2006, 45, 3216. Copyright © 2006 Wiley-VCH.*

The grafting method has two main advantages:

- Mesoporous silica support can be synthesized by standard procedures in large scales and then modified with the selected organosilanes.
- The mesostructure of the silica phase as well as the morphology of the particles are usually retained after the functionalization process.

1.3.5. Co-condensation procedure

Co-condensation method represents an alternative to synthesize organically functionalized mesoporous silica phases in which the silica precursor (e.g. TEOS) and the functional organosilane are incorporated in the synthetic mixture at the same time and condensate in the presence of a structure-directing agent (Figure 7). It consists on a one-pot synthesis, also called direct synthesis.

The resulting silica framework contains alkoxy functional groups intercalated in the main silica matrix, distributed homogenously both on the

external and internal surfaces, albeit, it is convenient to consider some disadvantages of the co-condensation method:

- The presence of increasing concentration of functional groups $(R'O)_3SiR$ in the reaction mixture may interfere with the formation of micellar aggregates, affecting the stability and the particle morphology in the final material, in extreme cases it can prevent the formation of the mesoporous structure.[98]
- Homo-condensation reactions between silane groups are favored and the homogeneous distribution of different organic functionalities in the framework cannot be guaranteed.
- The incorporated organic groups can lead to a reduction in the pore diameter, pore volume, and specific surface area.
- Finally, the removal of the surfactant template is limited to extractive methods, since calcinations would spoil or degrade of the organic functional groups.

Thus, even if some procedures for incorporating specific and common tryalkosylanes like APTES have been described, this method is less versatile since the procedure should be optimized in each particular case.

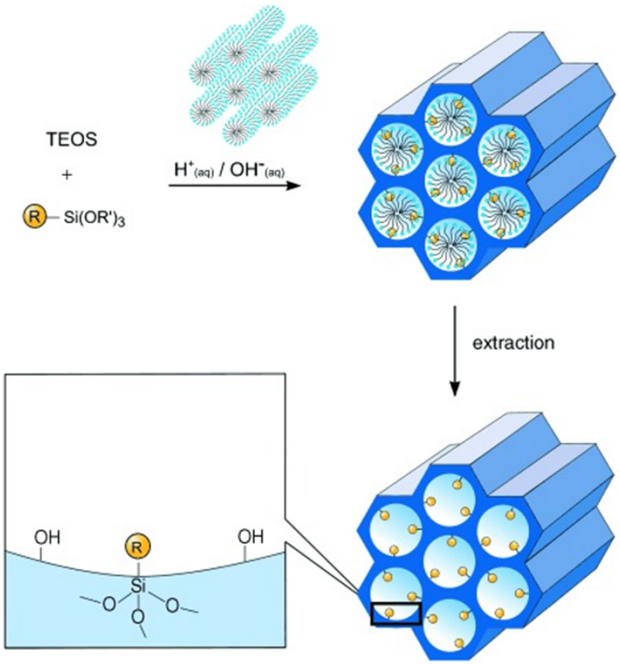

Figure 7. Schematic of the co-condensation method for organic functionalization of mesoporous silica materials. *Adapted from Angew. Chem. Int. Ed. 2006, 45, 3216. Copyright © 2006 Wiley-VCH*.

There is also the possibility to use silsesquioxane precursors that have a molecular structure of the type $(R'O)_3Si\text{-}R\text{-}Si(OR')_3$, being R the organic functional group to be introduced on the material. They are also called "single-source" precursors since they act as the precursor of the inorganic network and, at the same time, incorporate the organic functionality. The materials produced using this approach are called periodic mesoporous organosilicas (PMOs).[99] However, the variety of commercially available silsesquioxanes is smaller compared to the wide variety of tryalkoxysilanes and this strategy has been less employed.

1.3.6. Characterization of mesoporous silica materials

Different characterization techniques are routinely used to elucidate the structural and physico-chemical properties of hybrid mesoporous materials. Typically, when characterizing a hybrid mesoporous material the main features to be considered are: i) the integrity of the mesoporous scaffold, ii) the amount of organic matter that composes the final material and iii) particle morphology and size. The most common techniques used in the characterization of mesoporous materials are showed in table 1.

Table 1. Characterization techniques commonly used in the determination of textural and physico-chemical properties of hybrid mesoporous materials.

Characterization technique	Objective
X-Ray Diffraction	Meso-scale periodicity
Transmission electron microscopy	Pore order, particle size and morphology
Scanning electron microscopy	Particle morphology, pore size
Dynamic light scattering	Particle size
Nitrogen adsorption-desorption measurements	Determination of textural properties, pore size
Thermogravimetric analysis	Quantification of organic species incorporated in the material
Elemental analysis	Chemical composition of the material
Fourier transformed infrared spectroscopy	Characterization of functional groups
UV-Vis spectroscopy and fluorescence	Presence of chromophore organic groups

Powder X-Ray Diffraction (PXRD) is a non-destructive technique commonly used to identify the crystallographic symmetry of material phases at both the nano- and mesoscale. In a typical experiment, the sample is placed in a holder at the center between the source and the detector. The source emits X-ray radiation with a variant incident angle, and

the diffracted light is collected by the detector. PXRD patterns are plots of intensity (of diffracted light) as a function of the angle of the incident beam. According to Brag's law (Figure 8), the angles at which there are intensity peaks (reflections, due to constructive interferences) are determined by the distance between atomic planes in the ordered structure.

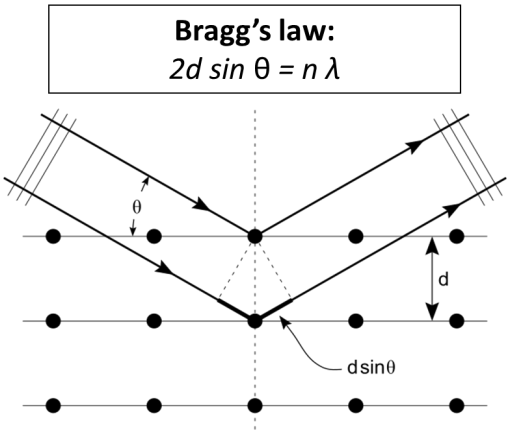

Figure 8. Illustration of Bragg's law which determines that there is a constructive interference (refraction peak) when $2d \sin \theta = n \lambda$ (where d is the spacing between diffracting planes, θ is the incident angle, n is any whole number and λ is the wavelength of the incident beam).

In the case of the mesoporous silica materials, the arrangement of Si and O atoms in the silica phase is amorphous, and the characteristic peaks on the PXRD pattern due to the periodic arrangement of the pores appear at low angles since the distance between planes of pores is large (compared to atomic planes distances in other kind of materials like for example metallic particles). Therefore, PXRD gives information about the arrangement of the pores in the mesoporous material. This technique is especially useful to verify the integrity of mesoporous scaffold after the modification steps that can potentially damage the structure. For instance, the diffractogram of mesoporous nanoparticles with an MCM-41 structure (Figure 9) shows a main characteristic peak at around 2.4° that is indexed

as the (100) Bragg peak, and three other secondary peaks are higher angles indexed as the (100), (200) and (210) Bragg peaks.

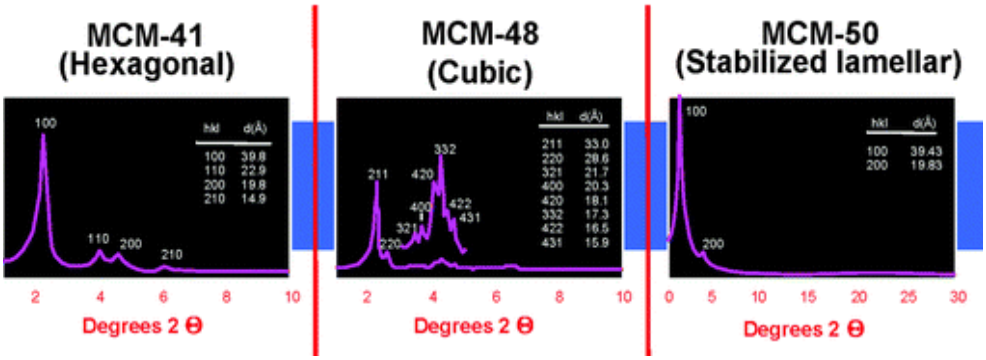

Figure 9. Characteristic PXRD patterns of the M41S family of mesoporous silica materials. *Adapted from Chem. Soc. Rev. 2013, 42, 3663. Copyright © 2013 The Royal Society of Chemistry.*

Transmission electron microscopy (TEM) allows to visualize the size and morphology of the materials with high resolution. Using TEM, the presence of pores on the material and their periodicity can be usually discerned. An example of MCM-41 mesoporous silica material is shown in figure 10. In addition, **scanning electron microscopy** (SEM) can also be used to study the particle size and morphology. Whereas TEM produces images by detecting primary electrons transmitted through the sample, SEM produces images by detecting secondary electrons which are emitted from the material surface due to excitation by the incident electron beam. Scanning Transmission Electron Microscopy coupled with energy dispersive X-ray spectroscopy (**STEM-EDX**) is used in some cases to map the presence of certain elements in the material. STEM-EDX is based on the fact that under excitation with a high-energy beam, a certain element will emit X-ray at specific wavelengths due to the excitation-relaxation of its electrons.

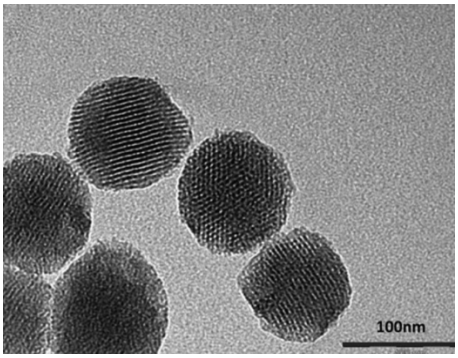

Figure 10. TEM images of MCM-41 nanoparticles.

Dynamic Light Scattering (DLS) is based on measuring the fluctuation in scattered light due to the Brownian motion of the particles in solution while it is irradiated with a laser beam. The particles move faster the smaller they are and thus the fluctuations can be related with the size of the particles. It serves for estimating the hydrodynamic diameter of the particles which is usually higher than the diameter determined by TEM. The zeta potential (charge on the surface of the material) of the nanoparticles can be also determined with DLS, by using a special cuvette with two electrodes.

Nitrogen adsorption-desorption isotherms is a fundamental technique in the characterization of mesoporous materials. It provides information about properties like specific surface area, specific pore volume, and pore size. These isotherms are plots of quantity of nitrogen adsorbed per gram of material as a function of the relative pressure. When the mesoporous scaffold has empty pores the quantity of nitrogen adsorbed is high due to its adsorption inside the pore channels. On the contrary, when the pores are filled with a cargo or have not been properly formed, the quantity of adsorbed nitrogen is significantly lower. Furthermore, there is a correlation between the shape of the isotherm plot (that can be grouped into 6 types) and the structure of the material (porous materials have isotherms of type IV and V).[100] The absence of hysteresis loops indicates the homogeneity of the pore network. Typically, the specific surface area of mesoporous materials is determined by applying the

Brunauer-Emmet-Teller (BET) method on the adsorption branch of the isotherm.[101] The pore size and specific pore volumes are calculated by applying the Barret-Joyner-Halenda (BJH) model also in the adsorption branch of the isotherm.[102]

Thermogravimetric analysis (TGA) register the loss in weight of the material as a function of the temperature so the overall percentage of organic matter can be calculated.

Elemental analysis (EA) is performed (using a special analyzer) by combustion of a small amount of sample (1-2 mg) and gives information about the percentage in weight of carbon, hydrogen, nitrogen and sulfur. Thus, the results can be related with the amount of organic functional molecules.

Fourier-transform infrared spectroscopy (FT-IR) shows specific IR absorption peaks of organic groups that are sometimes useful to discern the presence or absence of some functional group. The usefulness of this technique relies on the amount of functionalization, the groups and the absence of overlapping signals.

UV-visible spectrophotometry and **fluorescence** can be used, for several purposes, such as for monitoring the release of a fluorescent or colored cargo from the nanoparticles, checking nanoparticle fluorescence due to the incorporation of a certain fluorogenic chromophore, for conducting enzymatic assays, quantifying the amount of encapsulated cargo, and so on.

1.4 Stimuli-responsive gated materials. Advanced applications*

Obtaining hybrid materials able to respond to specific stimulus is a growing trend in fundamental and applied research. Specially, advanced systems made from porous materials functionalized with (bio)molecular gates, able to respond to a predefined stimulus, then allowing the movement of chemical or biochemical species from voids of porous supports to a solution, and vice versa are appealing.[103,104] Following this concept, several research groups are working in the development of new nanodevices in which the delivery of a certain cargo stored in a container can be triggered by applying selected external stimulus. Such gated materials are composed mainly of two subunits: i) a porous inorganic support in which a cargo is loaded and ii) certain molecular or supramolecular entities (the so-called molecular gates), generally grafted onto the external surface, which controls mass transport from the pores to the solution in response to specific stimulus (see Figure 11).

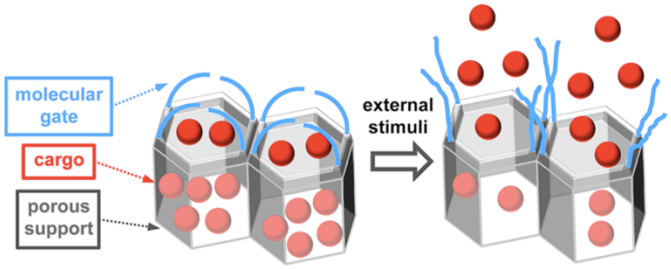

Figure 11. Schematic representation of a gated material for on-command controlled release. *Adapted from Chem. Rev. 2016, 116, 561. Copyright © 2016 American Chemical Society*.

**Text fragments and figures are reproduced with permission of "Aznar, E.; Oroval, M.; Pascual, L.; Murguía, J. R.; Martínez-Máñez, R.; Sancenón, F. Gated Materials for On-Command Release of Guest Molecules. Chem. Rev., 2016, 116, 561." Copyright © 2016 American Chemical Society.*

The first example of a molecular gate was reported by Fujiwara and coworkers in 2003.[105] From then on, multidisciplinary researchers have reported a variety of gated materials that respond to different stimuli such as light, temperature, magnetic fields, redox species, ions and biomolecules.[106a] Sensing/recognition as well as biomedical research has found a promising tool in gated-materials for on-command release.[107,108] Among the different inorganic supports, mesoporous silica nanoparticles (MSNs) as well as mesoporous silica microparticles predominate in the research for sensing and biomedical applications.[109] In addition, some groups have found other useful supports, for instance, core-shell nanoparticles with different cores (such as gold, magnetite (Fe_2O_3), platinum and upconversion particles) surrounded by a mesoporous silica shell,[110] anodic alumina[111] and bioactive glasses.[112]

Gating mechanisms are diverse and can rely on the rupture/formation of covalent bonds, electrostatic/supramolecular interactions, changes in the physical properties of molecules or macromolecules and so on. The possible gatekeepers in this respect are unlimited: polymers, supramolecular ensembles, inorganic nanoparticles, (bio)macromolecules, etc. A great number of works and reviews about responsive gated materials have been published in recent years, which gives a hint about the potential and possibilities of these technologies.[93,106,113] Below some relevant examples of gated materials are shown. These examples are classified according to their triggering stimuli. Enzyme-responsive systems for drug delivery applications will also be described, as this is one of the topics used in this PhD thesis.

1.4.1. Light responsive systems

Light is a powerful tool for controlling open/closed protocols in mesoporous systems. Reported examples that used light as trigger take advantage of (i) photodimerizations, cis−trans photoconversions; (ii) photocleavage of chemical bonds directly or assisted by photosensitizers; or (iii) photoinduced heating of gold nanoparticles (AuNPs). In light-driven

gated systems, cargo release can, in principle, be controlled spatially and temporally by fine-tuning the area and time of the light stimulus. Moreover, light has the advantage of being applicable from outside of the patient in a noninvasive manner, and it is easily focalisable in selected areas, avoiding irradiation of the surrounding tissue. However, UV light is unable to penetrate in deep tissues. Concerned by this fact, in the last years the attention has been centered in using the more tissue-penetrating NIR irradiation as a light source thanks to the use of metal clusters or two-photon active molecules. However, most of the work in this field still is in an incipient development. In addition, researchers have not always reported the light power supply used in their work, which difficult the reproduction of the gating mechanism performance.

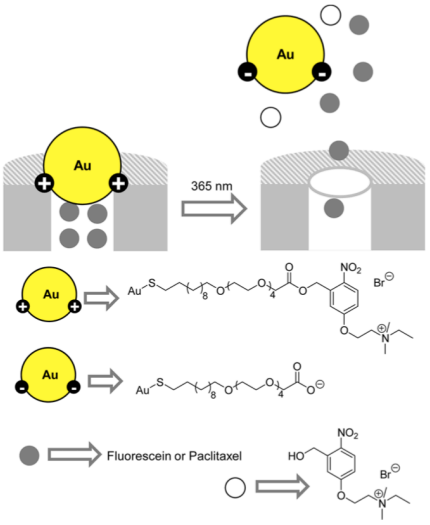

Figure 12. MSNs loaded with fluorescein and capped with the AuNPs that contained photocleavable o-nitrobenzyl moieties. Fluorescein was released upon irradiation at 365 nm.

Lin and co-workers prepared the first photolabile gated system with gold nanoparticles with average diameter of 5 nm, which contained the photoresponsive molecule thioundecyl-tetra-ethylene glycolester-o-nitrobenzylethyldimethylammonium bromide. Positively charged nanoparticles were able to interact with the negative silanol groups of

MSNs capping pores. The system was loaded with fluorescein.[114] The authors demonstrated that the system was capped in water, yet cargo delivery was observed upon photoirradiation with a 365 nm low-power (0.49 mW/cm^2) UV lamp for 10 min (see Figure 12). This was attributed to the photocleavage of the photolabile linker, which resulted in the formation of negatively charged thioundecyl-tetraethylene glycol-carboxylate-functionalized AuNPs that detached from the silica due to charge repulsion. To validate the feasibility of the system for intracellular drug delivery, a similar capped system was loaded with hydrophobic anticancer drug paclitaxel, and the system was tested in human liver and fibroblast cells. The material was efficiently endocytosed, as determined by flow cytometry. After a 10 min UV irradiation, cell viability significantly decreased in both cell lines. No toxicity of the nanomaterial without paclitaxel was detected before and after UV irradiation.

1.4.2. Temperature responsive systems

Several examples of gated materials, which are uncapped using temperature, have been described. Most of these capped materials used thermosensitive polymers that were able to deliver cargo after a temperature-dependent phase transition. Some other interesting examples, but less explored, involve melting double-stranded DNA sequences or also melting other organic coatings, such as paraffins. Temperature, as exogenous stimulus, has the advantage of a fine external control for tunable dose delivery. Furthermore, changes in temperature or the existence of different temperatures are a fingerprint in some diseases such as inflammation, infection, or even tumoral tissues, which can be used to specifically deliver selected cargos. However, the registered increase in temperature in such cases is no more than 4 or 5 °C, which needs highly sensitive systems working on a very narrow range of temperatures. The inability to respond in the window between 35 and 45 °C gives rise to systems not applicable in the biomedical field, while temperatures beyond 45 °C must be carefully used to avoid undesired cellular death.

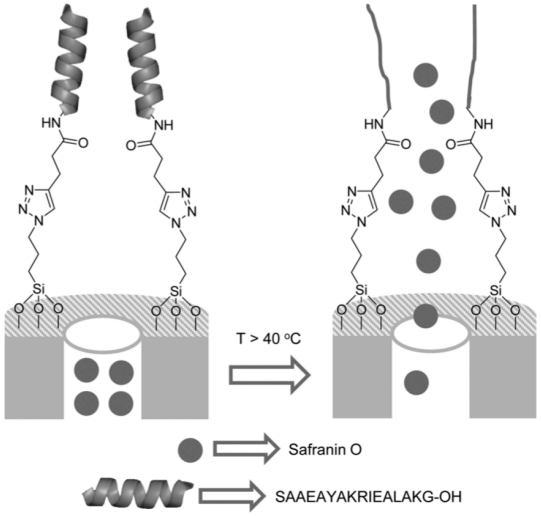

Figure 13. MSNs loaded with safranin O and capped with a peptide that adopted a bulky α-helical conformation at room temperature**.**

Martínez-Máñez et al.[115] reported a thermoresponsive material that was capped with a peptide. The concept was based on the use of the well-known temperature-controlled α-helix-to-disordered transformation, which occurs in certain peptides. The authors used a self-aggregating 17-mer peptide (H-SAAEAYAK-RIAEALAKG-OH, P), designed to adopt a high level of α-helical conformation, to cap the pores of MSNs. MSNs were loaded with safranin O and the external surface was functionalized with 3-(azidopropyl)triethoxisylane moieties. Finally, the corresponding 4-pentynoic-P derivative was grafted onto the surface through a “click” chemistry reaction as presented in Figure 13. Delivery studies in phosphate buffer, pH 7, and at different temperatures were carried out. At room temperature, organization of the peptide in α-helical bundles inhibited cargo release, while the transformation to a disordered conformation at a high temperature reduced the steric crowding around the pore outlets that allowed cargo release.

1.4.3. Magnetically and ultrasound responsive systems

Magnetic fields and ultrasound are also physical stimuli used for opening up molecular gates with the subsequent controlled delivery of an entrapped cargo. Both techniques allow a pulsatile delivery of the cargo, are noninvasive, can penetrate depth in tissues, and can be carefully controlled by changing frequency, power, cycles, and time of application. Magnetically triggered systems have the advantage of having an extra control and possibility of guidance of the gated support, for example, to accumulate in a selected tumor area (for biomedical purposes, where also tracking by MRI is possible) or even in industrial applications where separation and recovery of the gated particles could be of crucial interest. Regarding ultrasound, this technique offers the application of a stimulus without concern of residual radiation; however, their possible genotoxic effect even at moderate doses is today under study. Several examples of capped materials that were opened upon application of these stimuli have been described.

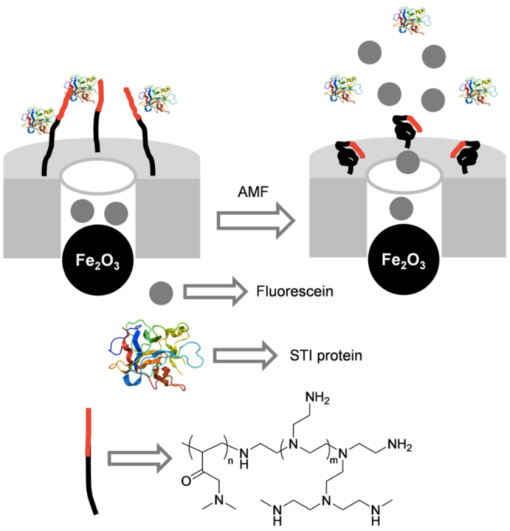

Figure 14. Superparamagnetic iron oxide nanocrystals coated with a mesoporous silica shell capped with the poly-NIPAM-block-PEI thermoresponsive copolymer.

Vallet and co-workers developed a magnetically triggered system capable of releasing small molecules from the pore voids of mesoporous silica and the proteins housed in a capping poly-NIPAM-block-PEI thermoresponsive copolymer at the same time.[116] For this purpose, the authors incorporated superparamagnetic iron oxide nanocrystals into a mesoporous silica matrix. Nanoparticles were functionalized with (trimethoxysilyl)propyl methacrylate, and poly-NIPAM-block-PEI polymer was grafted around the nanoparticles by radical polymerization. The pores of the silica support were loaded with fluorescein, and soybean trypsin inhibitor type II−S (STI) was incorporated into the copolymer shell (see Figure 14). The PNIPAM polymer exhibited a phase transition at a lower critical solution temperature (LCST) of approximately 32 °C in water. At temperatures around 30 °C, the copolymer was hydrated and blocked the release of both fluorescein and soybean trypsin inhibitor type II−S. At temperatures above LCST (around 40 °C), fluorescein and the protein were effectively released. Moreover, when the gated solid was exposed to an alternating magnetic field (AMF) of 24 kA m^{-1} and 100 kHz for 6 h, both the protein and fluorescein were delivered.

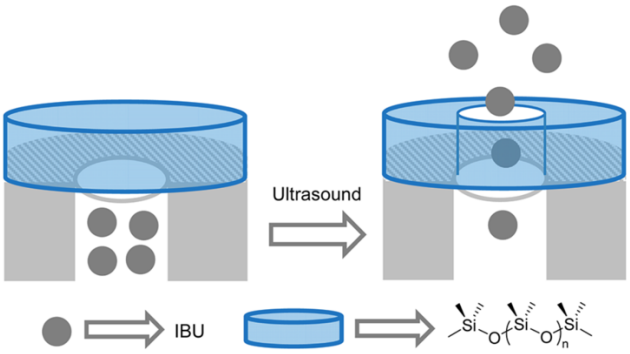

Figure 15. MSNs coated with a poly(dimethylsiloxane) thin film capable of IBU delivery upon ultrasound application.

Honma and co-workers developed a controlled delivery system using MSNs embedded in a poly(dimethylsiloxane) thin film, which was

responsive to ultrasound stimuli.[117] MSNs were loaded with ibuprofen (IBU) as model drug. Loaded MSNs were mixed with a poly(dimethylsiloxane) solution and dried to obtain a solid thin film that acts as cap (Figure 15). Kinetic experiments were performed by comparing the delivery behavior of the poly(dimethylsiloxane) loaded with IBU, either with or without MSNs. In the absence of ultrasound, films did not present significant cargo delivery, whereas both films exhibited drug delivery when irradiated with ultrasound. In the film with embedded MSNs, the amount of released drug was remarkably larger. The authors attributed this behavior to the generation of cavitations (formation, growth, and collapse of gas microbubbles) inside the polymeric matrix. Another remarkable achievement of the system was its pulsatile delivery capability.

1.4.4. Redox responsive systems

Since the birth of gated materials, the possibility of controlling mass transport aided by redox processes has been widely explored. This particular stimulus is appealing since endogenous reducing agents found at the intracellular level can be used as triggers. An increase in the concentration of such redox-active species has been reported for some diseases, such as cancer, and the wide bioapplicability of redox-responsive capped systems can be easily envisioned. Numerous examples have been described in this area, and they are summarized in two groups: (i) those based on redox-driven supramolecular interactions between macrocycles, such as cyclophanes, cyclodextrins, or cucurbiturils and wire-like moieties anchored to the surface of the porous support and (ii) those based on the rupture of disulfide bonds that bind material's surface and capping agents, such as biomolecules, inorganic nanoparticles, or polymers, to mesoporous material or that contribute to cap pores through the formation of disulfide-cross-linked layers. In this context, thiol-derivatized molecules and biomolecules can be easily prepared and used to obtain disulfide-linked gating mechanisms. In most cases, this fact simplifies the gated system because thiol-derivatized targeting ligands can adopt a double role (i.e., as redox-responsive gating ensemble and as selective targeting agent). Most

of the examples reported display a gating response in pure water, and some can be reoxidized to obtain reversible systems. Finally, some redox-responsive gated systems are frequently decorated with targeting ligands or agents to increase their suspensibility in biological environments. Some encouraging examples tested in *in vivo* models have demonstrated that gated materials loaded with cytotoxics can selectively reach a specific cell type and reduce the size of tumors and significantly decrease typical side effects.

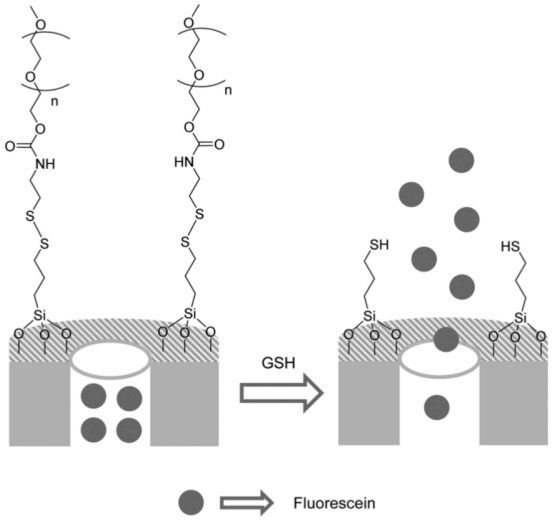

Figure 16. MSNs capped with PEG that contained a disulfide bond. Delivery was triggered by GSH.

Wang, Li, and co-workers developed MSNs functionalized on the outer surface with (3-mercaptopropyl)-triethoxysilane (MPTS) and loaded with fluorescein dye. PEG molecules were also anchored to the outer surface via a disulfide bond.[118] The PEG coating was obtained by adding PEG-SS-pyridine molecules to the thiol-functionalized MSNs, which resulted in an exchange reaction between the thiol end group on the outer surface of MSNs and the pyridyldisulfide groups at the end of the PEG-SS-pyridine molecules (Figure 16). Negligible dye release was observed in the absence of glutathione (GSH) over 20 h, whereas fluorescein achieved maximum delivery at 22 h in the presence of GSH. Cell uptake and cytotoxicity of

capped MSNs was investigated in MCF-7 cells. Confocal laser scanning microscopy demonstrated that the fluorescein-loaded capped material entered cells via endocytosis and that particles distributed mainly in the endosomal/lysosomal compartment. To test whether fluorescein was released from the cell-internalized nanomaterial by internal GSH content, MCF-7 cells were preincubated with 10 mM extracellular GSH. The intracellular fluorescein signal was significantly stronger under these conditions, which indicates that cargo release was due to intracellular GSH levels. Low cytotoxicity of the fluorescein-loaded capped material was observed in MCF-7 cells. Remarkably, the cytotoxicity of antineoplasic drug metothrexate in MCF-7 cells was clearly enhanced 2-fold when encapsulated in the nanomaterial and further increased after preincubation with 10 mM extracellular GSH.

1.4.5. pH responsive systems

pH is the most popular stimulus used to develop gated materials. In the reported examples, the open/close paradigm usually relies on changes in size/shape or attraction/repulsion interactions with other charged species due to proton addition or abstraction, the use of groups that can be hydrolyzed with pH or coatings that can be dissolved upon pH changes. Hence, researchers have used a wide variety of imaginative ensembles including amines, metallic complexes, macrocycles, different polymers, supramolecular ensembles such as layer-by-layer coatings, biomolecules as DNA, proteins, lipid bilayers, and even inorganic nanoparticles to control the release of selected cargos. pH-Driven gates are a promising tool to develop delivery systems for biomedicine. At the intracellular level, pH difference between the extracellular environment (pH 7) and endosomes and lysosomes (pH 5) is a useful tool to selectively release therapeutic agents directly in cells. Also, the acidic microenvironment found in many types of tumors, due to the production of lactic acid and hydrolysis of ATP, represents a pH difference between normal and tumor tissues that can be used for targeted delivery of payloads. pH-triggered systems offer the advantage of being totally autonomous, not requiring any extra equipment,

and in most cases, the closing and opening mechanism is reversible. Furthermore, pH-driven systems are not restricted to the biomedical field, and a number of applications may take advantage of a selective payload delivery when a change in pH takes place.

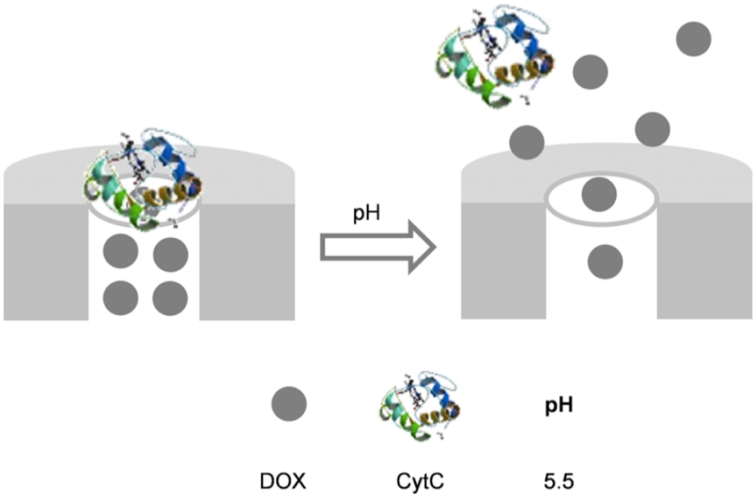

Figure 17. MSNs loaded with DOX and capped with CytC via electrostatic interactions. *Adapted from Chem. Rev. 2016, 116, 561. Copyright © 2016 American Chemical Society.*

Teng and co-workers [119] developed pH-responsive MSNs by using positively charged natural protein cytochrome C (CytC) as a pore blocker. CytC was attached to the silica surface by simple electrostatic interactions with the silanol groups. Pores were loaded with doxorubicin (DOX) (Figure 17). At pH 7.4, CytC prevented DOX release (16% in 72 h), whereas at an acidic pH (5.5), the zeta potential changes in MSNs induced the removal of CytC caps and allowed cargo release (54% in 72 h). Confocal laser scanning microscopy studies indicated that the DOX-loaded system was internalized by human breast cancer MCF-7 cells and that DOX was released from nanocarriers. Cytotoxicity and histological assays confirmed that the constructed CytC capped nanocarriers possessed lower toxicity than free DOX and unsealed drug carriers. Furthermore, the intratumoral administration of nanocarriers proved significantly more efficacious in tumor reduction than free DOX and unsealed drug carriers in xenograft MCF-7 cancer models.

1.4.6. Enzyme responsive systems

Mesoporous gated structures can also be tuned to respond to biomolecules such as enzymes. Enzymes are the catalysts of life and nature. Many chemical reactions in our bodies are triggered by enzymes. The role of enzymes is to accelerate or ease reactions required in the functioning of living organisms. They are involved in vital processes such as reactions needed to digest food, send nerve signals, contract muscles and many others.

Enzyme responsive systems presents high intrinsic specificity, which is an advantage to perform an accurate controlled release of the encapsulated cargo. This opens the possibility to design precise systems for very particular biomedical applications, as well as in sensing processes. For instance, the wide variety of enzymes present along the GIT, and their selective location (stomach, brush border, colon,) allows the design of very specific site release systems.

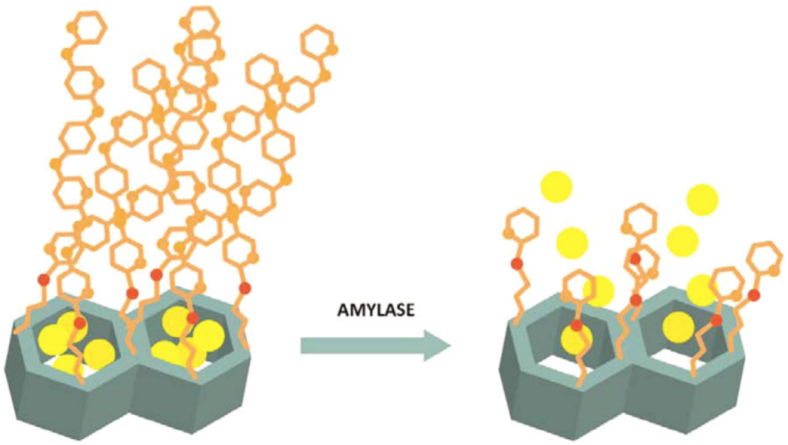

Figure 18. Schematic representation of an enzyme-driven molecular gate-like material functionalized with hydrolyzed starch. In the absence of pancreatin, starch derivatives (orange chains) hinder the release of the guest molecule (yellow spheres) from the porous support (gray container) by steric hindrance. In the presence of amylases, starch is hydrolyzed, which allows cargo delivery. *Reprinted with permission from J. Food Sci. 2015, 80 (11), E2511–E2512. Copyright © 2015 Institute of Food Technologists®.*

In line with this, Bernardos et al. functionalized the surface of a loaded MCM-41 support with 3 different commercially available hydrolyzed starches (Glucidex 47, 39, and 29) via the derivatization of starch with an alkoxysilane.[120] Cargo release was achieved by enzymatic hydrolysis in the presence of pancreatin (an enzyme cocktail that contains pancreatic amylase), which showed different release kinetics according to the degree of starch hydrolysis (Figure 18). The lower the hydrolysis rate of starch, the lower the delivery rate.[121]

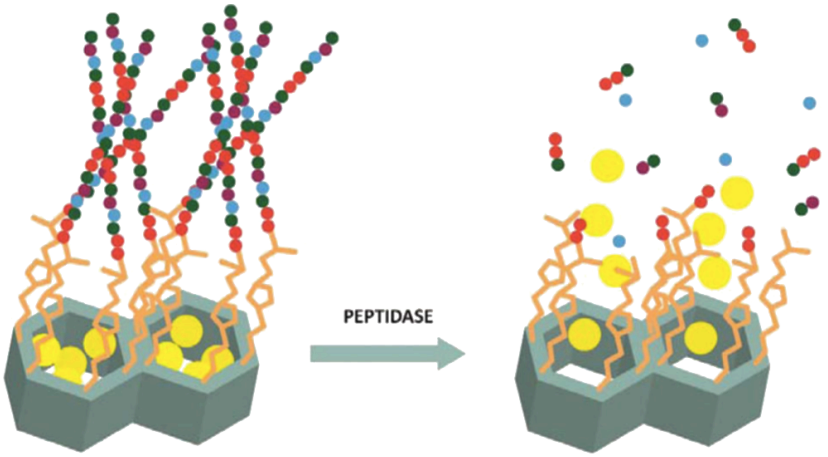

Figure 19. Schematic representation of an enzyme-driven molecular gate-like material capped with a peptide. In the absence of proteases, peptidic chains (dot chains) hinder the release of the guest molecules (yellow spheres) from the porous support (gray container) by steric hindrance. In the presence of peptidases, peptides are hydrolyzed and payload is delivered. *Reprinted with permission from J. Food Sci. 2015, 80 (11), E2511–E2512. Copyright © 2015 Institute of Food Technologists®.*

Bein and others prepared a gated that opened by the presence of protease.[122] The capping protocol consisted of attaching avidin to biotinylated mesoporous silica particles (MSPs). The addition of protease trypsin induced the hydrolysis of the attached avidin and cargo release. Along the same lines, Coll and others (2011) employed a click chemistry reaction to functionalize the external surface of MSPs with a peptide to develop a nanodevice capable of hampering cargo release. Delivery was observed in the presence of proteases (Figure 19).[123]

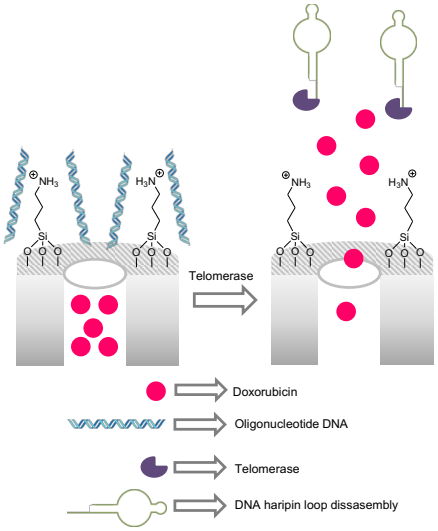

Figure 20. MSNs loaded with DOX and capped, through electrostatic interactions, with a DNA oligonucleotide containing the telomeric repeat complementary sequence and telomerase substrate [5'-(CCCTAA)nAATCCGTCGAGC AGAGTT-3']. Cargo release is observed in the presence of telomerase.

Srivastava and co-workers described a DNA wrapped MSNs loaded with DOX to target telomerase positive human and murine cancer cells.[124] Telomerase is a ribonucleoprotein involved in the protection and elongation of telomeres. The telomeres are a region of repetitive nucleotide sequences that protects the end of the chromosome and regulate the cell aging. In normal conditions, telomeres get shorter and telomerase enzyme is at very low levels in cells. In contrast, in cancer cells telomerase is overexpressed (Figure 20). The authors loaded MSNs with DOX, the silica surface functionalized with amino groups, and the oligonucleotide containing the telomeric repeat complementary sequences and telomerase substrate was electrostatically conjugated to the MSNs surface. The authors confirmed the telomerase dependent release disposing suspension of nanoparticles under different telomerase concentrations. A negligible cargo release was registered in the presence of buffer alone, whereas in the presence of telomerase a remarkable DOX delivery was observed. The telomerase recognized the substrate sequence and elongated the oligonucleotide cap.

This resulted in a change in the DNA conformation to hairpin loop conformation and the disassembly of the molecular gate. The anti-tumoral activity of the nanoparticles was studied in positive telomerase cells lines (DL, MCF-7 and K-562 cancer cells) and negative cells lines (U-2-OS) as a control. The system showed a significant targeting and thus a high cytotoxic effect in positive cancer cell lines. Finally, the prepared nanodevice was studied in a murine lymphoma model established in a DL tumor-bearing mouse by intraperitoneal administration of free DOX or nanoparticles respectively. The results demonstrated an enhanced effect in the tumor suppression and animals survival and recovery with the nanoparticles.

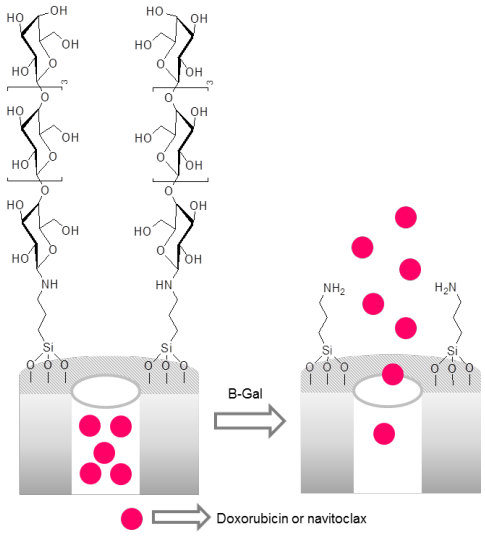

Figure 21. MSNs loaded with DOX or navitoclax and capped with a galacto-hexasaccharide. Cargo delivery is triggered in the presence of ß-galactosidase.

Serrano, Martínez-Máñez and co-workers designed a β-galactosidase responsive drug delivery system to target senescent cells.[125] MSNs were loaded with DOX and navitoclax drugs and the external surface was functionalized with amino groups which were reacted with a galacto-hexasaccharide (galactan) yielded the final materials. Galactan-capped nanoparticles were designed to be uncapped in senescent cells due to the overexpression of β-galactosidase enzyme that induced the hydrolysis of

the galacto-hexasaccharide cap (Figure 21). The authors studied the uncapping mechanism of the capped nanoparticles in the absence or presence of β-galactosidase from Aspergillus oryzae in water suspensions at pH 4.5. In the absence of the enzyme a negligible release of the drugs was observed, whereas in the presence of β-galactosidase a remarkable cargo delivery was found. The different synthetized nanoparticles were tested *in vitro* and *in vivo* in senescent models. Doxorubicin-loaded or navitoclax-loaded nanoparticles administered by tail vein injection to a SK-MEL-103 melanoma tumor-bearing nude mice model of chemotherapy-induced senescence, showed that galactan-functionalized nanodevice reached senescent cells in tumor and improving the inhibition of tumor growth. Moreover, a bleomycin-induced pulmonary fibrosis mouse model in C57BL/6 male mice was used and treated intravenously with the galactan-functionalized nanoparticles loaded with DOX. The solid targeted senescent cells in lungs and had the ability to restore pulmonary functions. In both cases, the galactan-functionalized nanoparticles reduced side effects of the free drugs.

1.5 References

1. Shah, N.K.; Rane, B.R.; Gujarathi, N.A. Developments in colon specific drug delivery systems—A review. Pharm. Sci. Monit. **2014**, 5, 95.
2. Singh, G.; Kumar, D.; Singh, M.; Sharma, D.; Kaur, S. Emerging techniques and challenges in colon drug delivery systems. J. Appl. Pharm. Sci. **2012**, 2, 139.
3. Malik K, Goswami L, Kothiyal P, Mukhopadhyay S. A Review on Colon Targeting Drug Delivery System: Novel Approaches, Anatomy and Evaluation. Pharma Innov. **2012**;1(9):12.
4. Lautenschläger, C.; Schmidt, C.; Fischer, D.; Stallmach, A. Drug Delivery Strategies in the Therapy of Inflammatory Bowel Disease. *Adv. Drug Deliv. Rev.* **2014**, *71*, 58–76.
5. Kaser, A.; Zeissig, S.; Blumberg, R. S. Inflammatory Bowel Disease. *Annu. Rev. Immunol.* **2010**, *28* (1), 573–621.
6. Xu, X.-M.; Zhang, H.-J. MiRNAs as New Molecular Insights into Inflammatory Bowel Disease: Crucial Regulators in Autoimmunity and Inflammation. *World J. Gastroenterol.* **2016**, *22* (7), 2206–2218.
7. Kim, D. H.; Cheon, J. H. Pathogenesis of Inflammatory Bowel Disease and Recent Advances in Biologic Therapies. Immune Netw **2017**, 17 (1), 25–40.
8. Neurath, M. F. Cytokines in Inflammatory Bowel Disease. Nat. Rev. Immunol. 2014, 14, 329.
9. Torres, J.; Mehandru, S.; Colombel, J.-F.; Peyrin-Biroulet, L. Crohn's Disease. *Lancet* **2017**, *389* (10080), 1741–1755.
10. Ungaro, R.; Mehandru, S.; Allen, P. B.; Peyrin-Biroulet, L.; Colombel, J.-F. Ulcerative Colitis. *Lancet* **2017**, *389* (10080), 1756–1770.
11. Leitner, G. C.; Vogelsang, H. Pharmacological- and Non-Pharmacological Therapeutic Approaches in Inflammatory Bowel Disease in Adults. *World J. Gastrointest. Pharmacol. Ther.* **2016**, *7* (1), 5–20.
12. Crohn, B. B. An Historic Note on Ulcerative Colitis. *Gastroenterology* **1962**, *42*, 366–367.
13. Crohn, B. B.; Ginzburg, L.; Oppenheimer, G. D. Regional Ileitis: A Pathologic and Clinical Entity. 1932. *Mt. Sinai J. Med.* **2000**, *67* (3), 263–268.
14. Ng, S. C.; Shi, H. Y.; Hamidi, N.; Underwood, F. E.; Tang, W.; Benchimol, E. I.; Panaccione, R.; Ghosh, S.; Wu, J. C. Y.; Chan, F. K. L.; et al. Worldwide Incidence and Prevalence of Inflammatory Bowel Disease in the 21st Century: A Systematic Review of Population-Based Studies. *Lancet* **2017**, *390* (10114), 2769–2778.
15. Meenan, J.; Grool, T. A.; Hommes, D. W.; Dijkhuizen, S.; ten Kate, F. J.; Wood, M.; Whittaker, M.; Tytgat, G. N.; van Deventer, S. J. Lexipafant (BB-882), a Platelet Activating Factor Receptor Antagonist, Ameliorates Mucosal Inflammation in an Animal Model of Colitis. *Eur. J. Gastroenterol. Hepatol.* **1996**.
16. Torres, M. I.; Ríos, A. Current View of the Immunopathogenesis in Inflammatory Bowel Disease and Its Implications for Therapy. *World Journal of Gastroenterology*. **2008**
17. Hardy, J. G.; Davis, S. S.; Wilson, C. G. *Drug Delivery to the Gastrointestinal Tract*; **1989**.
18. Jay, M.; Beihn, R. M.; Digenis, G. A.; Deland, F. H.; Caldwell, L.; Mlodozeniec, A. R. Disposition of Radiolabelled Suppositories in Humans. *J. Pharm. Pharmacol.* **1985**, *37* (4), 266–268.

19. Newton, A. M. J.; Lakshmanan, P. Effect of HPMC - E15 LV Premium Polymer on Release Profile and Compression Characteristics of Chitosan/ Pectin Colon Targeted Mesalamine Matrix Tablets and in Vitro Study on Effect of PH Impact on the Drug Release Profile. *Recent Pat. Drug Deliv. Formul.* **2014**, *8* (1), 46–62.
20. DeFilippis, E. M.; Longman, R.; Harbus, M.; Dannenberg, K.; Scherl, E. J. Crohn's Disease: Evolution, Epigenetics, and the Emerging Role of Microbiome-Targeted Therapies. *Curr. Gastroenterol. Rep.* **2016**, *18* (3), 13.
21. Neurath, M. F.; Travis, S. P. L. Mucosal Healing in Inflammatory Bowel Diseases: A Systematic Review. *Gut* **2012**, *61* (11), 1619–1635.
22. Hua, S.; Marks, E.; Schneider, J. J.; Keely, S. Advances in Oral Nano-Delivery Systems for Colon Targeted Drug Delivery in Inflammatory Bowel Disease: Selective Targeting to Diseased versus Healthy Tissue. *Nanomedicine* **2015**, *11* (5), 1117–1132.
23. Hu, Z.; Mawatari, S.; Shibata, N.; Takada, K.; Yoshikawa, H.; Arakawa, A.; Yosida, Y. Application of a Biomagnetic Measurement System (BMS) to the Evaluation of Gastrointestinal Transit of Intestinal Pressure-Controlled Colon Delivery Capsules (PCDCs) in Human Subjects. *Pharm. Res.* **2000**, *17* (2), 160–167.
24. Rana, S. V; Sharma, S.; Malik, A.; Kaur, J.; Prasad, K. K.; Sinha, S. K.; Singh, K. Small Intestinal Bacterial Overgrowth and Orocecal Transit Time in Patients of Inflammatory Bowel Disease. *Dig. Dis. Sci.* **2013**, *58* (9), 2594–2598.
25. Challa, T.; Vynala, V.; Allam, K. V. Colon Specific Drug Delivery Systems: A Review on Primary and Novel Approaches. *Int. J. Pharm. Sci. Rev. Res.* **2011**, *7*, 171–181.
26. Coupe, A. J.; Davis, S. S.; Wilding, I. R. Variation in Gastrointestinal Transit of Pharmaceutical Dosage Forms in Healthy Subjects. *Pharm. Res.* **1991**, *8* (3), 360–364.
27. Rao, K. A.; Yazaki, E.; Evans, D. F.; Carbon, R. Objective Evaluation of Small Bowel and Colonic Transit Time Using PH Telemetry in Athletes with Gastrointestinal Symptoms. *Br. J. Sports Med.* **2004**, *38* (4), 482–487.
28. Podolsky, D. K. Inflammatory Bowel Disease. *N. Engl. J. Med.* **2002**, *347* (6), 417–429.
29. Hebden, J. M.; Blackshaw, P. E.; Perkins, A. C.; Wilson, C. G.; Spiller, R. C. Limited Exposure of the Healthy Distal Colon to Orally-Dosed Formulation Is Further Exaggerated in Active Left-Sided Ulcerative Colitis. *Aliment. Pharmacol. Ther.* **2000**, *14* (2), 155–161.
30. Fallingborg, J.; Christensen, L. A.; Jacobsen, B. A.; Rasmussen, S. N. Very Low Intraluminal Colonic PH in Patients with Active Ulcerative Colitis. *Dig. Dis. Sci.* **1993**, *38* (11), 1989–1993.
31. Bratten, J.; Jones, M. P. New Directions in the Assessment of Gastric Function: Clinical Applications of Physiologic Measurements. *Dig. Dis.* **2006**, *24* (3–4), 252–259.
32. Nugent, S. G.; Kumar, D.; Rampton, D. S.; Evans, D. F. Intestinal Luminal PH in Inflammatory Bowel Disease: Possible Determinants and Implications for Therapy with Aminosalicylates and Other Drugs. *Gut* **2001**, *48* (4), 571–577.
33. Sasaki, Y.; Hada, R.; Nakajima, H.; Fukuda, S.; Munakata, A. Improved Localizing Method of Radiopill in Measurement of Entire Gastrointestinal PH Profiles: Colonic Luminal PH in Normal Subjects and Patients with Crohn's Disease. *Am. J. Gastroenterol.* **1997**, *92* (1), 114–118.
34. Collnot, E.-M.; Ali, H.; Lehr, C.-M. Nano- and Microparticulate Drug Carriers for Targeting of the Inflamed Intestinal Mucosa. *J. Control. Release* **2012**, *161* (2), 235–246.
35. Sinha, V. R.; Kumria, R. Colonic Drug Delivery: Prodrug Approach. *Pharm. Res.* **2001**, *18* (5), 557–564.
36. Gorbach, S. L. Intestinal Microflora. *Gastroenterology* **1971**, *60* (6), 1110–1129.

37. Simon, G. L.; Gorbach, S. L. The Human Intestinal Microflora. *Dig. Dis. Sci.* **1986**, *31* (9 Suppl), 147S–162S.
38. Moore, W. E. C.; Holdeman, L. V. Discussion of Current Bacteriological Investigations of the Relationships Between Intestinal Flora, Diet and Colon Cancer. *Cancer Res.* **1975**, *35* (11 Part 2).
39. Rubinstein, A. Microbially Controlled Drug Delivery to the Colon. *Biopharm. Drug Dispos.* **1990**, *11* (6), 465–475.
40. Scheline, R. R. Metabolism of Foreign Compounds by Gastrointestinal Microorganisms. *Pharmacol. Rev.* **1973**, *25* (4), 451–523.
41. Prasanth, V. V.; Jayaprakash, R.; Mathew, S. T. Colon Specific Drug Delivery Systems: A Review on Various Pharmaceutical Approaches. *Journal of Applied Pharmaceutical Science*. 2012, pp 163–169.
42. Chen, J.; Li, X.; Chen, L.; Xie, F. Starch Film-Coated Microparticles for Oral Colon-Specific Drug Delivery. *Carbohydr. Polym.* **2018**, *191*, 242–254.
43. Mrsny, R. J. The Colon as a Site for Drug Delivery. *J. Control. Release* **1992**, *22* (1), 15–34.
44. Sartor, R. B. Therapeutic Correction of Bacterial Dysbiosis Discovered by Molecular Techniques. *Proc. Natl. Acad. Sci. U. S. A.* **2008**, *105* (43), 16413–16414.
45. Liu, T.-C.; Stappenbeck, T. S. Genetics and Pathogenesis of Inflammatory Bowel Disease. *Annu. Rev. Pathol.* **2016**.
46. Patel, P. B.; Dhake, A. S. Multiparticulate Approach: An Emerging Trend in Colon Specific Drug Delivery for Chronotherapy. *J. Appl. Pharm. Sci.* **2011**, *1* (5), 59–63.
47. Xiao, B.; Merlin, D. Oral Colon-Specific Therapeutic Approaches toward Treatment of Inflammatory Bowel Disease. *Expert Opin. Drug Deliv.* **2012**, *9* (11), 1393–1407.
48. Lamprecht, A.; Yamamoto, H.; Takeuchi, H.; Kawashima, Y. Nanoparticles Enhance Therapeutic Efficiency by Selectively Increased Local Drug Dose in Experimental Colitis in Rats. *J. Pharmacol. Exp. Ther.* **2005**, *315* (1), 196–202.
49. Beloqui, A.; Coco, R.; Alhouayek, M.; Solinís, M. Á.; Rodríguez-Gascón, A.; Muccioli, G. G.; Préat, V. Budesonide-Loaded Nanostructured Lipid Carriers Reduce Inflammation in Murine DSS-Induced Colitis. *Int. J. Pharm.* **2013**, *454* (2), 775–783.
50. Desai, M. P.; Labhasetwar, V.; Amidon, G. L.; Levy, R. J. Gastrointestinal Uptake of Biodegradable Microparticles: Effect of Particle Size. *Pharm. Res.* **1996**, *13* (12), 1838–1845.
51. Schmidt, C.; Lautenschlaeger, C.; Collnot, E.-M.; Schumann, M.; Bojarski, C.; Schulzke, J.-D.; Lehr, C.-M.; Stallmach, A. Nano- and Microscaled Particles for Drug Targeting to Inflamed Intestinal Mucosa: A First in Vivo Study in Human Patients. *J. Control. Release* **2013**, *165* (2), 139–145.
52. Viscido, A.; Capannolo, A.; Latella, G.; Caprilli, R.; Frieri, G. Nanotechnology in the Treatment of Inflammatory Bowel Diseases. *J. Crohns. Colitis* **2014**, *8* (9), 903–918.
53. Date, A. A.; Hanes, J.; Ensign, L. M. Nanoparticles for Oral Delivery: Design, Evaluation and State-of-the-Art. *J. Control. Release* **2016**, *240*, 504–526.
54. Vass, P.; Démuth, B.; Hirsch, E.; Nagy, B.; Andersen, S. K.; Vigh, T.; Verreck, G.; Csontos, I.; Nagy, Z. K.; Marosi, G. Drying Technology Strategies for Colon-Targeted Oral Delivery of Biopharmaceuticals. *J. Control. Release* **2019**, *296*, 162–178.
55. Taghipour, Y. D.; Bahramsoltani, R.; Marques, A. M.; Naseri, R.; Rahimi, R.; Haratipour, P.; Panah, A. I.; Farzaei, M. H.; Abdollahi, M. A Systematic Review of Nano Formulation of Natural Products for the Treatment of Inflammatory Bowel Disease: Drug Delivery and Pharmacological Targets. *DARU J. Pharm. Sci.* **2018**, *26* (2), 229–239.

56. Zhang, M.; Merlin, D. Nanoparticle-Based Oral Drug Delivery Systems Targeting the Colon for Treatment of Ulcerative Colitis. *Inflamm. Bowel Dis.* **2018**, *24* (7), 1401–1415.
57. Naeem, M.; Bae, J.; Oshi, M. A.; Kim, M.-S.; Moon, H. R.; Lee, B. L.; Im, E.; Jung, Y.; Yoo, J.-W. Colon-Targeted Delivery of Cyclosporine A Using Dual-Functional Eudragit(®) FS30D/PLGA Nanoparticles Ameliorates Murine Experimental Colitis. *Int. J. Nanomedicine* **2018**, *13*, 1225–1240.
58. Oshi, M. A.; Naeem, M.; Bae, J.; Kim, J.; Lee, J.; Hasan, N.; Kim, W.; Im, E.; Jung, Y.; Yoo, J.-W. Colon-Targeted Dexamethasone Microcrystals with PH-Sensitive Chitosan/Alginate/Eudragit S Multilayers for the Treatment of Inflammatory Bowel Disease. *Carbohydr. Polym.* **2018**, *198*, 434–442.
59. Günter, E. A.; Popeyko, O. V. Calcium Pectinate Gel Beads Obtained from Callus Cultures Pectins as Promising Systems for Colon-Targeted Drug Delivery. *Carbohydr. Polym.* **2016**, *147*, 490–499.
60. Lee, Y.; Kim, J.; Kim, W.; Nam, J.; Jeong, S.; Lee, S.; Yoo, J.-W.; Kim, M.-S.; Jung, Y. Celecoxib Coupled to Dextran via a Glutamic Acid Linker Yields a Polymeric Prodrug Suitable for Colonic Delivery. *Drug Des. Devel. Ther.* **2015**, *9*, 4105–4113.
61. Qiao, H.; Fang, D.; Chen, J.; Sun, Y.; Kang, C.; Di, L.; Li, J.; Chen, Z.; Chen, J.; Gao, Y. Orally Delivered Polycurcumin Responsive to Bacterial Reduction for Targeted Therapy of Inflammatory Bowel Disease. *Drug Deliv.* **2017**, *24* (1), 233–242.
62. Naeem, M.; Kim, W.; Cao, J.; Jung, Y.; Yoo, J.-W. Enzyme/PH Dual Sensitive Polymeric Nanoparticles for Targeted Drug Delivery to the Inflamed Colon. *Colloids Surfaces B Biointerfaces* **2014**, *123*, 271–278.
63. Rafii, F.; Franklin, W.; Cerniglia, C. E. Azoreductase Activity of Anaerobic Bacteria Isolated from Human Intestinal Microflora. *Appl. Environ. Microbiol.* **1990**, *56* (7), 2146–2151.
64. Amidon, S.; Brown, J. E.; Dave, V. S. Colon-Targeted Oral Drug Delivery Systems: Design Trends and Approaches. *AAPS PharmSciTech* **2015**, *16* (4), 731–741.
65. Dagli, Ü.; Balk, M.; Yücel, D.; Ülker, A.; Över, H.; Saydam, G.; Şahin, B. The Role of Reactive Oxygen Metabolites in Ulcerative Colitis. *Inflamm. Bowel Dis.* **1997**, *3* (4), 260–264.
66. Simmonds, N. J.; Rampton, D. S. Inflammatory Bowel Disease--a Radical View. *Gut* **1993**, *34* (7), 865 LP – 868.
67. Grisham, M. B. Oxidants and Free Radicals in Inflammatory Bowel Disease. *Lancet* **1994**, *344* (8926), 859–861.
68. Zhang, Q.; Tao, H.; Lin, Y.; Hu, Y.; An, H.; Zhang, D.; Feng, S.; Hu, H.; Wang, R.; Li, X.; et al. A Superoxide Dismutase/Catalase Mimetic Nanomedicine for Targeted Therapy of Inflammatory Bowel Disease. *Biomaterials* **2016**, *105*, 206–221.
69. Sedghi, S.; Fields, J. Z.; Klamut, M.; Urban, G.; Durkin, M.; Winship, D.; Fretland, D.; Olyaee, M.; Keshavarzian, A. Increased Production of Luminol Enhanced Chemiluminescence by the Inflamed Colonic Mucosa in Patients with Ulcerative Colitis. *Gut* **1993**, *34* (9), 1191 LP – 1197.
70. Simmonds, N. J.; Allen, R. E.; Stevens, T. R. J.; Niall, R.; Van Someren, M.; Blake, D. R.; Rampton, D. S. Chemiluminescence Assay of Mucosal Reactive Oxygen Metabolites in Inflammatory Bowel Disease. *Gastroenterology* **1992**, *103* (1), 186–196.
71. Babbs, C. F. Oxygen Radicals in Ulcerative Colitis. *Free Radic. Biol. Med.* **1992**, *13* (2), 169–181.
72. Hofseth, A. B.; Ying, L.; Kotakadi, V. S.; Cui, X.; Jin, Y.; Hofseth, L. J.; Wood, P. A.; Windust, A.; Matesic, L. E.; Chiuzan, C.; et al. American Ginseng Suppresses

Inflammation and DNA Damage Associated with Mouse Colitis. *Carcinogenesis* **2008**, *29* (12), 2351–2359.
73. Seguí, J.; Gironella, M.; Sans, M.; Granell, S.; Gil, F.; Gimeno, M.; Coronel, P.; Piqué, J. M.; Panés, J. Superoxide Dismutase Ameliorates TNBS-Induced Colitis by Reducing Oxidative Stress, Adhesion Molecule Expression, and Leukocyte Recruitment into the Inflamed Intestine. *J. Leukoc. Biol.* **2004**, *76* (3), 537–544.
74. Wilcox, C. S. Effects of Tempol and Redox-Cycling Nitroxides in Models of Oxidative Stress. *Pharmacol. Ther.* **2010**, *126* (2), 119–145.
75. Xiao, B.; Laroui, H.; Viennois, E.; Ayyadurai, S.; Charania, M. A.; Zhang, Y.; Zhang, Z.; Baker, M. T.; Zhang, B.; Gewirtz, A. T.; et al. Nanoparticles with Surface Antibody against CD98 and Carrying CD98 Small Interfering RNA Reduce Colitis in Mice. *Gastroenterology* **2014**, *146* (5), 1289-300.e3019.
76. Hankard, F.; Cezard; Aigrain; Navarro; Peuchmaur. CD44 Variant Expression in Inflammatory Colonic Mucosa Is Not Disease Specific but Associated with Increased Crypt Cell Proliferation. *Histopathology* **1998**, *32* (4), 317–321.
77. Farkas, S.; Hornung, M.; Sattler, C.; Anthuber, M.; Gunthert, U.; Herfarth, H.; Schlitt, H. J.; Geissler, E. K.; Wittig, B. M. Short-Term Treatment with Anti-CD44v7 Antibody, but Not CD44v4, Restores the Gut Mucosa in Established Chronic Dextran Sulphate Sodium (DSS)-Induced Colitis in Mice. *Clin. Exp. Immunol.* **2005**, *142* (2), 260–267.
78. Xiao, B.; Zhang, Z.; Viennois, E.; Kang, Y.; Zhang, M.; Han, M. K.; Chen, J.; Merlin, D. Combination Therapy for Ulcerative Colitis: Orally Targeted Nanoparticles Prevent Mucosal Damage and Relieve Inflammation. *Theranostics* **2016**.
79. Naeem, M.; Choi, M.; Cao, J.; Lee, Y.; Ikram, M.; Yoon, S.; Lee, J.; Moon, H. R.; Kim, M. S.; Jung, Y.; et al. Colon-Targeted Delivery of Budesonide Using Dual PH- and Time-Dependent Polymeric Nanoparticles for Colitis Therapy. *Drug Des. Devel. Ther.* **2015**.
80. Cesar, A. L. A.; Abrantes, F. A.; Farah, L.; Castilho, R. O.; Cardoso, V.; Fernandes, S. O.; Araújo, I. D.; Faraco, A. A. G. New Mesalamine Polymeric Conjugate for Controlled Release: Preparation, Characterization and Biodistribution Study. *Eur. J. Pharm. Sci.* **2018**, *111*, 57–64.
81. IUPAC, Pure appl. Chem. **1972**, 31, 578.
82. X. S. Zhao, J. Mater. Chem. **2006**, 16, 623-625.
83. C. Perego, R. Millini, Chem. Soc. Rev. **2013**, 42, 3956-3976.
84. K. M. Thomas, Catal. Today, **2007**, 120, 389-398.
85. X. Liu, Y. Du, Z. Guo, S. Gunasekaran, C.-B. Ching, Y. Chen, S. S. J. Leong, Y. Yang, Micropor. Mesopor. Mater. **2009**, 122, 114-120.
86. C. Ispas, I. Sokolov, S. Andreescu, Anal. Bioanal. Chem. **2009**, 393, 543-554.
87. M. Vallet-Regi, M. Colilla, I. J. Izquierdo-Barba, J. Biomed. Nanotechnol. **2008**, 4, 1-15.
88. D. J. Wales, J. Grand, V. P. Ting, R. D. Burke, K. J. Edler, C. R. Bowen, S. Mintova, A. D. Burrows, *Chem. Soc. Rev.* **2015**, *44*, 4290–4321.
89. I. I. Slowing, B. G. Trewyn, S. Giri, V. S.-Y. Lin, Adv. Funct. Mater. **2007**,17, 1225-1236.
90. J. S. Beck, J. C. Vartuli, W. J. Roth, M. E. Leonowicz, C. T. Kresge, K. D. Schmitt, C. T. W. Chu, D.H. Olson, E. W. Sheppard, S. B. McCullen, J. B. Higgins, J. L. Schlenker, J. Am. Chem. Soc. **1992**, 114, 10834-10843.
91. C. T. Kresge, W. J. Roth, Chem. Soc. Rev. **2013**, 42, 3663-3670.
92. D. Zhao, J. Feng, Q. Huo, N. Melosh, G. H. Fredrickson, B. F. Chmelka, G. D. Stucky, Science **1998**, 279, 548-552.

93. [93] J. G. Croissant, Y. Fatieiev, A. Almalik, N. M. Khashab, Adv. Healthcare Mater. **2018**, 7, 1700831.
94. M. C. Llinàs, D. Sánchez-García, Afinidad LXXI 2014, 565, 20-31.
95. F. Hoffmann, M. Cornelius, J. Morell, M. Fröba, Angew. Chem. Int. Ed. **2006**, 45, 3216-3251.
96. A. Stein, B. J. Melde, R. C. Schroden, *Adv. Mater.* **2000**, *12*, 1403–1419.
97. F. de Juan, E. Ruiz-Hitzky, *Adv. Mater.* **2000**, *12*, 430–432.
98. A. Stein, B. J. Melde, R. C. Schroden, *Adv. Mater.* **2000**, *12*, 1403–1419.
99. B. Hatton, K. Landskron, W. Whitnall, D. Perovic, G. A. Ozin, Acc. Chem. Res. **2005**, 38, 305-312.
100. K. S. W. Sing, D. H. Everett, R. A. W. Haul, L. Moscou, R. A. Pierotti, J. Rouquerol, T.Siemieniewska, Pure Appl. Chem. **1985**, 57 ,603-619.
101. S. Brunauer, P. H. Emmett, T. Teller, J. Am. Chem. Soc. **1938**, 60, 309-319.
102. E. P. Barrett, L. G. Joyner, P. P. Halenda, J. Am. Chem. Soc. **1951**, 73, 373-380.
103. Ariga, K.; Ishihara, S.; Labuta, J.; Hill, J. P. Supramolecular Approaches to Nanotechnology: Switching Properties and Dynamic Functions. *Curr. Org. Chem.* **2011**, 15, 3719−3733.
104. Descalzo,A.B.; Martínez-Mañez,R.; Sancenoń,F.; Hoffmann,K.; Rurack, K. The Supramolecular Chemistry of Organic-Inorganic Hybrid Materials. *Angew. Chem., Int.* Ed. **2006**, 45, 5924−5948.
105. a) N. K. Mal, M. Fujiwara, Y. Tanaka, *Nature* **2003**, *421*, 350-353; b) N. K. Mal, M. Fujiwara, Y. Tanaka, T. Taguchi, M. Matsukata, *Chem. Mater.* **2003**, *15*, 3385-3394.
106. a) E. Aznar, M. Oroval, L. Pascual, J. R. Murguía, R. Martínez-Máñez, F. Sancenón, *Chem. Rev.* **2016**, *116*, 561-718; b) C. Coll, A. Bernardos, R. Martínez-Máñez, F. Sancenón, *Acc. Chem. Res.* **2013**, *46*, 339-349.
107. F. Sancenón, L. Pascual, M. Oroval, E. Aznar, R. Martínez-Máñez, *ChemistryOpen* **2015**, *4*, 418-437.
108. a) Z. Li, J. C. Barnes, A. Bosoy, J. F. Stoddart, J. I. Zink, *Chem. Soc. Rev.* **2012**, *41*, 2590-2605; b) Y. Wang, Q. Zhao, N. Han, L. Bai, J. Li, J. Liu, E. Che, L. Hu, Q. Zhang, T. Jiang, S. Wang, *Nanomedicine* **2015**, *11*, 313-327; c) R. R. Castillo, M. Colilla, M. Vallet-Regí, *Expert. Opin. Drug Deliv.* **2017**, *14*, 229-243.
109. a) A. Bernardos, A. Aznar, C. Coll, R. Martínez-Máñez, J. M. Barat, M. D. Marcos, F. Sancenón, A. Benito, J. Soto, *J. Control. Release* **2008**, *131,* 181-189; b) *E*. Aznar, M. Dolores Marcos, R. Martínez-Máñez, F. Sancenón, J. Soto, P. Amorós, C. Guillem, *J. Am. Chem. Soc.* **2009**, *131*, 6833-6843.
110. a) S. F. Lee, X. M. Zhu, Y. X. J. Wang, S. H. Xuan, Q. H. You, W. H. Chan, C. H. Wong, F. Wang, J. C. Yu, C. H. Cheng, K. C. Leung, *ACS Appl. Mater. Interfaces* **2013**, *5*, 1566-1574; b) W.-P. Li, P.-Y. Liao, C.-H. Su, C.-S. Yeh, *J. Am. Chem. Soc.* **2014**, *136*, 10062-10075; c) Z. F. Wang, X. Yang, J. Feng, Y. J. Tang, Y. Y. Jiang, N. Y. He, *Analyst* **2014**, *139*, 6088-6091; d) M. L. Yin, E. G. Ju, Z. W. Chen, Z. H. Li, J. S. Ren, X. G. Qu, *Chem. Eur. J.* **2014**, *20*, 14012-14017.
111. a) A. Ribes, E. Xifré-Pérez, E. Aznar, F. Sancenón, T. Pardo, L. F. Marsal, R. Martínez-Máñez, *Sci. Rep.* **2016**, *6*, 38649; b) L. Pla, E. Xifré-Pérez, A. Ribes, E. Aznar, M. D. Marcos, L. F. Marsal, R. Martínez-Máñez, F. Sancenón, *ChemPlusChem* **2017**, *82*, 337-341.
112. L. Polo, N. Gómez-Cerezo, E. Aznar, J.-L. Vivancos, F. Sancenón, D. Arcos, M. Vallet-Regí, R. Martínez-Máñez, *Acta Biomater.* **2017**, *50*, 114-126.

113. a) N. Song, Y.-W. Yang, *Chem. Soc. Rev.* **2015**, *44*, 3474-3504; b) J. Wen, K. Yang, F. Liu, Y. Xiu, S. Sun, *Chem. Soc. Rev.* **2017**, *46*, 6024-6045; c) J. Zhu, Y. Niu, Y. Li, Y. Gong, H. Shi, Q. Huo, Y. Liu, Q. Xu, *J. Mater. Chem. B.* **2017**, *5*, 1339-1352.
114. Vivero-Escoto, J. L.; Slowing, I. I.; Wu, C. W.; Lin, V. S. Y. Photoinduced Intracellular Controlled Release Drug Delivery in Human Cells by Gold-Capped Mesoporous Silica Nanosphere. *J. Am. Chem. Soc.* **2009**.
115. De La Torre, C.; Agostini, A.; Mondragón, L.; Orzáez, M.; Sancenón, F.; Martínez-Máñez, R.; Marcos, M. D.; Amorós, P.; Pérez-Payá, E. Temperature-Controlled Release by Changes in the Secondary Structure of Peptides Anchored onto Mesoporous Silica Supports. *Chem. Commun.* **2014**.
116. Baeza, A.; Guisasola, E.; Ruiz-Hernandez, E.; Vallet-Regí, M. Magnetically Triggered Multidrug Release by Hybrid Mesoporous Silica Nanoparticles. Chem. Mater. **2012**, 24, 517−524.
117. Kim, H.-J.; Matsuda, H.; Zhou, H.; Honma, I. Ultrasound-Triggered Smart Drug Release from a Poly(Dimethylsiloxane)– Mesoporous Silica Composite. *Adv. Mater.* **2006**, *18* (23), 3083–3088.
118. Cui, Y.; Dong, H.; Cai, X.; Wang, D.; Li, Y. Mesoporous Silica Nanoparticles Capped with Disulfide-Linked PEG Gatekeepers for Glutathione-Mediated Controlled Release. *ACS Appl. Mater. Interfaces* **2012**.
119. Tang, Y.; Teng, Z.; Liu, Y.; Tian, Y.; Sun, J.; Wang, S.; Wang, C.; Wang, J.; Lu, G. Cytochrome C Capped Mesoporous Silica Nanocarriers for PH-Sensitive and Sustained Drug Release. *J. Mater. Chem. B* **2014**.
120. Bernardos, A.; Mondragón, L.; Aznar, E.; Marcos, M. D.; Martínez-Máñez, R.; Sancenón, F.; Soto, J.; Barat, J. M.; Pérez-Payá, E.; Guillem, C.; et al. Enzyme-Responsive Intracellular Controlled Release Using Nanometric Silica Mesoporous Supports Capped with "Saccharides." *ACS Nano* **2010**, *4* (11), 6353–6368.
121. Pérez-Esteve, É.; Ruiz-Rico, M.; Martínez-Máñez, R.; Barat, J. M. Mesoporous Silica-Based Supports for the Controlled and Targeted Release of Bioactive Molecules in the Gastrointestinal Tract. *J. Food Sci.* **2015**, *80* (11), E2504–E2516.
122. Schlossbauer, A.; Kecht, J.; Bein, T. Biotin–Avidin as a Protease-Responsive Cap System for Controlled Guest Release from Colloidal Mesoporous Silica. *Angew. Chemie Int. Ed.* **2009**, *48* (17), 3092–3095.
123. Coll, C.; Mondragón, L.; Martínez-Máñez, R.; Sancenón, F.; Marcos, M. D.; Soto, J.; Amorós, P.; Pérez-Payá, E. Enzyme-Mediated Controlled Release Systems by Anchoring Peptide Sequences on Mesoporous Silica Supports. *Angew. Chemie Int. Ed.* **2011**, *50* (9), 2138–2140.
124. P. Srivastava, S. K. Hira, A. Sharma, M. Kashif, P. Srivastava, D. N. Srivastava, R. A. Singh, P. P. Manna, *Bioconjug. Chem*. **2018**, *29*, 2107-2119.
125. D. Muñoz-Espín, M. Rovira, I. Galiana, C. Giménez, B. Lozano-Torres, M. Paez-Ribes, S Llanos, S. Chaib, M. Muñoz-Martín, A. C. Ucero, G. Garaulet, F. Mulero, S. G. Dann, T. Van Arsdale, D. J. Shields, A. Bernardos, J. R. Murguía, R. Martínez-Máñez, M. Serrano, *EMBO Mol. Med.* **2018**, *10*, e9355.

Chapter 2

Objectives

Taking into account the growing interest in the development of Colon Drug Delivery Systems (CDDS) to improve the clinical outcome of colon related diseases, this PhD thesis has aimed to contribute to the progress of advanced therapeutical options for Inflammatory Bowel Disease by means of the development of several hybrid microsystems for controlled drug release in the colon.

In particular, we have focused on the design, preparation, characterization, release and *in vivo* studies in an induced-colitis model in Wistar rat of smart microdevices based on mesoporous silica microparticles equipped with enzyme responsive molecular gates and loaded with dyes or drugs.

The specific objectives are:

- To develop mesoporous silica microparticles containing magnetite nanoparticles to endow with magnetic properties the CDDS. The magnetic scaffold is loaded with the dye safranin O and capped with an organic molecule including an azo bond and a carbamate group (1).

Objectives

- To develop mesoporous silica microparticles including magnetite nanoparticles, loaded with safranin O dye or with hydrocortisone (2) and both capped with a Congo red dye derivative that includes an azo bond and a urea moiety.

- To develop mesoporous silica microparticles loaded with rhodamine B dye or with hydrocortisone (3) and capped with an olsalazine derivative that includes an azo bond and an amide group.

- To evaluate pharmacokinetics from (2) and (3) in healthy Wistar rats.

- To evaluate clinical efficacy of (2) and (3) in an *in vivo* model of induced colitis in Wistar rats.

Chapter 3

Functional Magnetic Mesoporous Silica Microparticles Capped with an Azo-Derivative: A Promising Colon Drug Delivery Device

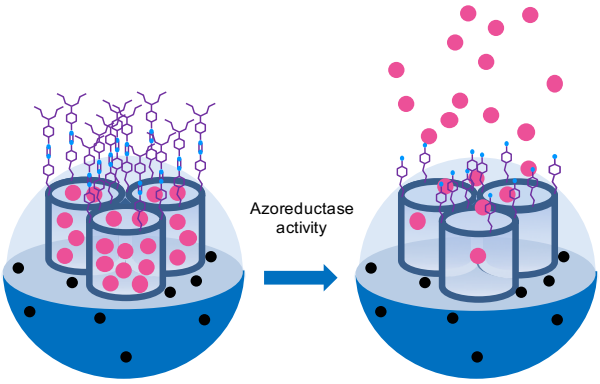

Functional Magnetic Mesoporous Silica Microparticles Capped with an Azo-Derivative: A Promising Colon Drug Delivery Device

Adrián H. Teruel [1,2], Carmen Coll [1,2], Ana M. Costero [1,2,3], Daniel Ferri [1,3], Margarita Parra [1,2,3], Pablo Gaviña [1,2,3], Marta González-Álvarez [4], Virginia Merino [1,5], M. Dolores Marcos [1,2,6,7], Ramón Martínez-Máñez [1,2,6,7,*] and Félix Sancenón [1,2,6,7]

[1] Interuniversity Research Institute for Molecular Recognition and Technological Development (IDM), Polytechnic University of Valencia, University of Valencia, 46100 Valencia, Spain

[2] CIBER of Bioengineering, Biomaterials and Nanomedicine (CIBER-BBN), 28029 Madrid, Spain

[3] Department of Organic Chemistry, University of Valencia, 46100 Valencia, Spain

[4] Engineering Department. Pharmacy and Pharmaceutical Technology Section, Miguel Hernandez University, 03550 Alicante, Spain

[5] Pharmacy and Pharmaceutical Technology and Parasitology, University of Valencia, 46100 Valencia, Spain

[6] Joint Research Unit in Nanomedicine and Sensors. Polytechnic University of Valencia, Health Research Institute Hospital La Fe, 46100 Valencia, Spain.

[7] Joint Unit CIPF-UPV of Mechanisms of Diseases and Nanomedicine, Valencia, Polytechnic University of Valencia, Prince Felipe Research Center, 46100 Valencia, Spain.

Published online: 10 February, 2018

(Reprinted with permission from ***Molecules*** **2018, *23*, 375.**

3.1 Abstract

Magnetic micro-sized mesoporous silica particles were used for the preparation of a gated material able to release an entrapped cargo in the presence of an azo-reducing agent and, to some extent, at acidic pH. The magnetic mesoporous microparticles were loaded with safranin O and the external surface was functionalized with an azo derivative 1 (bearing a carbamate linkage) yielding solid S1. Aqueous suspensions of S1 at pH 7.4 showed negligible safranin O release due to the presence of the bulky azo derivative attached onto the external surface of the inorganic scaffold. However, in the presence of sodium dithionite (azoreductive agent), a remarkable safranin O delivery was observed. At acidic pH, a certain safranin O release from S1 was also found. The pH-triggered safranin O delivery was ascribed to the acid-induced hydrolysis of the carbamate moiety that linked the bulky azo derivatives onto the mesoporous inorganic magnetic support. The controlled release behavior of S1 was also tested using a model that simulated the gastro intestinal tract.

3.2 Introduction

In recent years, the blending of coordination, molecular, supramolecular and biomolecular chemistry concepts with porous materials has led to the development of smart functional gated materials with multiple applications in different scientific and technological fields [1]. These hybrid materials are mainly composed by two subunits: (i) an inorganic porous support for cargo loading; and (ii) certain molecules acting as “molecular gates” for controlled cargo release upon the application of external stimuli [2].

One of the most commonly used inorganic supports in gated materials is mesoporous silica due to its outstanding features such as biocompatibility, inertness and chemical stability, high loading capacity and ease of functionalization using the well-known alkoxysilane chemistries [3]. Besides, mesoporous silica can be prepared as micro- or nanoparticles, the

diameter of the pores can also be adjusted from the typical 2–3 nm range to ca. 6–10 nm (to include inside the porous network biomolecules such as small peptides, DNA fragments or enzymes) and can be prepared including other nanoparticles (for example, magnetite) in their structure endowing the final support with novel features [4–6].

These “gated materials” have been extensively used in controlled release processes [7–10] as well as in sensing/recognition protocols (when a dye or fluorophore is released in the presence of a target molecule) [11] and, very recently, in abiotic communication networks involving several gated nanodevices [12,13]. Dealing with controlled drug release, the preparation of carriers able to deliver certain drugs at-will and on the site of action, minimizing secondary effects, is a benchmark in the treatment of different diseases [14].

From another point of view, colon drug delivery systems (CDDS) have been developed for their use in two main applications: (i) to deliver macromolecular drugs, such as protein or peptides that found in the colon a better environment to be absorbed without losing activity because of the relatively low proteolytic enzyme activity and good absorption (e.g., insulin, calcitonin, and vasopressin); and (ii) to increase the efficacy in prevention and treatment of colon related diseases (e.g., irritable bowel syndrome, inflammatory bowel diseases (IBD), and colorectal cancer) [15,16]. In fact, the development of CDDS is an excellent strategy to deliver certain drugs in colon, decreasing adverse effects and enhance drug efficacy. With this aim, smart formulations for targeting colon such as pH-responsive biodegradable polymers, time-dependent formulations, pressure responsive systems, osmotic controlled materials, bio-adhesive systems, enzyme triggered prodrugs or drugs coated with enzyme-sensitive polymers have been recently developed [17–19].

Despite these examples, the use of hybrid organic–inorganic gated materials based on mesoporous silica for the development of CDDS is still an almost unexplored field. For the preparation of these CDDS silica-based nanodevices, enzymes produced by colon microbiota (azoreductase, β-galactosidase, β-xylosidase, nitroreductase, glycosidase deaminase, etc.) are ideal candidates to be used as external triggers [20,21].

Bearing in mind our interest in the development of silica-based gated materials for controlled release applications [22–29], we report herein the preparation of capped a micro-sized silica mesoporous solid containing magnetic nanoparticles (S1) as a suitable carrier to release an entrapped cargo in colon. Although not specifically tested in this present work, the magnetic character of the prepared nanodevice may be useful to enhance the retention time of the particles in the part of interest of the intestinal tract (for instance in colon). Moreover, particles S1 are loaded with a dye and capped with an azoderivative attached to the external surface of the inorganic matrix by means of a carbamate group. We demonstrated that the presence of the bulky azoderivative onto the external surface of S1 inhibited cargo release, whereas in the presence of a reducing agent delivery was observed. The solid was also able to deliver the cargo to some extent at acidic pH. A study on payload release from S1 in a simulated digestive process in mouth, stomach, small intestine and colon is also reported.

3.3 Results and discussion

3.3.1. Synthesis of Gated Magnetic Micro-Sized Mesoporous Silica Particles

Magnetic nanoparticles (MNPs) coated with oleic acid were prepared by a co-precipitation procedure that used a mixture of $FeCl_3$ and $FeCl_2$ and ammonium hydroxide [30]. Moreover, mesoporous silica was prepared following the “atrane route” with small modifications [31,32]. In this synthetic protocol, n-cetyltrimethylammonium bromide was used as structural directing agent and tetraethylortosilicate as silica source. MNPs were suspended in water and incorporated into the synthesis crude before the addition of NaOH. The resulting brownish powder was washed and the surfactant was subsequently removed by calcination. This procedure yielded the final magnetic micro-sized inorganic solid (**S0**). Once the magnetic mesoporous support was synthesized, the pores of the siliceous

phase were loaded with safranin O (as a model drug in our study) and the external surface functionalized with the bulky azo-containing derivative **1**. This synthetic protocol yielded micro-sized magnetic solids **S1** (see Scheme 1). It was expected that the bulky azo-containing derivative **1** would inhibit dye leaching from the pores, whereas safranin O delivery should be observed in the presence of sodium dithionite (able to hydrolyze azo linkages) or partially at acidic pH (due to the hydrolysis of the carbamate moiety in **1**).

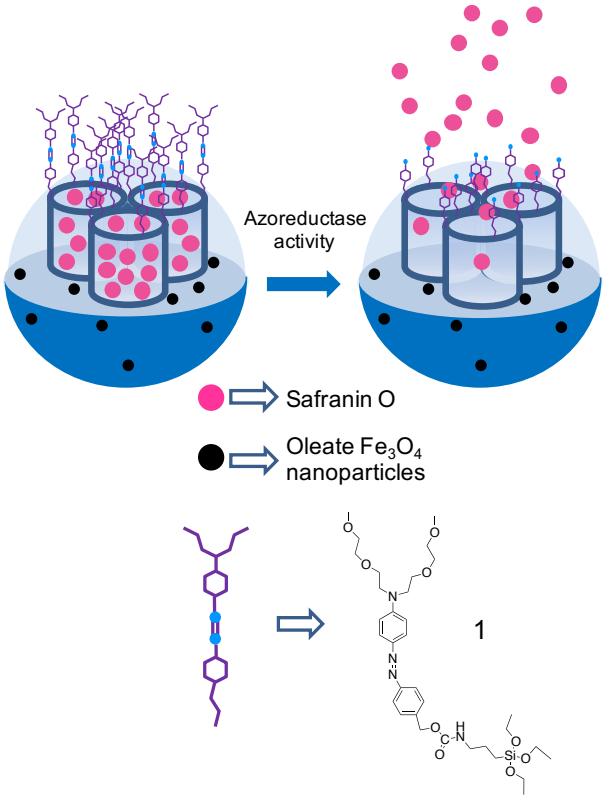

Scheme 1. Magnetic micrometric silica mesoporous supports loaded with safranin O and capped with azo derivative (1). Safranin O is released in the presence of an azoreductor.

The synthesis of azo-containing alkoxysilane derivative **1** (see Scheme 2) starts with the mesylation of 2-methoxyethanol (**1a**) in dichloromethane that yielded **1b** [33]. Then, in a second step, **1b** was reacted with the disodium salt of N-phenyldiethanolamine (**1c**) obtaining the

oligoethylenglycol derivative **1d**. Afterwards, **1d** was reacted with the diazonium salt of 4-aminobenzyl alcohol (**1e**) yielding azo derivative 1f. Finally, azo-containing trialkoxysilane derivative **1** was obtained upon reaction between **1f** and (3-isocyanatopropyl) triethoxysilane (**1g**). The final azo-containing trilakoxysilane derivative (**1**) was fully characterized using ^{1}H- and 13C-NMR and HRMS.

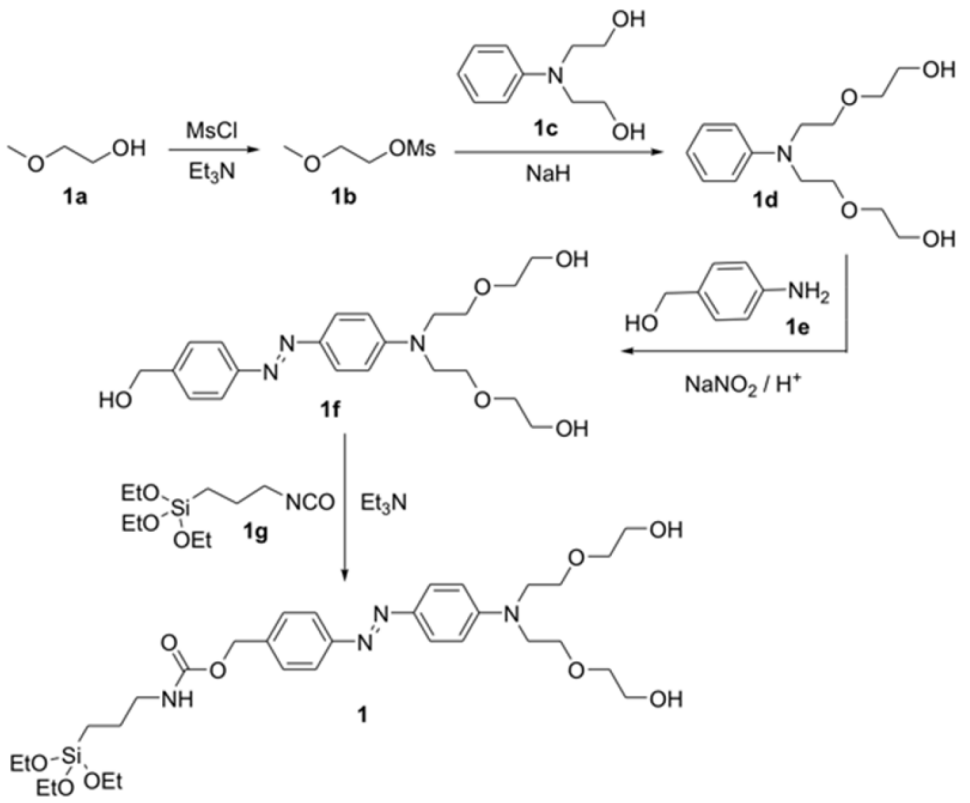

Scheme 2. Synthetic route used for the preparation of azoderivative **1**. 2-methoxyethanol (**1a**); 2-methoxyethyl methanesulfonate (**1b**); N-phenyldiethanolamine (**1c**); oligoethylenglycol derivative (**1d**); 4-aminobenzyl alcohol (**1e**); azo derivative (**1f**); (3-isocyanatopropyl) triethoxysilane (**1g**).

3.3.2. Characterization of the Prepared Materials

S0 and **S1** were characterized using powder X-ray diffraction (PXRD), transmission electron microscopy (TEM), scanning transmission electron microscopy (STEM), N_2 adsorption–desorption isotherms and thermogravimetric analysis. Figure 1 shows the PXRD patterns (at high and low angles) of oleate-stabilized MNPs, the magnetic mesoporous microparticles as-made, **S0** and **S1**. PXRD of oleate-coated MNPs (see also Figure 1) showed the five typical high-angle reflections of magnetite phase indexed as (220), (311), (400), (511) and (440) Bragg peaks. The same peaks were observed for the as-made microparticles, **S0** and **S1** materials but with a marked decrease in intensity (Figure 1). This intensity loss was ascribed to the inclusion of MNPs into the inorganic mesoporous matrix. Low angle PXRD pattern of as-made microparticles (Figure 1) displayed the typical reflections of a hexagonal-ordered mesoporous system that can be indexed as (100), (110), (200) and (210) Bragg peaks. A shift of the (100) peak in calcined **S0** solid was clearly observed. This displacement is consistent with an approximate cell contraction of 3.64 Å and is attributed to the condensation of silanol groups during the calcination step. The presence of the characteristic (100) reflection in the diffraction spectrum of **S1** clearly indicated that the mesoporous structure was preserved throughout the filling process with safranin O and the anchoring of the azo derivative **1**.

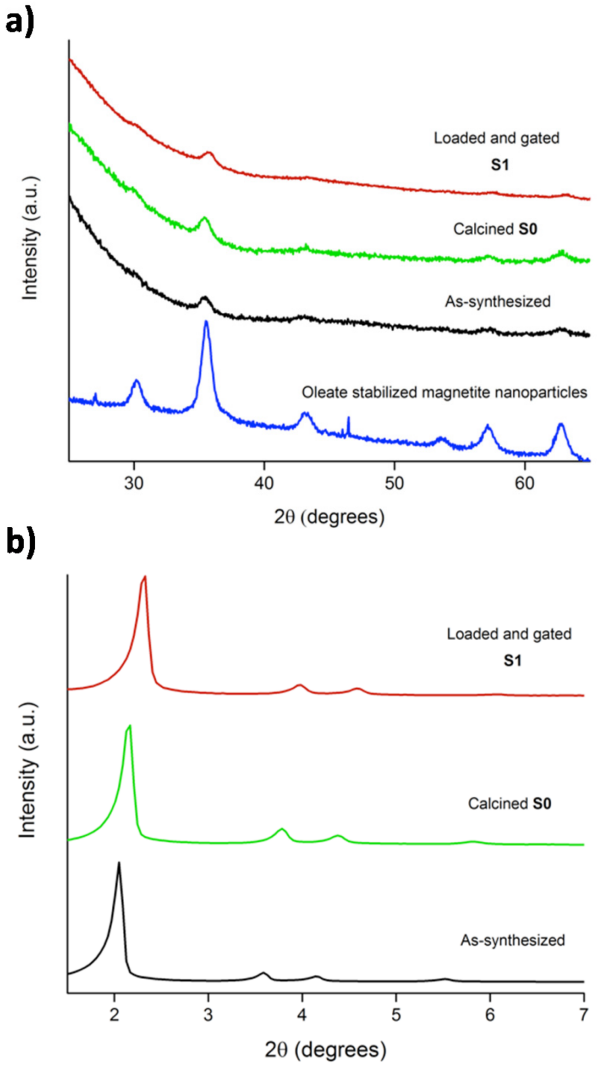

Figure 1. Powder X-rays patterns at: (**a**) high angles; and (**b**) low angles of oleate stabilized magnetite (Fe_3O_4) nanoparticles and magnetic micrometric mesoporous silica particles as-synthesized, **S0** and **S1**.

Figure 2 shows transmission electron microscopy (TEM) images of solid **S0**. As could be seen, the typical porosity associated with the mesoporous inorganic support was present. Besides, MNPs were observed as small dark dots. Scanning transmission electron microscopy (STEM) images of

solid **S0** (iron mapping) indicated that MNPs are randomly distributed through the mesoporous silica microparticles (Figure 3). Moreover, to assess the magnetic behavior of **S0**, field dependent magnetization curves measured at 298 K were obtained. The obtained curves (see Figure 4) displayed no hysteresis loops and showed coercivity values near zero, in agreement with a typical superparamagnetic behavior at room temperature. The saturation magnetization value for **S0** was 1.5 emu/g. This magnetization value is not far from those reported in the literature for other magnetic mesoporous silica particles, which are typically in the 1.7–10 emu/g range [30].

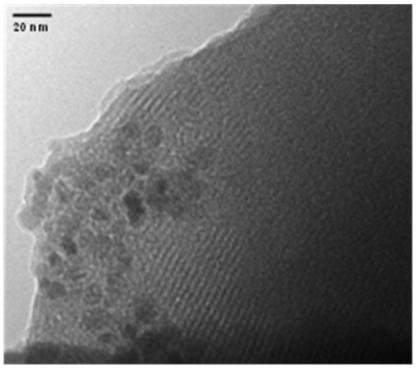

Figure 2. TEM image of micrometric mesoporous silica particles containing magnetite nanoparticles (**S0**).

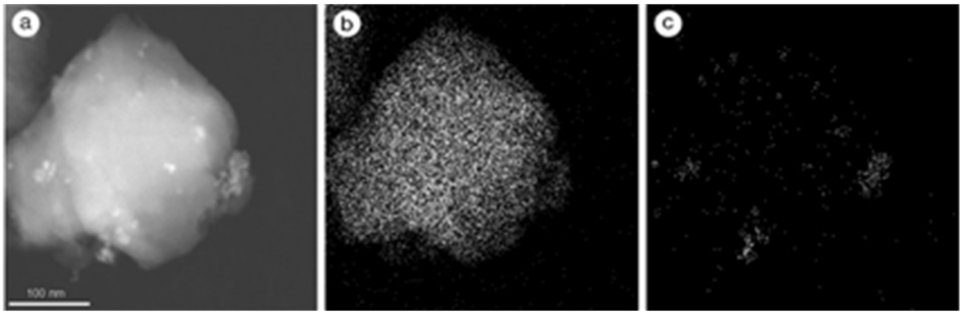

Figure 3. (**a**) STEM images of micrometric mesoporous silica particles containing magnetite nanoparticles (**S0**); (**b**) silica mapping; and (**c**) iron mapping.

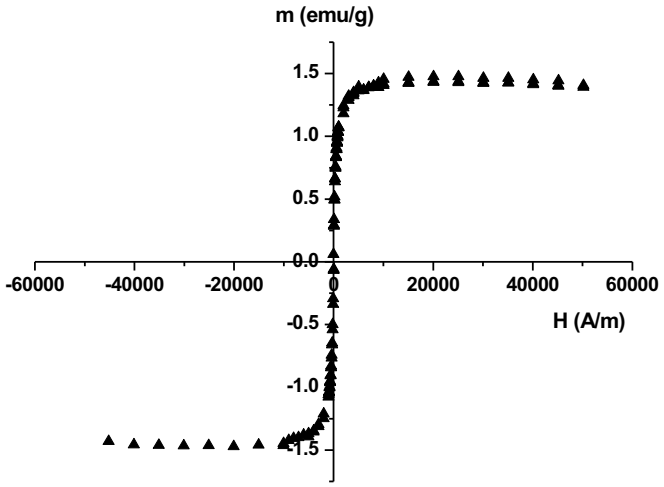

Figure 4. Field-dependent magnetization curves at room temperature of **S0** microparticles.

N_2 adsorption–desorption studies of **S0** and **S1** were also carried out (Figure 5). As could be seen, solid **S0** showed a typical curve for mesoporous silica materials, with an adsorption step at intermediate P/P_0 values (0.2–0.4). This isotherm is classified as type IV in which the absorption step deals with nitrogen condensation inside the mesopores. The pore diameter of **S0** was calculated by the Barret-Joyner-Halenda (BJH) method [34]. The narrow BJH pore distribution observed and the absence of a hysteresis loop in the 0.2–0.4 P/P_0 interval suggested the existence of uniform cylindrical mesopores. Values of pore diameter of 2.83 nm and pore volume of 0.94 $cm^3\ g^{-1}$, calculated on the adsorption branch of the isotherm, were found. Pore diameter estimated from TEM images agree with this value. The application of the Brunauer-Emmett-Teller (BET) model [35] gave a value of 1057 $m^2\ g^{-1}$ for the total specific surface. On the other hand, the N_2 adsorption–desorption isotherms of solid **S1** are typical of mesoporous systems with partially filled mesopores, and a decrease in both the adsorbed N_2 volume and the specific surface area was clearly observed (Table 1). This reduction in the BET surface, compared with that

of **S0**, was ascribed to the loading of pores with safranin O and the functionalization of the surface with the bulky azo derivative **1** in **S1**.

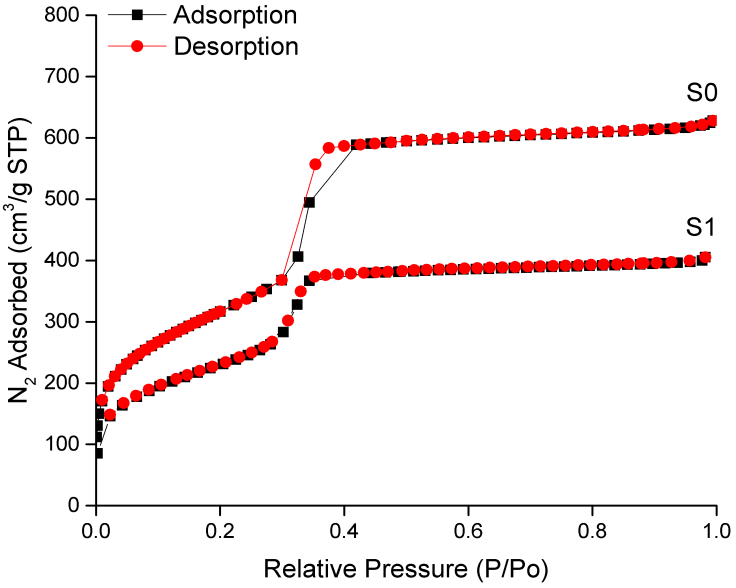

Figure 5. N_2 adsorption–desorption isotherms for **S0** and **S1** materials.

Table 1. BET specific surface values, pore volumes and pore sizes for **S0** and **S1**.

Solid	S_{BET} ($m^2\ g^{-1}$)	pore volume [1] ($cm^3\ g^{-1}$)	pore size [1,2] (nm)
S0	1057	0.94	2.83
S1	834	0.68	-

[1] Total pore volume according to the BJH model. [2] Pore size estimated by using the BJH model applied on the adsorption branch of the isotherm, for $P/P_0 < 0.6$, which can be associated to the surfactant generated mesopores.

Total organic matter on solid **S1** was determined by thermogravimetric analysis (see Supplementary Materials) and ^{1}H-NMR (Table 2). The amount of anchored azo derivative onto **S1** was determined by ^{1}H-NMR upon dissolving the corresponding sample in HF/D_2O in the presence of tetraethyl ammonium bromide as internal standard (Table 2) [36]. Besides, energy dispersive X-ray spectroscopy (EDX, 20 kV) was used to determine Si and Fe content in **S1** microparticles. EDX measurements showed a value of 5.9 for the Si/Fe ratio in the final **S1** solid.

Table 2. Content of total organic matter (in g) per gram of SiO_2, content of azo derivative (in g) per gram of SiO_2 and dye released (in µg) per mg of solid in **S1**.

Solid	Organic Content (g/g SiO_2)	Azo Derivative (g/g SiO_2)	Dye Release (µg/mg solid)
S1	0.0469	0.043	0.69

3.3.3. Cargo Release from S1

Payload release from solid **S1** at acidic (2.0 and 4.5) and neutral (7.4) pH in the presence or absence of the azoreductor agent sodium dithionite was studied [37,38]. These pH values were selected taking into account the possible use of **S1** as nanodevice for controlled release in colon: pH 2.0 is typical of gastric juices, pH 4.5 is found in the transition from stomach to intestines (this pH can also be found in the colon of IBD patients), and a neutral pH ranging 6.5–7.4 is typically found in the intestine. In a typical experiment, 2 mg of **S1** were suspended in water at selected pH values, the final suspensions stirred at 37.5 ºC and aliquots were taken at scheduled times. The aliquots were centrifuged to remove the solid and the release of safranin O to the solution monitored by measuring fluorescence at 571 nm upon excitation at 520 nm. Cargo release profile for solid **S1** is shown in Figure 6. Aqueous suspensions of **S1** showed negligible safranin O release at neutral pH. However, as a clear contrast, a marked delivery of entrapped safranin O was seen in the presence of sodium dithionite (more than 80% of maximum dye delivered after 4 h). The observed delivery is attributed to the presence of sodium dithionite, which can reduce azo groups in the capping molecule **1** resulting in pore opening and safranin O release [37,38]. At acidic pH (2.0 and 4.5), a sustained safranin O release was also observed. Delivery of entrapped safranin O was ascribed to a hydrolysis of carbamate moieties, which linked the bulky azo derivative **1** onto the external surface of **S1**. Maximum release of safranin O for **S1** was ca. 0.51 µg/mg solid at pH 7.4 in the presence of sodium dithionite.

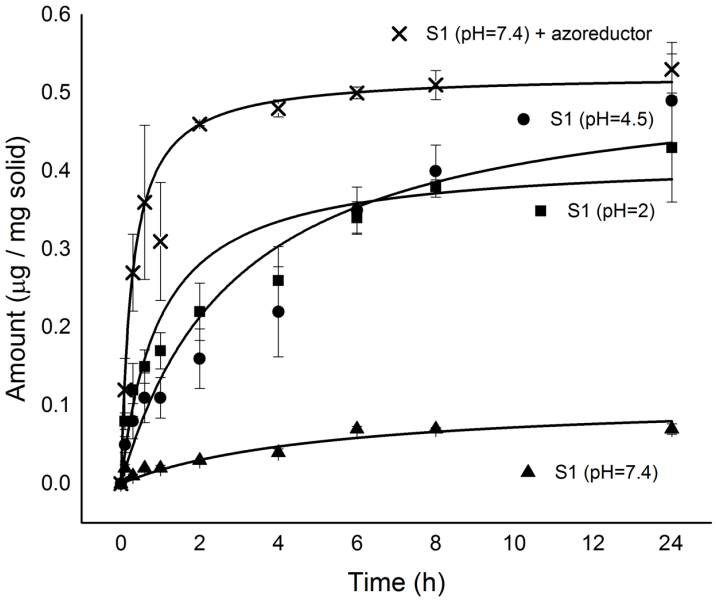

Figure 6. Release kinetics of safranin O from **S1** in water at pH ≈ 2 (square), pH ≈ 4.5 (circle), pH ≈ 7.4 (triangle) and pH ≈ 7.4 in the presence of azoreductor agent sodium dithionite (SD, 57.4 mM) (cross).

3.3.4. *In Vitro* Digestion Model Assay

Despite the partial payload delivery from **S1** at acidic pH shown above, it has to be noted that permanence of the particles in the stomach is usually less than 2 h and therefore only a partial cargo delivery from **S1** is expected to occur before targeting colonic tissues. In fact, to study in depth the possible application of azo-gated magnetic microparticles as suitable particles for cargo delivery in colon, payload delivery from **S1** was further tested in a model of digestion using simulated solutions. The model used was a modification of that introduced by Oomen and co-workers [39,40] that is a three-step procedure simulating digestive process in mouth, stomach and small intestine. Moreover, we introduced a fourth step to simulate the digestive process in colon. In a typical experiment, 2 mg of solid (**S1**) were suspended in simulated saliva (5 min at 37.5 °C) and then simulated gastric juice (stomach) was added and the mixture stirred 2 h.

Afterwards, duodenal simulated juice, bile and bicarbonate solution (small intestine) were added and the suspension stirred for two more hours. Finally, sodium dithionite was added and it was left for 24 h to mimic the colon environment and the presence of azoreductases. Safranin O release in the entire process was evaluated via monitorization of the emission at 571 nm upon excitation at 520 nm. The obtained results are shown in Figure 7.

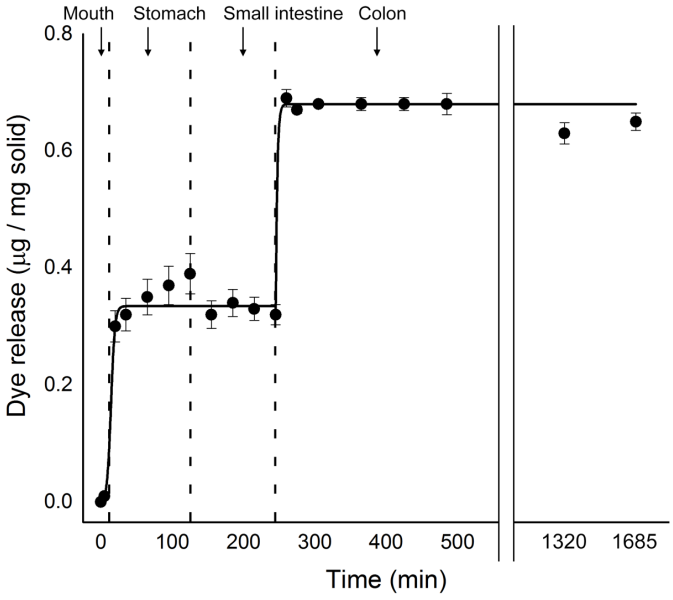

Figure 7. Release kinetics of Safranin O from **S1** in simulated gastro-intestinal tract (GIT) fluids.

As shown in Figure 7, a nearly “zero release” was observed during the first 5 min when solids were in contact with simulated saliva. In contact with gastric juice, a safranin O delivery of ca. 0.3 µg/mg solid was found and ascribed to partial pore opening due to the acidic environment. In small intestine conditions, no further delivery of safranin O was observed. However, a marked cargo release was found in simulated colon conditions and related with the presence of sodium dithionite, which can reduce azo bonds of the capping ensemble in **S1**.

3.4 Materials and Methods

3.4.1. General Techniques

Transmission electron microscopy (TEM), scanning transmission electron microscope (STEM), powder X-ray diffraction (PXRD), thermogravimetric analysis (TGA), N_2 adsorption–desorption, nuclear magnetic resonance (NMR), Fourier transform infrared spectroscopy (FT-IR) and fluorescence spectroscopy techniques were employed to characterize the synthesized materials. TEM and STEM images were acquired using a JEOL JEM-1010 and a JEOL JEM 2100F microscopes (Akishima, Japan), respectively. PXRD measurements were performed on a Bruker D8 Advance diffractometer (Billerica, MA, USA) using CuKα radiation. TGA were carried out on a TGA/SDTA 851e Mettler Toledo balance (Greifensee, Switzerland), using an oxidant atmosphere (air, 80 mL/min) with a heating program consisting on a heating ramp of 10 °C per minute from 393 to 1273 K and an isothermal heating step at this temperature for 30 min. N_2 adsorption–desorption isotherms were recorded with a Micromeritics ASAP 2010 automated sorption analyzer (Norcross, GA, USA). The samples were degassed at 120 °C under vacuum overnight. The specific surface areas were calculated from the adsorption data in the low pressure range using the Brunauer-Emmett-Teller (BET) model. Pore size was determined following the Barrett-Joyner-Halenda (BJH) method. ^{1}H NMR spectra were recorded using a Bruker AV400 spectrometer (Billerica, MA, USA). Infrared spectra were recorded using a Bruker Tensor 27 equipment (Billerica, MA, USA). Fluorescence measurements were carried out in a PerkinElmer EnSpire Multimode Plate Reader (Waltham, MA, USA).

3.4.2. Chemicals

The chemicals tetraethylorthosilicate (TEOS), *n*-cetyltrimethyl-ammonium bromide (CTABr), sodium hydroxide, triethanolamine ($TEAH_3$), (3-isocyanatopropyl) triethoxysilane, iron(III) chloride hexahydrate, iron(II)

chloride tetrahydrate, oleic acid, safranin O dye, 2-methoxyethanol, triethylamine, methanesulfonyl chloride, hydrochloric acid, *N*-phenyldiethanolamine, anhydrous acetonitrile, sodium hydride, 4-aminobenzyl alcohol, sodium nitrite, sodium dithionite and all chemicals for the digestive fluids were provided by Sigma-Aldrich (Madrid, Spain). Magnesium sulfate, sodium carbonate, and all the analytical-grade solvents were purchased from Scharlab (Barcelona, Spain). Aluminum oxide was acquired from Merck (Madrid, Spain). All products were used as received.

3.4.3. Synthesis of Oleic Acid-coated Magnetic Nanoparticles (MNPs)

MNPs were prepared using a modified co-precipitation method. In a typical procedure, $FeCl_3 \cdot 6H_2O$ (24.0 g, 0.089 mol) and $FeCl_2 \cdot 4H_2O$ (9.8 g, 0.049 mol) were dissolved in deionized water (100 mL) under nitrogen atmosphere with vigorous stirring at 80 °C. Then ammonium hydroxide (50 mL) was added quickly into the solution. The colour of the solution immediately turned black and then oleic acid (3.8 g, 0.013 mol) was added after 30 min. The reaction was kept at 80 °C for 1.5 h. The final oleic acid-coated MNPs were washed with deionized water until neutral pH. Afterwards, the MNPs were transferred into a chloroform solution (30 mg MNPs/mL $CHCl_3$).

3.4.4. Synthesis of Mesoporous Silica Microparticles Containing MNPs (S0)

A chloroform suspension of MNPs (6 mL, 30 mg MNPs/mL $CHCl_3$) was mixed with an aqueous solution of CTABr (8 mL, 10 mg/mL) and the resulting suspension was treated with ultrasounds and heated. Finally, ultrasounds were applied again and the suspension was passed through nylon filters (0.45 μM) to ensure MNPs homogeneity. Magnetic micro-sized MCM-41 particles were synthesized following the so-called “atrane route”. For this purpose, a solution of $TEAH_3$ (25.79 g, 0.173 mol) and NaOH (2 mL of a 6 M solution) was heated to 120 °C and then cooled down to 70 °C, at this moment TEOS (11 mL, 0.045 mol) was added and the crude reaction was heated up to 120 °C. The crude reaction was left cooling down again and CTABr (4.68 g, 0.013 mol) was added at 118 °C. Next, water

containing MNPs (74 mL of distilled water + 6 mL of the MNPs CTABr-water suspension) was slowly added with vigorous stirring at 70 °C. Besides, NaOH (10 mL of a 0.1 M solution) was added to obtain a pH ≈ 10.9. After a few minutes, a brownish suspension was formed. This mixture was aged in an autoclave at 100 °C for 24 h. The resulting powder was collected by filtration and washed with water. Finally, the solid was dried at 70 °C. To prepare the final solid (**S0**), the as-synthesized microparticles were calcined at 550 °C using oxidant atmosphere for 5 h to remove the template.

3.4.5. Synthesis of 1b

2-Methoxyethanol (**1a**, 16 mL, 0.2 mol) was dissolved in dichloromethane (270 mL) in a 2 L round-bottomed flask. The solution was kept in an ice bath for 15 min, and then triethylamine (55.2 mL, 0.4 mol) was added to the solution. Afterwards, a solution of methanesulfonyl chloride in dichloromethane (0.32 mol in 48 mL) was added dropwise for 60 min to the initial reaction crude. After this addition, reaction was stirred at room temperature for another 90 min period. Then, the crude was poured onto a water/ice mixture containing concentrated hydrochloric acid (50 mL), and the organic layer was separated, washed three times with brine and dried with anhydrous $MgSO_4$. Dichloromethane was eliminated in a rotary evaporator to give **1b** as yellow oil (25.16 g, 0.18 mol, 91% yield). Spectroscopic data were coincident with those reported in the literature.

3.4.6. Synthesis of 1d

N-phenyldiethanolamine (**1c**, 3.90 g, 0.021 mol) was dissolved in dry acetonitrile (70 mL) and then the flask was purged several times with argon to remove oxygen and water. Then, sodium hydride (1.2 g, 0.05 mol) was gradually added at room temperature, after which a white precipitate appeared. On the other hand, **1b** (6 g, 0.043 mol) was dissolved in anhydrous acetonitrile (30 mL) and then added dropwise to the generated dianionic salt of **1c**. After this addition, the crude reaction was heated at

reflux for 24 h. Then, the reaction mixture was filtered off and the organic solvent was eliminated using a rotary evaporator, yielding a yellow oil. The product **1d** (1.25 g, 4 mmol, 20% yield) was purified using column chromatography with aluminum oxide and hexane/ethyl acetate (8:2 *v*/*v*) as the eluent. Spectroscopic data were consistent with those reported in the literature.

3.4.7. Synthesis of 1f

4-aminobenzyl alcohol (**1e**, 414 mg, 3.36 mmol) was dissolved in hydrochloric acid (150 mL, 4 mol L^{-1}). This solution was slowly added to water (25 mL) containing sodium nitrite (232 mg, 3.36 mmol) at 5 °C. The generated diazonium salt of **1e** was immediately added to an aqueous solution containing **1d** (1 g, 3.36 mmol). The reaction was allowed to react for 30 min at 5 °C and for 30 min at room temperature. The final dark red crude was neutralized with a saturated sodium carbonate solution and the organic product was extracted with dichloromethane. Organic layers were dried with $MgSO_4$ filtered off and the solvent was eliminated in a rotary evaporator. Product **1f** (250 mg, 0.58 mmol, 17% yield) was isolated as a dark red-orange solid through column chromatography with aluminum oxide and hexane/ethyl acetate (3:2 *v*/*v*) as the eluent. ^{1}H-NMR (400 MHz, $CDCl_3$): δ = 7.84 (d, 4H), 7.46 (d, 2H), 6.79 (d, 2H), 4.75 (s, 2H), 3.74–3.49 (m, 16H), 3.38 ppm (s, 6H); ^{13}C: δ = 50.2, 57.4, 58.1, 67.3, 69.7, 70.9, 110.6, 121.2, 126.5, 127.4, 141.1, 154.9, 156.4 ppm.

3.4.8. Synthesis of 1

In a first step, **1f** (520 mg, 1.2 mmol) was dissolved in chloroform (20 mL). Then, excess of alkoxysilane derivative **1g** (468 µL, 1.8 mmol) and triethylamine (468 µL, 0.003 mmol) were added under argon atmosphere. The crude reaction was allowed to react for 72 h at 60 °C. Afterwards, the solvent was eliminated in a rotary evaporator and the reaction crude was washed 3 times with cold hexane to remove impurities. Compound **1** was isolated as orange oil (550 mg, 0.810 mmol, 67% yield). ^{1}H-NMR (400

MHz, $CDCl_3$): δ = 7.76 (d, 4H), 7.38 (d, 2H), 6.72 (d, 2H), 5.06 (s, 2H), 4.68 (s, 1H), 3.75 (q, 6H), 3.62–3.47 (m, 16H), 3.31 (s, 6H), 3.14 (t, 2H), 1.56 (m, 2H), 1.15 (t, 9H), 0.56 (t, 2H) ppm; ^{13}C: δ = 160.9, 142.3, 139.4, 129.9, 128.5, 127.6, 122.4, 119.1, 114.2, 111.8, 100.2, 72.1, 70.8, 68.5, 65.3, 59.2, 51.4, 32.1, 29.9, 29.5, 22.8, 14.3, 1.2 ppm. HRMS-EI *m*/*z*: calcd for $C_{33}H_{54}N_4O_9Si$ 678.3660; found: 677.2403 ($M - H^+$).

3.4.9. Synthesis of S1

Magnetic mesoporous silica microparticles (**S0**, 270 mg) were suspended in an acetonitrile solution (10 mL) of safranin O (75 mg, 0.8 mmol/g **S0**) under argon atmosphere. The obtained suspension was then stirred at room temperature overnight to achieve maximum loading of the pores. Afterward, **1** (550 mg, 3 mmol/g **S0**) was dissolved in anhydrous acetonitrile (8 mL) and was added to the microparticle/dye suspension. The mixture was stirred at room temperature for 6 h in an argon atmosphere. **S1** was isolated by centrifugation, washed several times with acetonitrile and was finally dried at 40 °C for 24 h.

3.4.10. Controlled Release Studies

Controlled release studies from **S1** were tested at different pH values (i.e., 2.0, 4.5 and 7.4) and in the presence of a reductive environment (sodium dithionite, which is known to reduce azo linkages). In a typical experiment, 2 mg of the corresponding solid were suspended in water at the selected pH (2 mL) and aliquots were extracted at given times (0, 5 min, 20 min, 40 min, 1 h, 2 h, 4 h, 6 h, 8 h, and 24 h), centrifuged to remove the solid and supernatants were loaded into a 96-well plate to measure safranin O fluorescence at 571 nm (excitation at 520 nm). Controlled release from **S1** microparticles were also tested in *in vitro* digestion conditions using simulated solutions for saliva, gastric juice, duodenal juice and bile [39,40]. *In vitro* digestion experiments were carried out with **S1** (2 mg) at 37 °C (temperature of the human body) and stirring at 12,000 rpm (to ensure the correct suspension of the microparticles). Digestions started

by adding simulated saliva fluid (320 µL) and incubating for 5 min. Then, simulated gastric juice (630 µL) was added, and the mixture was stirred for 2 h. Later, simulated duodenal juice (630 µL), bile (320 µL) and a bicarbonate solution (1 M, 100 µL) were added simultaneously and the mixture was stirred for another 2 h. Finally, colon fluid was simulated by adding sodium dithionite (20 mg, 57.4 mM/2 mL). Aliquots were taken at given times (0, 5, 20, 35, 65, 95, 125, 155, 185, 215, 245, 260, 275, 305, 365, 425, 485, 1320 and 1685 min), centrifuged and supernatants were loaded into a 96 well plate to measure safranin O fluorescence. Calibration curves, in water, simulated small intestine fluid and simulated colon fluid, were performed to assess the amounts of safranin O released from solid **S1** in the different environments.

3.5 Conclusions

As summary, here we have reported the synthesis and characterization of magnetic mesoporous silica microparticles loaded with safranin O and capped with bulky azo derivative bearing pH-hydrolysable moieties (carbamate group). At neutral pH, the capped material showed a negligible safranin O release. However, at neutral pH, addition of a reducing agent such as sodium dithionite (mimicking azoreductase enzyme) induced a marked safranin O release. The observed delivery was ascribed to a reduction of the azo bonds that induced a fall in the steric crowding around pore outlets with subsequent dye delivery. Moreover, a partial payload release was also observed at acidic pH. Delivery studies in a digestion model indicated an important part of the payload was released in colon. These particles are expected to find applications as smart controlled drug delivery systems in the colon mucosa (e.g., for IBD patients) due to the presence of azoreductase enzymes produced by bacteria in the colon microbiota. Besides, its ability to release the cargo at acidic pH, opens the possibility to improve the performance of these carriers for drug delivery in ulcerative colitis and Crohn's disease in which a marked decrease in the pH of the colon happens [41,42]. Moreover, these microparticles (**S1**) were

equipped with magnetic nanoparticles to potentially apply magnetic fields to enhance the retention time of the solids in colon. Similar magnetic microparticles to those reported here and loaded with a drug (e.g., 5-ASA) are promising materials for the oral treatment of colon related diseases. Further *in vivo* studies in this line will be performed in due course.

Acknowledgements

We thank the Spanish Government (projects MAT2015-64139-C4-1-R and AGL2015-70235-C2-2-R (MINECO/FEDER)) and the Generalitat Valenciana (project PROMETEOII/2014/047) for support. AHT thanks to the Spanish MEC for his FPU grant. The authors also thank the Electron Microscopy Service at the Universitat Politècnica de València for support. SCSIE (Universitat de València) is also gratefully acknowledged for all the equipment employed. NMR was registered at the U26 facility of ICTS "NANBIOSIS" at the Universitat de València. The authors thanks L. A. Villaescusa for his helpful discussion about the ^{1}H-NMR analysis of the composition of loaded and functionalized supports.

3.6 References

1. Descalzo, A.B.; Martínez-Máñez, R.; Sancenón, F.; Hoffmann, K.; Rurack, K. The supramolecular chemistry of organic-inorganic hybrid materials. *Angew. Chem. Int. Ed.* **2006**, *45*, 5924. [Google Scholar] [CrossRef] [PubMed]
2. Giménez, C.; de la Torre, C.; Gorbe, M.; Aznar, E.; Sancenón, F.; Murguía, J.R.; Martínez-Máñez, R.; Marcos, M.D.; Amorós, P. Gated mesoporous silica nanoparticles for the controlled delivery of drugs in cancer cells. *Langmuir* **2015**, *31*, 3753. [Google Scholar] [CrossRef] [PubMed]
3. Stein, A. Advances in microporous and mesoporous solids—Highlights of recent progress. *Adv. Mater.* **2003**, *15*, 763. [Google Scholar] [CrossRef]
4. Mekaru, H.; Lu, J.; Tamanoi, F. Development of mesoporous silica-based nanoparticles with controlled release capability for cancer therapy. *Adv. Drug Deliv. Rev.* **2015**, *95*, 40. [Google Scholar] [CrossRef] [PubMed]
5. Baeza, A.; Vallet-Regí, M. Smart mesoporous silica nanocarriers for antitumoral therapy. *Curr. Top. Med. Chem.* **2015**, *15*, 2306. [Google Scholar] [CrossRef] [PubMed]
6. Ling, D.; Lee, N.; Hyeon, T. Chemical synthesis and assembly of uniformly sized iron oxide nanoparticles for medical applications. *Acc. Chem. Res.* **2015**, *48*, 1276. [Google Scholar] [CrossRef] [PubMed]

7. Aznar, E.; Oroval, M.; Pascual, L.; Murguía, J.R.; Martínez-Máñez, R.; Sancenón, F. Gated materials for on-command release of guest molecules. *Chem. Rev.* **2016**, *116*, 561. [Google Scholar] [CrossRef] [PubMed]
8. Li, Z.; Barnes, J.C.; Bosoy, A.; Stoddart, J.F.; Zink, J.I. Mesoporous silica nanoparticles in biomedical applications. *Chem. Soc. Rev.* **2012**, *41*, 2590. [Google Scholar] [CrossRef] [PubMed]
9. Doane, T.L.; Burda, C. The unique role of nanoparticles in nanomedicine: imaging, drug delivery and therapy. *Chem. Soc. Rev.* **2012**, *41*, 2885. [Google Scholar] [CrossRef] [PubMed]
10. Llopis-Lorente, A.; Lozano-Torres, B.; Bernardos, A.; Martínez-Máñez, R.; Sancenón, F. Mesoporous silica materials for controlled delivery based on enzymes. *J. Mater. Chem. B.* **2017**, *5*, 3069. [Google Scholar] [CrossRef]
11. Sancenón, F.; Pascual, L.; Oroval, M.; Aznar, E.; Martínez-Máñez, R. Gated silica mesoporous materials in sensing applications. *ChemistryOpen* **2015**, *4*, 418. [Google Scholar] [CrossRef] [PubMed]
12. Giménez, C.; Climent, E.; Aznar, E.; Martánez-Máñez, R.; Sancenón, F.; Marcos, M.D.; Amorós, P.; Rurack, K. Towards chemical communication between gated nanoparticles. *Angew. Chem. Int. Ed.* **2014**, *53*, 12629. [Google Scholar] [CrossRef] [PubMed]
13. Llopis-Lorente, A.; Díez, P.; Sánchez, A.; Marcos, M.D.; Sancenón, F.; Martínez-Ruíz, P.; Villalonga, R.; Martínez-Máñez, R. Interactive models of communication at the nanoscale using nanoparticles that talk to one another. *Nat. Commun.* **2017**, *8*, 15511. [Google Scholar] [CrossRef] [PubMed]
14. Coburn, J.M.; Kaplan, D.L. Engineering biomaterial-drug conjugates for local and sustained chemotherapeutic delivery. *Bioconj. Chem.* **2015**, *26*, 1212. [Google Scholar] [CrossRef] [PubMed]
15. Shah, N.K.; Rane, B.R.; Gujarathi, N.A. Developments in colon specific drug delivery systems—A review. *Pharm. Sci. Monit.* **2014**, *5*, 95. [Google Scholar]
16. Singh, G.; Kumar, D.; Singh, M.; Sharma, D.; Kaur, S. Emerging techniques and challenges in colon drug delivery systems. *J. Appl. Pharm. Sci.* **2012**, *2*, 139. [Google Scholar]
17. Malik, K.; Goswami, L.; Kothiyal, P.; Mukhopadhyay, S. A review on colon targeting drug delivery system: Novel approaches, anatomy and evaluation. *Pharma. Innov. J.* **2012**, *1*, 1. [Google Scholar]
18. Lautenschläger, C.; Schmidt, C.; Fischer, D.; Stallmach, A. Drug delivery strategies in the therapy of inflammatory bowel disease. *Adv. Drug Deliv. Rev.* **2014**, *71*, 58. [Google Scholar] [CrossRef] [PubMed]
19. Hua, S.; Marks, E.; Schneider, J.J.; Keely, S. Advances in oral nano-delivery systems for colon targeted drug delivery in inflammatory bowel disease: Selective targeting to diseased versus healthy tissue. *Nanomedicine***2015**, *11*, 1117. [Google Scholar] [CrossRef] [PubMed]
20. Sinha, V.R.; Kumria, R. Microbially triggered drug delivery to the colon. *Eur. J. Pharm. Sci.* **2003**, *18*, 3. [Google Scholar] [CrossRef]
21. Rubinstein, A. Microbially controlled drug delivery to the colon. *Biopharm. Drug Dispos.* **1990**, *11*, 465. [Google Scholar] [CrossRef] [PubMed]
22. Oroval, M.; Díez, P.; Aznar, E.; Coll, C.; Marcos, M.D.; Sancenón, F.; Villalonga, R.; Martínez-Máñez, R. Self-regulated glucose-sensitive neoglycoenzyme-capped mesoporous silica nanoparticles for insulin delivery. *Chem. Eur. J.* **2017**, *23*, 1353. [Google Scholar] [CrossRef] [PubMed]

23. García-Fernández, A.; García-Laínez, G.; Ferrándiz, M.L.; Aznar, E.; Sancenón, F.; Alcaraz, M.J.; Murguía, J.R.; Marcos, M.D.; Martínez-Máñez, R.; Costero, A.M.; et al. Targeting inflammasome by the inhibition of caspase-1 activity using capped mesoporous silica nanoparticles. *J. Control. Release* **2017**, *248*, 60. [Google Scholar] [CrossRef] [PubMed]
24. Ultimo, A.; Giménez, C.; Bartovsky, P.; Aznar, E.; Sancenón, F.; Marcos, M.D.; Amorós, P.; Bernardo, A.R.; Martínez-Máñez, R.; Jiménez-Lara, A.M.; et al. Targeting innate immunity with dsRNA-conjugated mesoporous silica nanoparticles promotes antitumor effects on breast cancer cells. *Chem. Eur. J.* **2016**, *22*, 1582. [Google Scholar] [CrossRef] [PubMed]
25. Aznar, E.; Coll, C.; Marcos, M.D.; Martínez-Máñez, R.; Sancenón, F.; Soto, J.; Amorós, P.; Cano, J.; Ruiz, E. Borate-driven gatelike scaffolding using mesoporous materials functionalised with saccharides. *Chem. Eur. J.***2009**, *15*, 6877. [Google Scholar] [CrossRef] [PubMed]
26. Bringas, E.; Köysüren, O.; Quach, D.V.; Mahmoudi, M.; Aznar, E.; Roehling, J.D.; Marcos, M.D.; Martínez-Máñez, R.; Stroeve, P. Triggered release in lipid bilayer-capped mesoporous silica nanoparticles containing SPION using an alternating magnetic field. *Chem. Commun.* **2012**, *48*, 5647. [Google Scholar] [CrossRef] [PubMed]
27. Agostini, A.; Mondragón, L.; Bernardos, A.; Martínez-Máñez, R.; Marcos, M.D.; Sancenón, F.; Soto, J.; Costero, A.; Manguan-García, C.; Perona, R.; et al. Targeted cargo delivery in senescent cells using capped mesoporous silica nanoparticles. *Angew. Chem. Int. Ed.* **2012**, *51*, 10556. [Google Scholar] [CrossRef] [PubMed]
28. de la Torre, C.; Casanova, I.; Acosta, G.; Coll, C.; Moreno, M.J.; Albericio, F.; Aznar, E.; Mangues, R.; Royo, M.; Sancenón, F.; et al. Gated mesoporous silica nanoparticles using a double-role circular peptide for the controlled and target-preferential release of doxorubicin in CXCR4-expresing lymphoma cells. *Adv. Funct. Mater.* **2015**, *25*, 687. [Google Scholar] [CrossRef]
29. Polo, L.; Gómez-Cerezo, N.; Aznar, E.; Vivancos, J.L.; Sancenón, F.; Arcos, D.; Vallet-Regí, M.; Martínez-Máñez, R. Molecular gates in mesoporous bioactive glasses for the treatment of bone tumors and infection. *Acta Biomater.* **2017**, *50*, 114. [Google Scholar] [CrossRef] [PubMed]
30. Zhang, J.; Li, X.; Rosenholm, J.M.; Gu, H. Synthesis and characterization of pore size-tunable magnetic mesoporous silica nanoparticles. *J. Colloid Interface Sci.* **2011**, *361*, 16. [Google Scholar] [CrossRef] [PubMed]
31. Kresge, C.T.; Leonowicz, M.E.; Roth, W.J.; Vartuli, J.C.; Beck, J.S. Ordered mesoporous molecular sieves synthesized by a liquid-crystal template mechanism. *Nature* **1992**, *359*, 710. [Google Scholar] [CrossRef]
32. El Haskouri, J.; Cabrera, S.; Caldés, M.; Alamo, J.; Beltrán, A.; Marcos, M.D.; Amorós, P.; Beltrán, D. Ordered mesoporous materials: Composition and topology control through chemistry. *Int. J. Inorg. Mater.* **2001**, *3*, 1157. [Google Scholar] [CrossRef]
33. Mas, N.; Agostini, A.; Mondragón, L.; Bernardos, A.; Sancenón, F.; Marcos, M.D.; Martínez-Máñez, R.; Costero, A.M.; Gil, S.; Merino-Sanjuán, M.; et al. Enzyme-responsive silica mesoporous supports capped with azopyridinium salts for controlled delivery applications. *Chem. Eur. J.* **2013**, *19*, 1346. [Google Scholar] [CrossRef] [PubMed]

34. Barrett, E.P.; Joyner, L.G.; Halenda, P.P. The determination of pore volume and area distributions in porous substances. I. Computations from nitrogen isotherms. *J. Am. Chem. Soc.* **1951**, *73*, 373. [Google Scholar] [CrossRef]
35. Brunauer, S.; Emmett, P.H.; Teller, E. Adsorption of gases in multimolecular layers. *J. Am. Chem. Soc.* **1938**, *60*, 309. [Google Scholar] [CrossRef]
36. Pérez-Esteve, E.; Ruiz-Rico, M.; de la Torre, C.; Villaescusa, L.A.; Sancenón, F.; Marcos, M.D.; Amorós, P.; Martínez-Máñez, R.; Barat, J.M. Encapsulation of folic acid in different silica porous supports: A comparative study. *Food Chem.* **2016**, *196*, 66. [Google Scholar] [CrossRef] [PubMed]
37. Lee, S.H.; Moroz, E.; Castagner, B.; Leroux, J.C. Activatable cell penetrating peptide-peptide nucleic acid conjugate via reduction of azobenzene PEG chains. *J. Am. Chem. Soc.* **2014**, *136*, 12868. [Google Scholar] [CrossRef] [PubMed]
38. Yang, Y.Y.; Grammel, M.; Raghavan, A.S.; Charron, G.; Hang, H.C. Comparative analysis of cleavable azobenzene-based affinity tags for bioorthogonal chemical proteomics. *Chem. Biol.* **2010**, *17*, 1212. [Google Scholar] [CrossRef] [PubMed]
39. Versantvoort, C.H.; Oomen, A.G.; Van de Kamp, E.; Rompelberg, C.J.; Sips, A.J. Applicability of an in vitro digestion model in assessing the bioaccessibility of mycotoxins from food. *Food Chem. Toxicol.* **2005**, *43*, 31. [Google Scholar] [CrossRef] [PubMed]
40. Oomen, A.G.; Rompelberg, C.J.; Bruil, M.A.; Dobbe, C.J.; Pereboom, D.P.; Sips, A.J. Development of an in vitro digestion model for estimating the bioaccessibility of soil contaminants. *Arch. Environ. Contam. Toxicol.***2003**, *44*, 281. [Google Scholar] [CrossRef] [PubMed]
41. Fallingborg, J.; Christensen, L.A.; Jacobsen, B.A.; Rasmussen, S.N. Very low intraluminal colonic pH in patients with active ulcerative colitis. *Dig. Dis. Sci.* **1993**, *38*, 1989. [Google Scholar] [CrossRef] [PubMed]
42. Sasaki, Y.; Hada, R.; Nakajima, H.; Fukuda, S.; Munakata, A. Improved localizing method of radiopill in measurement of entire gastrointestinal pH profiles: Colonic luminal pH in normal subjects and patients with Crohn's disease. *Am. J. Gastroenterol.* **1997**, *92*, 114. [Google Scholar] [PubMed]

3.7 Supporting Information

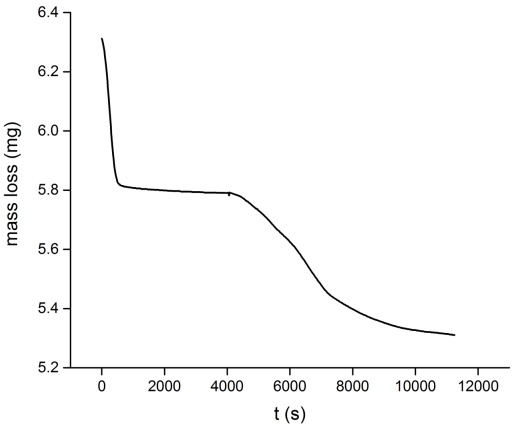

Figure SI-1. TGA curves of **S1** magnetic microparticles.

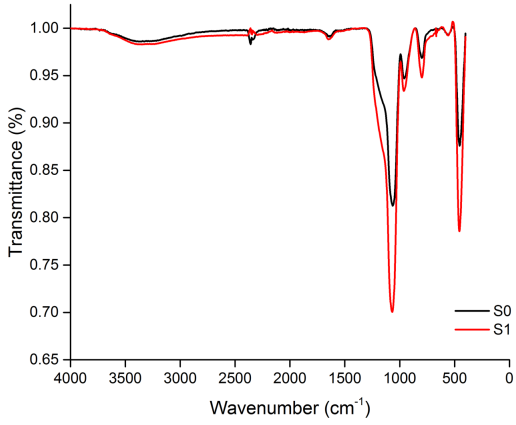

Figure SI-2. FTIR spectra of magnetic micro-sized inorganic solid (**S0**) and of the final loaded and capped microparticles (**S1**).

Chapter 4

Smart gated magnetic silica mesoporous particles for targeted colon drug delivery: New approaches for inflammatory bowel diseases treatment

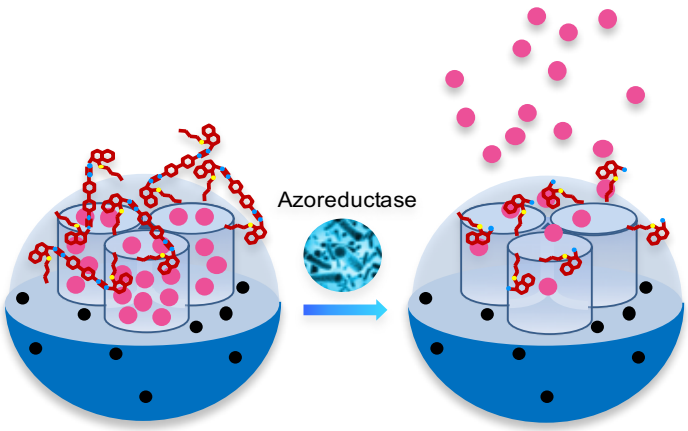

Smart gated magnetic silica mesoporous particles for targeted colon drug delivery: New approaches for inflammatory bowel diseases treatment

Adrián H. Teruel [a,b], Édgar Pérez-Esteve [a], Isabel González-Álvarez [c], Marta González-Álvarez [c], Ana M. Costero [a,b,d], Daniel Ferri [a,d], Margarita Parra [a,b,d], Pablo Gaviña [a,b,d], Virginia Merino [a,e], Ramón Martínez-Máñez [a,b,f,g,*] and Félix Sancenón [a,b,f,g]

[a] Instituto Interuniversitario de Investigación de Reconocimiento Molecular y Desarrollo Tecnológico (IDM), Universitat Politècnica de València, Universitat de València, Spain

[b] CIBER de Bioingeniería, Biomateriales y Nanomedicina (CIBER-BBN), Spain

[c] Departamento de Ingeniería, Sección de Farmacia y Tecnología Farmacéutica, Universidad Miguel Hernandez, Alicante 03550, Spain

[d] Departamento de Química Orgánica, Universitat de València, Doctor Moliner 50, Valencia 46100, Spain

[e] Departamento de Farmacia y Tecnologia Farmacéutica, Universitat de València, Valencia 46100, Spain

[f] Instituto de Investigación Sanitaria La Fe, Unidad Mixta de Investigación en Nanomedicina y Sensores, Universitat Politècnica de València, Valencia, Spain

[g] Unidad Mixta UPV-CIPF de Investigación en Mecanismos de Enfermedades y Nanomedicina, Centro de Investigación Príncipe Felipe, Universitat Politècnica de València, Valencia, Spain

Published online: 10 May, 2018

(Reprinted with permission from ***J. Control. Release*** **2018, 281, 58–69.**

4.1 Abstract

Magnetic mesoporous silica microparticles were loaded with safranin O (**S1**) and with hydrocortisone (**S2**) and the outer surface functionalized with a bulky azo derivative bearing urea moieties. Aqueous suspensions of both solids at pH 7.4 showed negligible payload release whereas a marked delivery was observed in the presence of sodium dithionite due to the rupture of the azo bonds. Besides, a moderate cargo release was observed at acidic pH due to the hydrolysis of the urea bonds that linked the azo derivative onto the external surface of the inorganic scaffolds. *In vitro* digestion models showed that **S1** and **S2** microparticles could be used for the controlled release of payload in the reducing colon environment (in which azoreductase enzymes are present). On the other hand, *in vivo* pharmacokinetic studies in rats showed that safranine O release from **S1** microparticles was concentrated in colon. The performance of **S2** microparticles for the treatment of colitis in rats (induced by oral administration of a 2,4,6-trinitrobenzenesulfonic acid solution) was tested. The controlled release of hydrocortisone from **S2** in the colon of injured rats induced marked reduction in colon/body weight ratio and in clinical activity score. Also, histological studies showed a marked decrease in inflammation followed by intensive regeneration and almost normal mucosal structure of the individuals treated with **S2**. Besides, the use of a magnetic belt increased the therapeutic performances of **S2** due to an enhanced retention time of the particles in the colon.

4.2 Introduction

Inflammatory bowel diseases (IBD) are autoimmune, inflammatory, chronic malignances affecting the gastrointestinal tract tissue, mainly the colon, which is a difficult area to treat [1–5]. Although the etiology of IBD is still unknown, some authors have reported that a mix of genetic, environmental factors and some dietetic habits may favor the establishment and proliferation of these diseases. There are two main diseases classified

as IBD, ulcerative colitis and Crohn's disease [3,4]. Ulcerative colitis affects exclusively the colon mucosa (first layer from the luminal face) and the injuries caused present a continuous distribution. Meanwhile, Crohn's disease affects all layers (transmural) along the gastrointestinal tract from the mouth until the last portion of the rectus, with injuries distributed in patches (injured areas surrounded by healthy areas). IBD have a big impact in our society since its incidence and prevalence is continuously increasing in both, developed and developing countries [6–8]. Most common treatments for IBD are based on non-specific anti-inflammatory drugs focused on the relief of ulcers and fissures or the damaged tissue [9–11]. These treatments present some disadvantages such as the presence of adverse effects or the low drug efficacy due to the drug systemic absorption in the first segment of the small intestine. Taking this into account, the development of new drug carriers for oral IBD treatment to decrease adverse effects and enhance drug efficacy is a research field with marked interest. With this aim, smart formulations for targeting colon such as pH-responsive biodegradable polymers, time-dependent formulations, pressure responsive systems, osmotic controlled materials, bioadhesive systems, enzyme triggered prodrugs or drugs coated with enzyme-sensitive polymers have been recently developed [12–14]. In fact, enzymes produced by colon microbiota (such as azoreductase, β-galactosidase, β-xylosidase, nitroreductase, glycosidase deaminase) are ideal candidates to be used as external triggers in the preparation of smart controlled release carriers [15–17].

From another point of view, the blending of material and supramolecular chemistry concepts has resulted in recent years in the development of innovative examples of smart hybrid organic-inorganic micro or nanodevices able to perform programmed functions [18]. In the vast realm of these smart nanodevices those equipped with “molecular gates” are highly appealing because allow mass transport upon application of an external trigger [19]. These “gated materials” are generally formed by two components: (i) an inorganic porous support, which is able to entrap selected chemicals, and (ii) supramolecular or (bio)molecular entities, grafted onto the outer surface, which control cargo release upon application

of an external stimuli [20]. Dealing with the inorganic supports mesoporous silica has been extensively used for the preparation of these "gated materials". This is due to its positive features, such as relatively well-known functionalization chemistry, inertness, chemical stability, presence of controlled pore diameter within the nanometric range (ca. 2–3 nm), and large specific surfaces (up to 1200 m^2 g^{-1}) and specific volumes [21]. Besides, mesoporous silica can be prepared in the form of nano or microparticles. A high number of gated materials containing different payloads and able to selectively deliver their cargo upon application of chemical, physical or biochemical stimuli have been reported [19]. In fact, the incorporation of gate-like ensembles on the external surface of mesoporous silica particles is a suitable and promising approach to design devices with applications in controlled release protocols in biological, pharmaceutical and medical fields [22,23]. "Gated materials" have mainly been used for drug delivery applications, and the preparation of carriers able to release certain drugs on the site of action at-will, minimizing secondary effects is a benchmark in the treatment of different diseases. Gated mesoporous supports have also been applied recently in sensing/ recognition protocols and in chemical communication networks [24–26]. However, it is also apparent from the literature that, gated hybrid organic-inorganic materials have not been used for the development of smart formulations for IBD treatment.

Bearing in mind our interest in the development of silica-based gated materials for controlled release applications [27–34], we report herein the preparation of micro-sized silica mesoporous solids containing magnetic nanoparticles (**S1** and **S2**) as potential systems designed to release an entrapped cargo in colon. The magnetic character of the solids may be useful to enhance the retention time of the particles in the part of interest of the intestinal tract (ileum or colon). Particles **S1** and **S2**, contained a dye (safranin O) and a model drug (hydrocortisone) in the pores were capped with a bulky azo derivative by means of a urea bond. We demonstrated that the presence of bulky azoderivatives onto the external surface of **S1** and **S2** inhibited cargo delivery yet both solids were able to deliver their cargo in the presence of a reducing agent (sodium dithionite) and to some extent at

acidic pH (due to partial hydrolysis of urea bonds that linked the azo derivative onto the inorganic support). Studies on cargo delivery from **S1** in a simulated digestive process in mouth, stomach, small intestine and colon is also reported. Finally, *in vivo* studies with **S1** were also performed to check the pharmacokinetics of this new nanodevice and **S2** was used to prove its efficacy in an *in vivo* ulcerative colitis model.

4.3 Materials and Methods

4.3.1. Chemicals

The chemicals tetraethylorthosilicate (TEOS), n-cetyltrimethyl-ammonium bromide (CTABr), sodium hydroxide, triethanolamine ($TEAH_3$), (3-isocyanatopropyl)triethoxysilane, iron(III) chloride hexahydrate, iron(II) chloride tetrahydrate, oleic acid, safranin O, triethylamine, Congo red, sodium dithionite, hydrocortisone, and 2,4,6-trinitrobenzenesulfonic acid solution (TNBS), were provided by Sigma-Aldrich. Disodium hydrogen phosphate, sodium dihydrogen phosphate, potassium dihydrogen phosphate, sodium chloride, potassium chloride, sodium acetate anhydrous and all the analytical-grade solvents were purchased from Scharlab. Isoflurane, pentobarbital (dolethal®) was acquired from the animal facilities. All products were used as received.

4.3.2. Synthesis of oleic acid-coated magnetic nanoparticles (MNPs)

MNPs were prepared using a modified co-precipitation method. In a typical procedure, $FeCl_3 \cdot 6H_2O$ (24.0 g, 0.089 mol) and $FeCl_2 \cdot 4H_2O$ (9.8 g, 0.049 mol) were dissolved in deionized water (100 mL) under nitrogen atmosphere with vigorous stirring at 80 °C. Then ammonium hydroxide (50 mL) was added quickly into the solution. The color of the solution immediately turned black and then oleic acid (3.8g, 0.013 mol) was added after 30 min. The reaction was kept at 80 °C for 1.5 h. The final oleic acid-coated MNPs were washed with deionized water until neutral pH.

Afterward, the MNPs were transferred into a chloroform solution (30 mg MNPs/mL $CHCl_3$).

4.3.3. Synthesis of mesoporous silica microparticles containing MNPs (S0)

A chloroform suspension of MNPs (6 mL, 30 mg MNPs/mL $CHCl_3$) was mixed with an aqueous solution of CTABr (8 mL, 10 mg/mL) and the resulting mixture was homogenized (using a sonicator) and heated. Finally, the suspension was sonicated again and passed through nylon filters (0.45 μM) to ensure MNPs homogeneity. Magnetic micro-sized MCM-41 particles were synthesized following the so-called "atrane route". For this purpose, a solution of $TEAH_3$ (25.79 g, 0.173 mol) and NaOH (2 mL of a 6 M solution) was heated to 120 °C and then cooled down to 70 °C, at this moment TEOS (11 mL, 0.045 mol) was added and the crude reaction was heated up to 120 °C. The crude reaction was left cooling down again and CTABr (4.68 g, 0.013 mol) was added at 118 °C. Next, water containing MNPs (74 mL of distilled water +6 mL of the MNPs CTABr-water suspension) was slowly added with vigorous stirring at 70 °C. Besides, NaOH (10 mL of a 0.1 M solution) was added to obtain a pH ≈ 10.9. After a few minutes, a brownish suspension was formed. This mixture was aged in an autoclave at 100 °C for 24 h. The resulting powder was collected by filtration and washed with water. Finally, the solid was dried at 70 °C. To prepare the final solid (**S0**), the as-synthesized microparticles were calcined at 550°C using oxidant atmosphere for 5 h in order to remove the template.

4.3.4. Synthesis of 1

Congo red (**1a** in Scheme 2, 8.1 g, 10 mmol) was dissolved in anhydrous N,N-dimethylformamide (120 mL) and then (3-Isocyanato-propyl)triethoxysilane (**1b** in Scheme 2, 5.21 mL, 20 mmol) and trimethylamine (2 droplets) were added under argon atmosphere. The crude reaction was allowed to react for 36 h at 100 °C. The solvent was eliminated in a rotary evaporator and the final product **1** isolated as dark

red oil (11.4 g, 10 mmol, 96% yield). ^{1}H NMR (400 MHz, DMSO-D6): δ = 8.79 (d, 2H), 8.47 (d, 2H), 8.36 (s, 2H), 8.12 (d, 4H), 7.96 (d, 4H), 7.78 (br s, 2H), 7.61 (t, 2H), 7.51 (t, 2H), 5.83 (br s, 2H), 3.73 (q, 12H), 2.93 (m, 4H), 1.40 (m, 4H), 1.14 (t, 18H), 0.51 (t, 4H) ppm; ^{13}C: δ = 158.3, 152.4, 145.9, 140.1, 132.4, 131.9, 129.1, 128.3, 127.5, 125.0, 124.4, 123.9, 122.9, 118.3, 57.8, 56.2, 42.2, 23.8, 18.5, 18.2, 7.4 ppm. HRMS-EI m/z: calcd for $C_{52}H_{64}N_8O_{14}S_2Si_2$ 572.1766; found: 544.3443 (M-2 EtOH from the trialkoxysilane group).

4.3.5. Synthesis of S1

MCM-41 magnetic mesoporous silica microparticles (**S0**, 160 mg) were suspended in an acetonitrile solution (10mL) of safranin O (45 mg, 0.8 mmol/g **S0**) under argon atmosphere. The obtained suspension was then stirred at room temperature overnight. Afterward, **1** (1.89 g, 10 mmol/g **S0**) was dissolved in anhydrous N,N-dimethylformamide (25mL) and was added to the microparticle/dye suspension. The mixture was stirred at room temperature for 6h in an argon atmosphere. **S1** was isolated as a dark red solid, after several DMF and H_2O washes, by centrifugation and was dried at 40 °C for > 24 h.

4.3.6. Synthesis of S2

MCM-41 magnetic mesoporous silica microparticles (**S0**, 330 mg) were impregnated with 3.34 mL of a hydrocortisone ethanolic solution (15 mg/mL) in a 2 cycles impregnation procedure. At this respect, 330 mg of **S0** were sunk in 1.67 mL of hydrocortisone ethanolic solution. Then the particles were left drying at 40 °C for 30 min (this step was performed two-times). Afterward, **1** (3.9 g, 10 mmol/g **S0**) was dissolved in a DMF-water 95:5 v/v solution (50 mL) and was added to the loaded microparticles. The mixture was stirred at room temperature for 6h. **S2** was isolated as a red solid, after several ethanol and H_2O washes, by centrifugation and was dried at 60 °C overnight.

4.3.7. Characterization

Transmission electron microscopy (TEM), scanning transmission electron microscopy (STEM), powder X-ray diffraction (PXRD), thermogravimetric analysis (TGA), N_2 adsorption-desorption, nuclear magnetic resonance (NMR), Fourier transform infrared spectroscopy (FT-IR) and high-performance liquid chromatography (HPLC) techniques were employed to characterize the synthesized materials. TEM and STEM images were acquired using a JEOL JEM-1010 and a JEOL JEM 2100F microscopes, respectively. PXRD measurements were performed on a Bruker D8 Advance diffractometer using CuKα radiation. TGA were carried out on a TGA/SDTA 851e Mettler Toledo balance, using an oxidant atmosphere (air, 80 mL/min) with a heating program consisting on a heating ramp of 10 °C per minute from 393 to 1273 K and an isothermal heating step at this temperature for 30 min. N_2 adsorption-desorption isotherms were recorded with a Micromeritics ASAP 2010 automated sorption analyzer. The samples were degassed at 120 °C under vacuum overnight. The specific surface areas were calculated from the adsorption data in the low pressure range using the Brunauer–Emmett–Teller (BET) model. Pore size was determined following the Barrett-Joyner-Halenda (BJH) method. 1H NMR spectra were recorded using a Bruker AV400 spectrometer. Infrared spectra were recorded using a Bruker Tensor 27 equipment. The HPLC instrument consisted of a Hitachi LaChrom Elite liquid chromatograph (Hitachi Ltd., Tokyo, Japan) equipped with an auto-sampler (module L-2200), UV detector (model L-2400) and a Kromaphase 100 C18 (150 mm × 4.6 mm i.d., 5-μm particle size analytical column (Scharlab, Barcelona, Spain) was used for separations.

4.3.8. Release Studies

Controlled release studies from S1 and S2 were performed at different pH values (i.e. 2.0, 4.5 and 7.4) and in the presence of a reductive environment (sodium dithionite, which is known to reduce azo linkages). In a typical experiment, 2 mg of the corresponding solid were suspended in

water at the selected pH (2 mL) and aliquots were extracted at given times (0, 5min, 20min, 40min, 1h, 2h, 4h, 6h, 8h, and 24h) and centrifuged to remove the solid before analyzing. Controlled release experiments were done in triplicate in order to obtain standard deviation values.

Controlled release from **S1** and **S2** microparticles was also tested under *in vitro* digestion conditions using simulated solutions for saliva, gastric juice, duodenal juice and bile. *In vitro* digestion experiments were carried out with **S1** and **S2** (2 mg) at 37 °C (temperature of the human body) and stirring at 100 rpm (in order to ensure the correct suspension of the microparticles). Digestions started by adding simulated saliva fluid (320 µL) and incubating for 5 min. Then, simulated gastric juice (630 µL) was added, and the mixture was stirred for 2 h. Later, simulated duodenal juice (630 µL), bile (320 µL) and a bicarbonate solution (1 M, 100 µL) were added simultaneously and the mixture was stirred for another 2 h. Finally, colon fluid was simulated by adding sodium dithionite (2 mg/mL). Aliquots were taken at given times from the beginning of the assay (0, 5, 20, 35, 65, 95, 125, 155, 185, 215, 245, 260,275, 305, 365, 425, 485, 1320 and 1685 min), centrifuged and then analyzed.

To quantify the amount of cargo released **S1** supernatants were loaded into 96 well plate to measure safranin O fluorescence at 571 nm (excitation at 520 nm). For **S2** samples, supernatants were analyzed by HPLC to measure the hydrocortisone released. Calibration curves were used to assess the amounts of safranin O and hydrocortisone released from solids **S1** and **S2** in the different environments tested.

4.3.9. Hydrocortisone quantification

Hydrocortisone was determined by reversed-phase HPLC according to the method described by Navarro and co-workers with several modifications [35]. The HPLC instrument consisted of a Hitachi LaChrom Elite liquid chromatograph (Hitachi Ltd., Tokyo, Japan) equipped with an auto-sampler (module L-2200) and UV detector (model L-2400). A Kromaphase 100 C18 (150 mm × 4.6 mm i.d., 5-µm particle size analytical column) (Scharlab, Barcelona, Spain) was used for separations. The

mobile phase consisted of (A) water and (B) acetonitrile. The program was isocratic for 15 min with 70% A and 30% B. The wavelength of the UV detector was set at 245 nm. Hydrocortisone was quantified according to the external standard method (since no matrix effect was observed) using a calibration curve of the peak area against the compound concentration. The applicability of this method was evaluated by performing a recovery study. For this purpose, digestion fluids were fortified with hydrocortisone at five different concentration levels. In all cases, recovery values, which were estimated from measured versus added amounts of hydrocortisone, were close to 100%. Thus, the results obtained demonstrated the applicability of the proposed methodology for the accurate determination of hydrocortisone in the different fluid samples.

4.3.10. *In vivo* pharmacokinetic studies

Male Wistar rats were used in accordance with 2010/63/EU directive of 22 September 2010 regarding the protection of animals used for scientific experimentation. The Ethics Committee for Animal Experimentation of the University approved the experimental protocols (Spain, code A1330354541263). Male Wistar rats weighing 300 ± 30 g were anesthetized as described in in situ perfusion to allow cannula implantation 24h before the experiment. A previously described jugular vein permanent cannulation method was used [36]. The implanted cannula allows blood sampling. The animals were randomly assigned (n = 10 to 12) to the following groups: Group 1: A volume of 1 mL of safranin O solution (150 μg/mL saline) was given orally. Group 2: A volume of 1.75 mL of a suspension containing 60 mg of **S1** (that should release ca. 150 μg of safranin O) was given orally. Group 3: A volume of 1.75 mL of a suspension containing 60 mg of **S1** (that should release ca. 150μg of safranin O) was given orally. In addition, the subjects in this group wore a magnetic belt in the lower part in the waist to increase the retention time of the microparticles in the last segment of the bowel.

Blood samples (0.6–0.7 mL) were withdrawn with heparinized syringes, and replaced by heparinized saline (10 IU/mL) at established sampling

times (t=15′, 30′, 45′, 1h, 2h, 3h, 4h and 5h). Plasma was immediately separated by centrifugation (10,000 rpm for 10 min) and then frozen at −20 °C until analysis. At the end of the 5 h the subjects were sacrificed and the cecum, colon and feces were collected and processed to analyze the presence of safranin O. Cecum, colon and feces were separated, suspended into buffer solution (phosphate, pH 6.8), and then centrifuged. Samples were taken and analyzed by HPLC (Waters Alliance® e2695, Milford, MA, USA) with fluorescence detector using 520 and 585 nm as excitation and emission wavelengths (Waters 2486, Milford, MA, USA). As mobile phase acetonitrile:water 30:70 v/v with 1% of trifuoroacetic acid was used. A Novapack C18 (WATERS®) cartridge-type column (5 µm, 4 mm × 200 mm) was used. Temperature was set at 25 °C, 50 µL of injection volume were used and a flow of 1 mL/min was fixed. The method was previously validated with adequate linearity, precision and accuracy (R > 0.99 and coefficient of variation < 5%).

4.3.11. *In vivo* efficacy studies. Induction of colonic inflammation

The studies reported here adhere to the Principles of Laboratory Animal Care and were approved by the institutional ethics committee of the University of Valencia (Spain) according to RD 1201/2005. These studies were carried out on male Wistar rats aged 8–12 weeks and weighing 275–325 g. Animals were housed in an air-conditioned room at 22 ± 3 °C, 55 ± 5% humidity, 12 h light/dark cycles and allowed free access to water and laboratory chow for the duration of the studies. To induce the model of chronic inflammation in the rat colon, the method described by Morris and co-workers was followed with several slight modifications [37]. Briefly, rats were arbitrarily separated into treatment groups, with free access to water and then anesthetized with isoflurane. A graduated rubber canula was inserted rectally into the colon in such a way that the tip was 8 cm proximal to the anus. Then, 0.6 mL of a solution of TNBS (78 mg/kg body weight) dissolved in 50% ethanol (v/v) was instilled into the lumen of the colon through the rubber probe (total volume 0.6 mL solution). The induction and

development of inflammation was monitored every day during the 10 days that lasted the assays.

4.3.12. Treatment studies design

Rats were divided into 5 groups: Group 1 (positive control group, 3 rats) was administered with saline solution (1.5 mL). Group 2 (8 rats) received a suspension of **S0** microparticles (60 mg in 1.5 mL of saline). Group 3 (8 rats) received a hydrocortisone solution (1.5 mg in 1.5 mL of saline). Group 4 (8 rats) received a suspension of **S2** microparticles (60 mg in 1.5 mL of saline). Group 5 (4 rats) received a suspension of **S2** (60 mg in 1.5 mL of saline) and a magnetic belt was attached to the waist of each rat.

The dose of hydrocortisone that received groups three to five, 5.58 mg/kg/day, was calculated from the dose administered to humans [38]. All administrations were done by means of an oral gavage, once a day for three days in the period of the most intensive inflammation (days 3, 4 and 5 after TNBS administration).

4.3.13. Assessment of colonic injury and inflammation

During the 10 days that lasted the assay animals were monitored and clinical activity score of colitis was calculated. At day 10 (after TNBS administration) the rats were killed with an overdose of anesthesia (dolethal®) then the abdomen was opened and the distal colon was removed. The samples of inflamed tissue were excised to measure the ratios of distal colon weight to body weight (colon/body ratio) and later a histological evaluation was carried out.

4.3.14. Clinical activity score system

Colitis activity was quantified with a clinical score assessing weight loss, stool consistency and rectal bleeding [39,40].

Control	Range	Score
% Weight loss	< 1%	0
	1–5%	1
	5–10%	2
	10–20%	3
	> 20%	4
Stool consistency	Well-formed pellets	0
	Pasty and semi-formed stools	2
	Liquid stools or absence	4
Bleeding	No blood	0
	Positive finding	2
	Gross bleeding	4

The sum of these scores formed the clinical score that ranges from 0 (healthy) to 12 (maximal activity of colitis). Rats that died or had to be sacrificed before day 10 were given a score of 12.

4.3.15. Determination of colon/body weight ratio

Once the animals were sacrificed, the abdomen was opened and the distal colon was rapidly excised and opened longitudinally along the mesenteric edge. The colon was washed with 0.9% (w/v) saline and placed with the mucosal surface upward over a glass plate and then weighted [41]. The ratio of the 8 cm segment distal colon weight was calculated as an index of colonic tissue edema.

4.3.16. Myeloperoxidase activity

The activated neutrophils into the inflamed tissue has peroxidase enzyme substantially expressed. For this reason, myeloperoxidase activity can be measured as index of inflammation. Myeloperoxidase activity was analyzed according to established method with some modification [42]. Colon tissue in presence of 750 µL of HTAB buffer (0.5% in 80 mM phosphate buffer pH 5.4) on ice was homogenized and centrifuged (−4 °C,

10,000 rpm) during 15 min. Supernatant was taken and incubated at 37 °C during 5 min with the mixture: 75 μL of phosphate buffer pH 7.4, 10 μL of phosphate buffer pH 5.4 and 0.026% hydrogen peroxide (10 μL). After that, 20 μL of TMB 18 mM (dissolved in 8% DMF) were added to the previous mixture and intubated. The reaction was stopped after 10 min by the adding of 15 μL of H_2SO_4 2 N. Myeloperoxidase activity was determined in the supernatant by spectrophotometric measures at 450 nm.

4.3.17. Histological evaluation

Two tissue samples (3 cm distal and proximal samples) were excised from each colon and maintained in paraformaldehyde (4%, v/v) for 24 h and then changed to a paraformaldehyde (0.4%, v/v) medium for microscopic studies. These tissue samples were processed routinely and embedded in paraffin. Longitudinal sections (5 μm) were stained with hematoxylin and eosin. Microscopic assessment by light microscope was performed blind on coded slices.

4.3.18. Statistical analysis

To compare the clinical activity score and the colon/body weight ratio between groups the t-student test was performed using SPSS version 22.0 for Windows (SPSS Inc., USA).

4.4 Results and discussion

4.4.1. Synthesis of gated magnetic micro-sized mesoporous silica particles

Magnetic nanoparticles (MNPs) coated with oleic acid were prepared by a co-precipitation procedure that used a mixture of $FeCl_3$ and $FeCl_2$ and ammonium hydroxide [43]. Moreover, mesoporous silica was prepared following the “atrane route” with small modifications [44,45]. In this synthetic

protocol n-cetyltrimethylammonium bromide (CTABr) was used as structural directing agent and tetraethylortosilicate (TEOS) as silica source. MNPs were suspended in water and incorporated into the synthesis crude before the addition of NaOH. The resulting brownish powder was washed and the surfactant was subsequently removed by calcination. This procedure yielded the final magnetic mesoporous silica micro-sized inorganic solid (**S0**). Once the magnetic mesoporous support was synthesized, the pores of the siliceous phase were loaded with safranin O or hydrocortisone (as a model drug in our study) and the external surface functionalized with the bulky azo derivative **1**. This synthetic protocol yielded micro-sized magnetic solids **S1** and **S2** (see Scheme 1). It was expected that the bulky azo derivative **1** would inhibit the leaching of the cargos from the pores. Moreover, cargo delivery was expected to be observed in the presence of sodium dithionite (able to broke azo linkages) or partially at acidic pH (due to partial hydrolysis of the urea moiety that linked azo derivative **1** onto the external surface of the inorganic support).

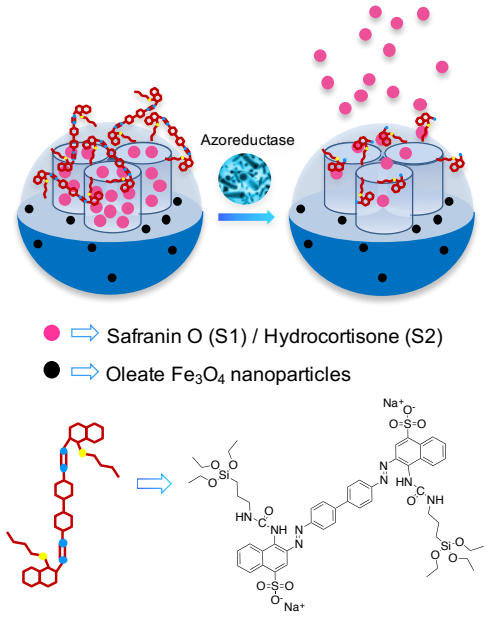

Scheme 1. Magnetic micrometric silica mesoporous support loaded with safranin O (**S1**) or hydrocortisone (**S2**) and capped with a bulky azo derivative. Safranin O or hydrocortisone were released in the presence of an azoreductor.

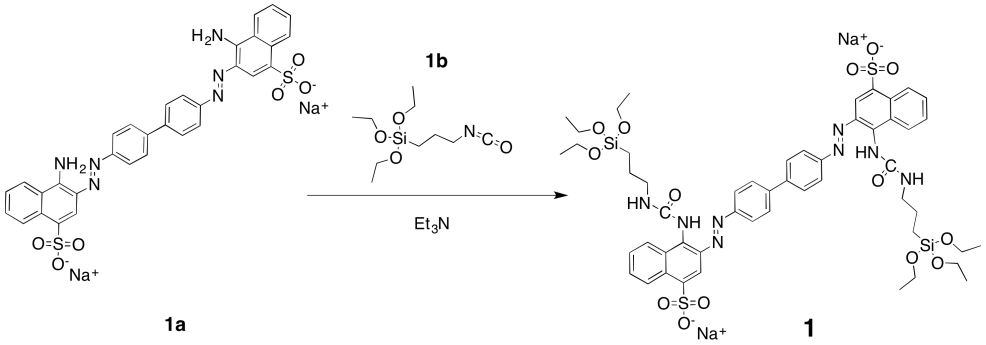

Scheme 2. Synthetic route for the preparation of **1**.

Azo derivative **1** was obtained in a one-step procedure (Scheme 2) reacting Congo red (**1a**) with (3-isocyanatopropyl)triethoxysilane (**1b**). The final azo derivative containing a trilakoxysilane moiety (**1**) was fully characterized using ^{1}H and ^{13}C NMR and HRMS.

4.4.2. Characterization of the materials

All the prepared materials were characterized using powder X-ray diffraction (PXRD), transmission electron microscopy (TEM), scanning transmission electron microscopy (STEM), N_2 adsorption-desorption isotherms and thermogravimetric measurements. Fig. 1 shows the PXRD patterns (at high and low angles) of oleate-stabilized MNPs, the magnetic mesoporous microparticles as-made, **S0**, **S1** and **S2**. PXRD of oleate-coated MNPs (see Fig. 1) showed the five typical high-angle reflections of magnetite phase indexed as (220), (311), (400), (511) and (440) Bragg peaks. The same peaks were observed for the as-made microparticles, **S0**, **S1** and **S2** materials but with a marked decrease in intensity (see again Fig. 1). This intensity loss was ascribed to the inclusion of MNPs into the inorganic mesoporous matrix. Low angle PXRD pattern of as-made microparticles (Fig. 1) displayed the typical reflections of a hexagonal-ordered mesoporous system that can be indexed as (100), (110), (200) and (210) Bragg peaks. A shift of the (100) peak in calcined **S0** solid was clearly observed. This displacement is consistent with an approximate cell

contraction of 3.64 Å and is attributed to the condensation of silanol groups during the calcination step. The presence of the characteristic (100) reflection in the diffraction pattern of **S1** and **S2** clearly indicated that the mesoporous structure was preserved throughout the filling process with safranin O (**S1**) or hydrocortisone (**S2**) and the anchoring of the azo derivative **1** onto the external surface of the microparticles.

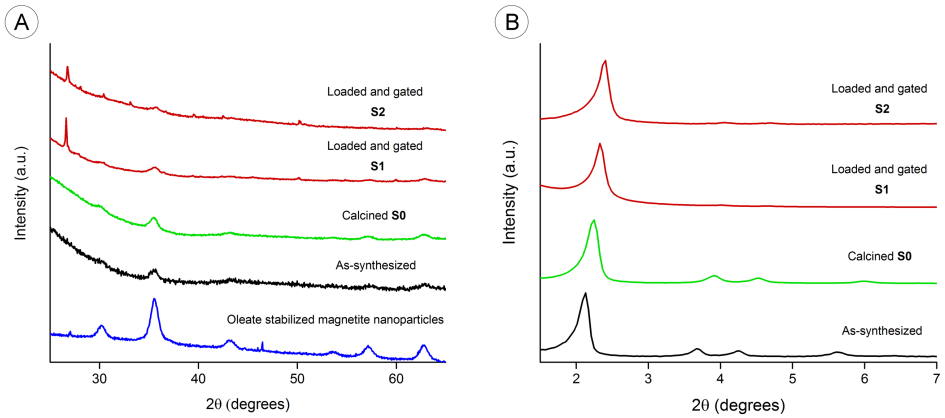

Fig 1. Powder X-ray patterns at A) high angles and B) low angles of oleate-stabilized MNPs, magnetic micrometric mesoporous silica particles as-synthesized, **S0**, **S1** and **S2**.

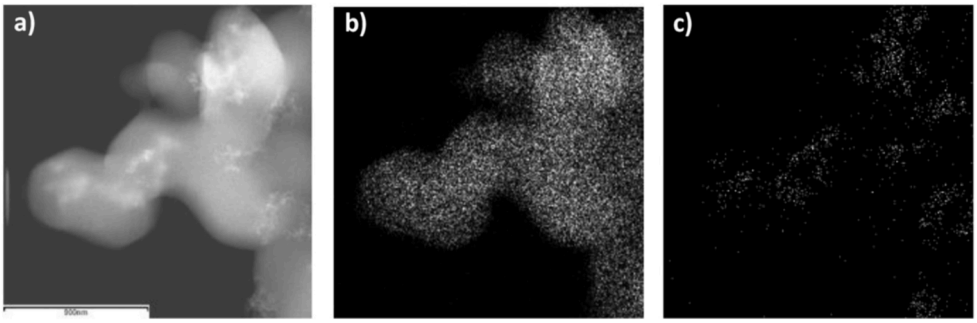

Fig 2. (a) STEM images of **S0** microparticles, (b) silica mapping, and (c) iron mapping.

TEM images of solid **S2** showed the typical porosity associated with MCM-41 mesoporous silica (see Supporting information). Besides, MNPs were observed, as small dark dots randomly distributed. STEM images of

solid **S0** (iron mapping) indicated that MNPs are uniformly distributed through the mesoporous silica microparticles (Fig. 2). Moreover, in order to assess the magnetic behavior of **S0**, field dependent magnetization curves measured at 298 K were obtained. The curves displayed no hysteresis loops and showed coercivity values near zero, in agreement with a typical superparamagnetic behavior at room temperature. The saturation magnetization value for **S0** was 1.5 emu/g. This magnetization value is close to those reported in the literature for other magnetic mesoporous silica particles, which are typically in the 1.7–10 emu/g range [43].

Table 1. BET specific surface area values, pore volumes and pore sizes for **S0**, **S1** and **S2**.

	S_{BET} ($m^2\,g^{-1}$)	Pore volume[a] ($cm^3\,g^{-1}$)	Pore size[a,b] (nm)
S0	1097	0.95	2.66
S1	552	0.43	–
S2	355	0.17	–

[a] Total pore volume according to the BJH model.

[b] Pore size estimated by using the BJH model applied on the adsorption branch of the isotherm, for $P/P_0 < 0.6$, which can be associated to the surfactant generated mesopores.

N_2 adsorption-desorption studies on **S0**, **S1** and **S2** were also carried out (see Supporting Information). Solid **S0** showed a typical curve for mesoporous silica materials, with an adsorption step at intermediate P/P_0 values (0.2–0.4). The isotherm was classified as type IV in which the absorption step deals with nitrogen condensation inside the mesopores. The pore diameter of **S0** was calculated using the Barret-Joyner-Halenda (BJH) method [46]. The narrow BJH pore distribution observed and the absence of a hysteresis loop in the 0.2–0.4 P/P_0 interval suggested the existence of uniform cylindrical mesopores. Values of pore diameter of 2.66 nm and pore volume of 0.95 $cm^3\,g^{-1}$, calculated on the adsorption branch of the isotherm, were found. Pore diameter estimated from TEM images agree with this value. The application of the Brunauer–Emmett–Teller (BET) model gave a value of 1097 $m^2\,g^{-1}$ for the total specific surface area [47].

On the other hand, the N_2 adsorption-desorption isotherms of solids **S1** and **S2** are typical of mesoporous systems with partially filled mesopores, and a significant decrease in both the adsorbed N_2 volume and the specific surface was clearly observed (Table 1). This reduction in the BET surface, compared with that of **S0**, was ascribed to the loading of pores with safranin O (**S1**) or hydrocortisone (**S2**) and the functionalization of the external surface with the bulky azo derivative **1** (for both solids).

Table 2. Content of total organic matter (in g) per gram of SiO_2, content of azo derivative (in g) per gram of SiO_2 and dye/drug released (in μg) per mg of solid in **S1** and **S2**.

Solid	Organic content (g/g SiO_2)	Gate (g/g SiO_2)	Dye/drug release (μg/mg solid)
S1	0.19	0.13	2.4
S2	0.41	0.15	28.1

Total organic matter on solids **S1** and **S2** was determined by thermogravimetric analysis and ^{1}H NMR (Table 2). The amount of azo derivative anchored onto **S1** and **S2** was determined by ^{1}H NMR upon dissolving the corresponding sample in NaOD/D_2O in the presence of tetraethyl ammonium bromide as internal standard [48]. The organic content in solid **S1** was lower than that found in **S2**. This is consistent with the higher specific surface observed for **S1** (see Table 1) and suggests that loading hydrocortisone into the pores of the inorganic scaffold was more effective than that for safranin O (to obtain **S1**).

FT-IR analysis comparing the calcined framework (**S0**) with the loaded and gated material (**S2**) were carried out to confirm the functionalization of the material (see Supporting Information). **S0** microparticles presented two main bands at 1062 and 954 cm^{-1} that corresponds to Si-O-Si stretching vibrations. Both bands were also present in the FT-IR spectrum of **S2** microparticles. Besides, **S2** also showed signals at 2935 and 2877 cm^{-1} typical of CeH stretching vibrations and attributed to the loaded hydrocortisone and the grafted azo derivative **1**. Moreover, the typical carbonyl (from the urea that linked **1** onto the external surface of the

inorganic scaffold) and azo stretching vibrations appeared at 1635 and 1562 cm^{-1} in **S2** microparticles.

4.4.3. Cargo release from S1 and S2

Payload release from solids **S1** and **S2** at acidic (2.0 and 4.5) and neutral (7.4) pH was tested. Besides, the controlled release behavior of both solids at neutral pH (7.4) in the absence or presence of the reducing agent sodium dithionite was also studied [49,50]. These pH values were selected taking into account the possible use of **S2** as vehicle for controlled release in colon and inflammatory bowel disease scenarios. At this respect, pH 2.0 is typical of gastric juices, pH 4.5 is found in the transition from stomach to intestines (this pH can also be found in stomach in fed conditions and in the colon of IBD patients), whereas pH 7.4 is typically found in the intestine. On the other hand, sodium dithionite mimics the presence of azoreductase enzymes on the colon. Cargo release profile for solid **S1** and **S2** are shown in Figs. 3 and 4.

As could be seen in Fig. 3, aqueous suspensions of **S1** showed negligible safranin O release at neutral pH. However, as a clear contrast, a marked delivery of entrapped safranin O was seen in the presence of sodium dithionite, showing a sustained release profile that reaches ca. 80% of maximum dye delivered after 4 h. The observed delivery is attributed to the sodium dithionite, which is able to reduce azo groups in the capping molecule **1** resulting in pore opening and safranin O release. At pH 4.5, **S1** showed a low dye delivery (ca. 20% of maximum dye released after 8 h). At pH 2.0, safranin O delivery reaches 60% of the maximum drug release after 8 h. The observed release at acidic pH is attributed to the hydrolysis of urea group in highly acidic environment. Maximum release of safranin O from **S1** was 2.4 μg/mg solid at pH 7.4 in the presence of a reducing agent. For **S2** solid, a nearly “zero” release of hydrocortisone at pH 7.4 was observed whereas a sustainable delivery of the drug (ca. 75% of maximum hydrocortisone release after 6 h) was produced in the presence of sodium dithionite (see Fig. 4). Again, cargo release was ascribed to the reduction of the azo bond by the reducing agent. However, in contrast with the

controlled release behavior of **S1** in acidic environments, a “zero” release of hydrocortisone at pH 4.5 and 2.0 was observed. Maximum release of hydrocortisone from **S2** was 28.1 µg/mg solid at pH 7.4 in the presence of a sodium dithionite. This different behavior is tentatively attributed to the lower solubility of hydrocortisone at acidic pH when compared with safranin O.

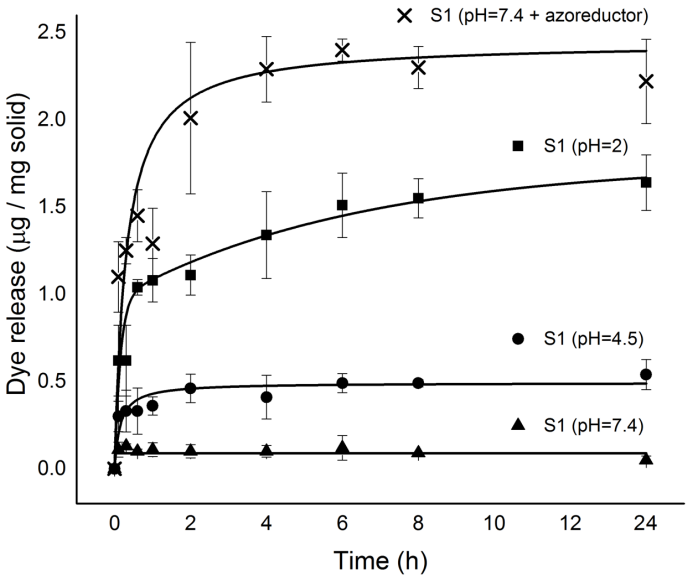

Fig. 3. Release kinetics of safranin O from **S1** in aqueous solution at pH ≈ 2 (square), pH ≈ 4.5 (circle), pH ≈ 7.4 (triangle) and pH ≈ 7.4 in the presence of sodium dithionite (2 mg/mL) (cross).

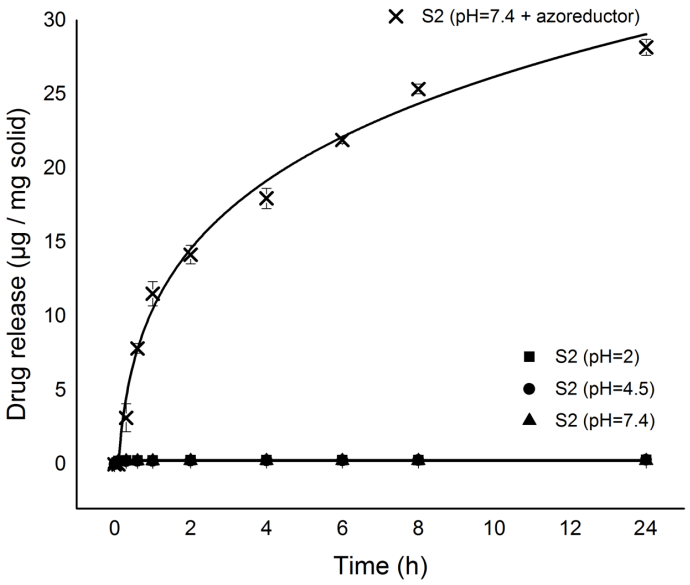

Fig. 4. Release kinetics of hydrocortisone from **S2** in aqueous solution at pH≈2 (square), pH≈4.5 (circle), pH≈7.4 (triangle) and pH≈7.4 in the presence of sodium dithionite (2 mg/mL) (cross).

4.4.4. *In vitro* digestion model assay

Despite the partial payload delivery from **S1** at acidic pH shown above, it has to be noted that permanence of the particles in the stomach is usually < 2h and therefore only a partial cargo delivery is expected to occur before targeting colonic tissues. In fact, in order to study more in-depth, the possible application of the prepared magnetic microparticles as suitable carriers for cargo delivery in colon, payload release from **S1** was further tested in a model of digestion using simulated solutions. The model used was a modification of the introduced by Oomen and co-workers which is a three-step procedure simulating digestive process in mouth, stomach and small intestine [51,52]. Moreover, we introduced a fourth step to simulate the digestive process in colon. The results obtained with **S1** microparticles are shown in Fig. 5.

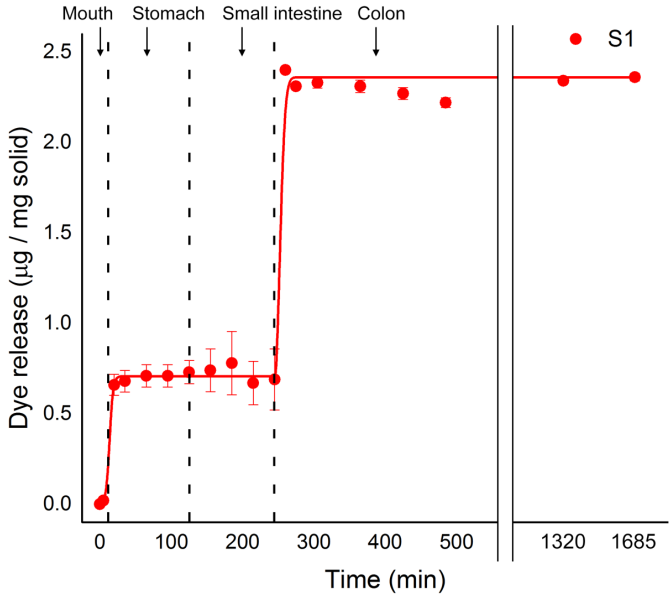

Fig. 5. Release kinetics of safranin O from **S1** in simulated GIT fluids.

As could be seen in Fig. 5, a nearly "zero release" was observed during the first 5 min in which the solid was in contact with simulated saliva. However, a moderate cargo release (0.6 µg/mg of safranin O for **S1**) was observed in the stomach due to partial pore opening (hydrolysis of the urea bond that linked the bulky azo derivative onto the microparticle surface) in the acidic environment of this part of the GIT. In conditions simulating small intestine, no further delivery of safranin O was observed. Finally, a marked cargo release was found in simulated colon conditions (1.8 µg/mg of safranin O for **S1**). This marked delivery observed is clearly related with the presence of sodium dithionite, which is able to reduce azo bonds of the capping ensemble in **S1** microparticles.

4.4.5. *In vivo* pharmacokinetics studies

To prove the specific colon delivery and quantify cargo release from the synthesized microparticles in plasma and colon, *in vivo* pharmacokinetic studies were carried out. For this purpose, male Wistar rats were divided into three groups (see section 4.3.10 in Materials and methods). Rats in

group 1 were treated with 1 mL of safranin O solution (150 μg/ mL saline). The subjects from group 2 were treated with 1.75 mL of a suspension of **S1** microparticles (containing 60 mg of solid that releases ca. 150 μg of safranin O). Finally, group 3 rats were subjected to the same treatment than those in group 2 but, in addition, a magnetic belt in the lower part of the waist was implemented in order to increase the retention time of the microparticles in the last segment of the bowel due to the presence of magnetic nanoparticles in **S1**. Safranin O concentrations in plasma are shown in Fig. 6. As could be seen, subjects from group 1 (that received the safranin O solution) showed high plasma levels of the dye (maximum value was ca. 0.35 μg/mL after 30 min). However, rats in group 2 and 3 presented negligible safranin O systemic absorption. The marked decrease of safranin O in the plasma of the subjects pertaining to groups 2 and 3 indicate a remarkable protection of the cargo in **S1** that inhibited absorption of the cargo in the intestine.

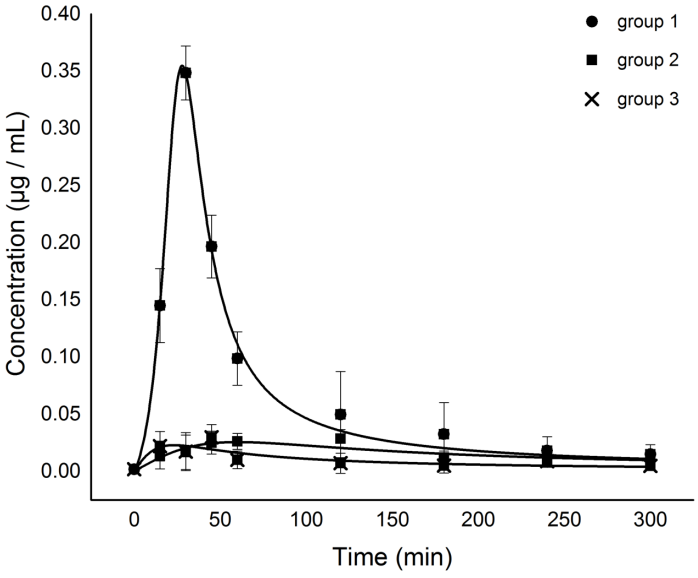

Fig. 6. Safranin O concentration (μg/mL) in plasma for subjects of group 1 (safranin O solution), group 2 (**S1** suspension) and group 3 (**S1** suspension + magnetic belt).

Besides, the presence of safranin O in cecum, colon and feces released from the particles was also evaluated. As could be seen in Fig. 7, subjects in group 1 showed negligible safranin O levels in cecum, colon and feces. Moreover, the levels of the dye in cecum and feces (for the individuals of groups 2 and 3 treated with **S1**) were lower when compared to levels observed in colon. The remarkable concentration of safranin O in colon for subjects from groups treated with **S1** (2 and 3) strongly suggested that microparticles were opened selectively in the reductive environment of this part of the GIT. Besides, safranin O levels in colon of individuals of group 3 are significantly higher than those found for rats in group 2. This fact was ascribed to the enhanced retention of **S1** microparticles in the colon because of the presence of the magnetic belt.

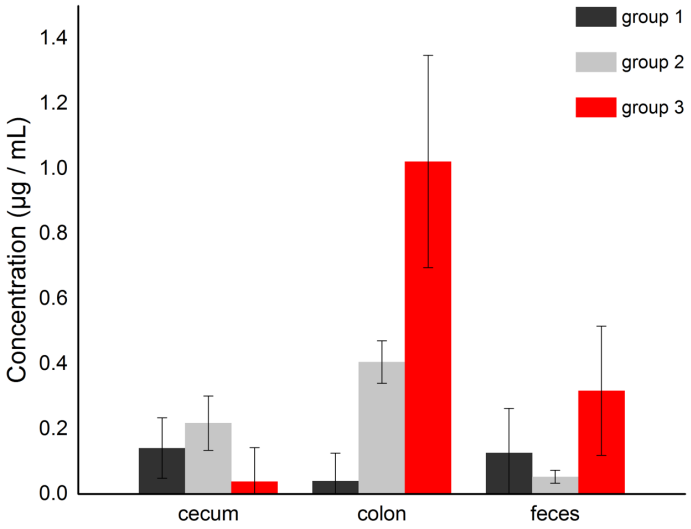

Fig. 7. Safranin O concentration (µg/mL) released from the particles in cecum, colon and feces for subjects of group 1 (safranin O solution), group 2 (**S1** suspension) and group 3 (**S1** suspension + magnetic belt).

The results presented above evidence the specific safranin O delivery into the colon and the avoidance of systemic absorption when rats were treated with **S1**. Moreover, improved results (in terms of concentration of dye in colon) were obtained for rats wearing a magnetic belt.

4.4.6. *In vivo* efficacy studies. Induction of colonic inflammation

In order to test the *in vivo* efficacy of the prepared microparticles a model of chronic inflammation in colon was used. For this purpose, male Wistar rats were treated with an enema containing trinitrobenzene sulfonic acid (TNBS) in ethanol-water 1:1 v/v mixture (see section 4.3.11 in Materials and methods for details). The main advantages of this model are its simplicity, reproducibility and time and dose related development of inflammation [53,54]. The development of the inflammation was monitored daily. It was observed that rats suffered from diarrhea and weight-loss but not rectal bleeding.

The efficacy of the magnetic microparticles loaded with hydrocortisone (**S2**) for the treatment of TNBS-induced colitis in rats was assessed. For this purpose, rats were divided into five groups (see section 4.3.12 in Materials and methods for details). Rats in group 1 were treated with 1.5 mL of saline solution (positive control). Group 2 was formed by rats treated with a suspension (60 mg in 1.5 mL of saline) of **S0** microparticles (as a control to assess the effect of the inorganic magnetic scaffold). Individuals in group 3 received a hydrocortisone solution (1.5 mg in 1.5 mL of saline). A suspension of **S2** microparticles (60 mg in 1.5 mL of saline) was administered to rats pertaining to group 4. Finally, group 5 was constituted by rats treated with a suspension of **S2** (60 mg in 1.5 mL of saline) wearing also a magnetic belt to evaluate if there was any improvement when the retention time of microparticles at the end of the GIT was lengthened. The efficacy of **S2** microparticles was evaluated by comparing the clinical activity score (see section 4.3.13 in Materials and methods), colon/body ratio (in g/g) and histological damage among the different groups.

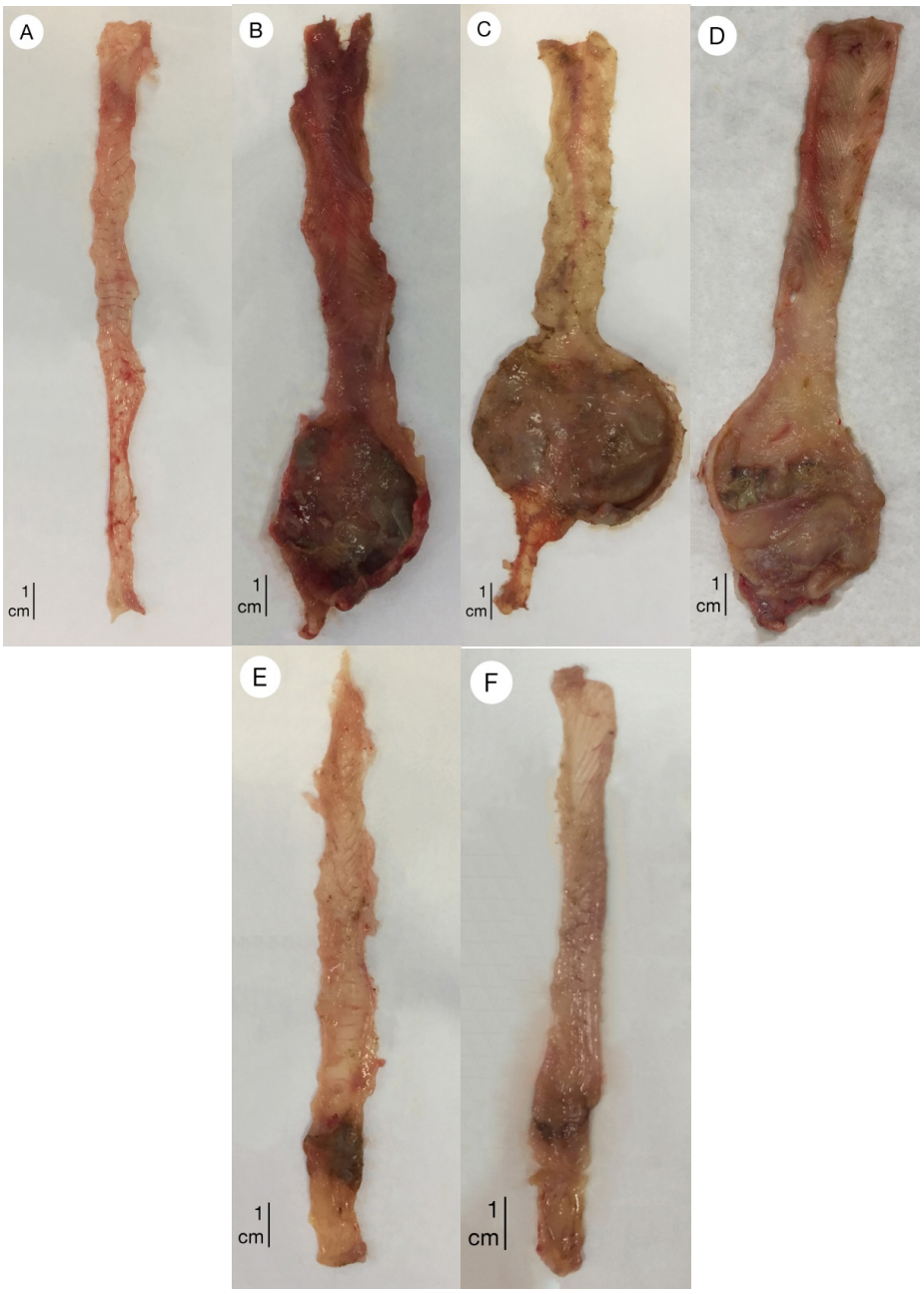

Fig. 8. Pictures of rat colon after the induction of colitis with TNBS sacrificed on day 10. A) healthy control (no TNBS administered); B) group 1 as positive control (treated with saline solution); C) group 2 (treated with **S0**); D) group 3 (treated with hydrocortisone); E) group 4 (treated with a **S2** suspension); F) group 5 (treated with **S2** + magnetic belt).

In a first step, the colon appearance of rats pertaining to groups 1–5 was visually assessed (Fig. 8). All rats from groups 1 to 5 were killed on day 10. Fig. 8A show the typical aspect of a healthy colon in rats not treated with TNBS. Fig. 8B and C show opened colons of rats pertaining to groups 1 (treated with saline as positive control) and 2 (administered with a suspension of **S0** microparticles). Both colons are closely similar showing necrotic tissue and presented a thick and rigid bowel. When hydrocortisone was administered (rats of group 3, see Fig. 8D) some tissues started to heal, necrotic zones and thickened tissues decreased to some extent but they were still largely present. As clear contrast, colon of rats treated with **S2** microparticles (Fig. 8E) showed middle to mild injuries with the presence of necrotic areas but with tissues no longer thickened. Finally, Fig. 8F showed the open colon of a rat pertaining to group 5 (treatment with **S2** microparticles and the rats wearing a magnetic belt). As could be seen, the aspect of the colon resembles that of healthy individuals (see Fig. 8A) presenting small injuries. The observed results pointed to a selective release of the entrapped hydrocortisone in **S2** microparticles in the colon of TNBS-treated rats.

Besides, the efficacy of the treatment of **S2** coupled to a magnetic field was higher than that found with the microparticles alone. This fact was ascribed to the enhanced retention time of **S2** microparticles in colon that resulted in a more effective delivery of hydrocortisone in the injured tissues. In fact, after the treatment, rats from group 4 and 5 started to gain weight and have normal stool. Besides, some of the rats from group 3 (receiving hydrocortisone solution) gained weight and improved their health condition as well. On the contrary, rats treated with saline solution or **S0** (groups 1 and 2) continued losing weight and had diarrhea during all the experiment time.

In a second step, the effects of different formulations on the colon/ body ratio and clinical activity score were assessed (see section 4.3.14 in Materials and methods). The obtained results are shown in Figs. 9 and 10. As could be seen in Fig. 9, the colon/body ratio in TNBS-treated rats administered with saline (positive control) was in the 0.30–0.33 g/g interval. Nearly the same interval was observed for rats in group 2 (treated with **S0**

microparticles). However, as a clear contrast, a marked reduction in the colon/body ratio for rats in groups 4 and 5 was observed (ca. 0.04–0.19 g/g for individuals treated with **S2** and wearing a magnetic belt). These reductions in the colon/body ratio indicated that **S2** microparticles reached the site of action and released hydrocortisone more efficiently. These results contrast with those obtained in group 3 (rats treated with hydrocortisone administered orally as a solution) that presented high variability with cases of real improvements mixed with individuals in which no effect was observed. This was reflected in a large colon/body ratio range (0.05–0.30 g/g) and suggested that hydrocortisone is probably adsorbed before the drug reaches the site of action.

Almost the same results were obtained with the clinical activity score (see Fig. 10). Colitis activity was quantified with a clinical score assessing weight loss, stool consistency and rectal bleeding. The sum formed the clinical score that ranges from 0 (healthy) to 12 (maximal activity of colitis) [39,40]. Rats that died or had to be sacrificed before day 10 were given a score of 12. As could be seen in Fig. 10, rats in group 1 (treated only with saline) presented a clinical score in the 7–9.5 range indicative of marked colitis activity. Besides, a marked reduction of the clinical activity score was observed in the groups treated with **S2** microparticles (4 and 5) indicative of a proper delivery of hydrocortisone in the injured colonic tissue.

Moreover, myeloperoxidase measurements agree with the clinical activity score obtained. These measurements indicated a myeloperoxidase activity decrease of 47% after administration of free hydrocortisone. However, after oral administration of **S2** microparticles in rats, a marked 94% decrease in myeloperoxidase activity was observed. This reduction in enzyme activity clearly indicated that inflammation was reduced with the **S2** administration.

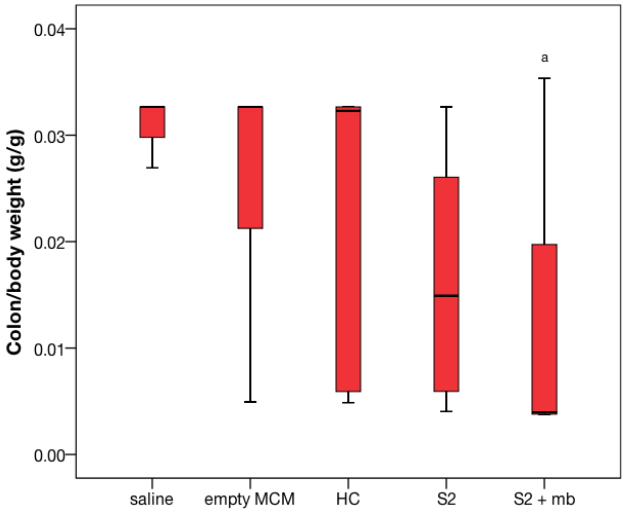

Fig. 9. Colon/body weight ratio of animals with TNBS-induced colitis after treatment with saline solution (group 1, positive control), **S0** (group 2), hydrocortisone (group 3), **S2** (group 4) and **S2** + magnetic belt (group 5). In each box is represented the median value, 25% and 75% percentils, minimal and maximal values ([a] statistical significant difference ($P < 0.05$) compared to saline).

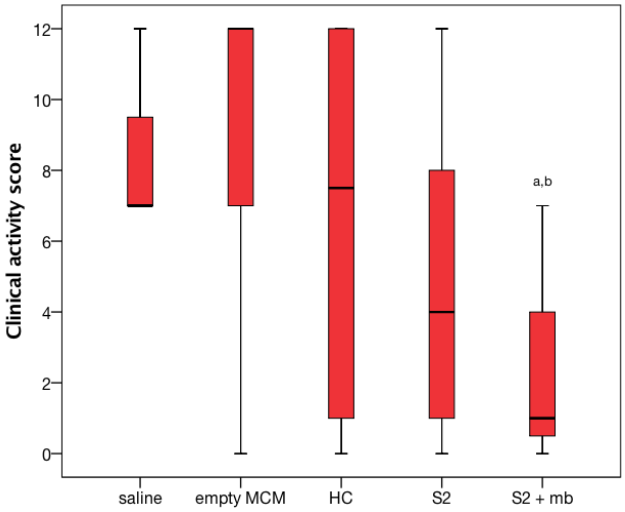

Fig. 10. Clinical activity score of animals with TNBS-induced colitis after treatment with saline solution (group 1, positive control), **S0** (group 2), hydrocortisone (group 3) **S2** (group 4) and **S2** + magnetic belt (group 5). In each box is represented the median value, 25% and 75% percentils, minimal and maximal values ([a,b] statistical significant difference ($P < 0.05$) compared to saline and empty MCM, respectively).

4.4.7. Histological evaluation

Finally, a histological examination of colon tissues of a healthy rat (control without TNBS administration), and of individuals treated with saline (group 1), **S0** (group 2), hydrocortisone (group 3), **S2** (group 4) and **S2** + magnetic belt (group 5) was carried out. All samples were taken from rats sacrificed on the 10th day after administration of TNBS (see section 4.3.15 in Materials and methods). The obtained results are shown in Fig. 11. Rats without TNBS treatment showed a normal colon structure with healthy mucosa, enterocytes and goblet cells and between them connective tissue (lamina propria), muscularis mucosae and normal submucosa and muscularis externa (see Fig. 11A). Tissues of individuals of groups 1 and 2 showed loss of the necrotic mucosa and substitution with granulation tissue. A strong inflammatory process was present in the lamina propria, submucosa and muscularis externa (Fig. 11B and C). As can be seen in Fig. 11B and C, process of ulceration with fibrinoid necrosis of the mucosal surface and granulation tissue below the necrotic tissue were observed. Animals in group 3 presented superficial erosion, thinning of the mucosa accompanied by thickening of the muscularis mucosae, and a chronic inflammatory process that affects the mucosa and submucosa with early development of lymphoid follicles (see Fig. 11D). Besides, few parts with normal mucosa structure but presence of strong follicular hyperplasia in the muscularis externa and parts with necrosis, loss of mucosa and substitution with granulation tissue and inflammation process were also observed (see again Fig. 11D). On the other hand, animals that received **S2** microparticles treatment (groups 4 and 5) showed substantially normal mucosal structure with slight presence of chronic inflammation in the muscularis propria (see Fig. 11E and F).

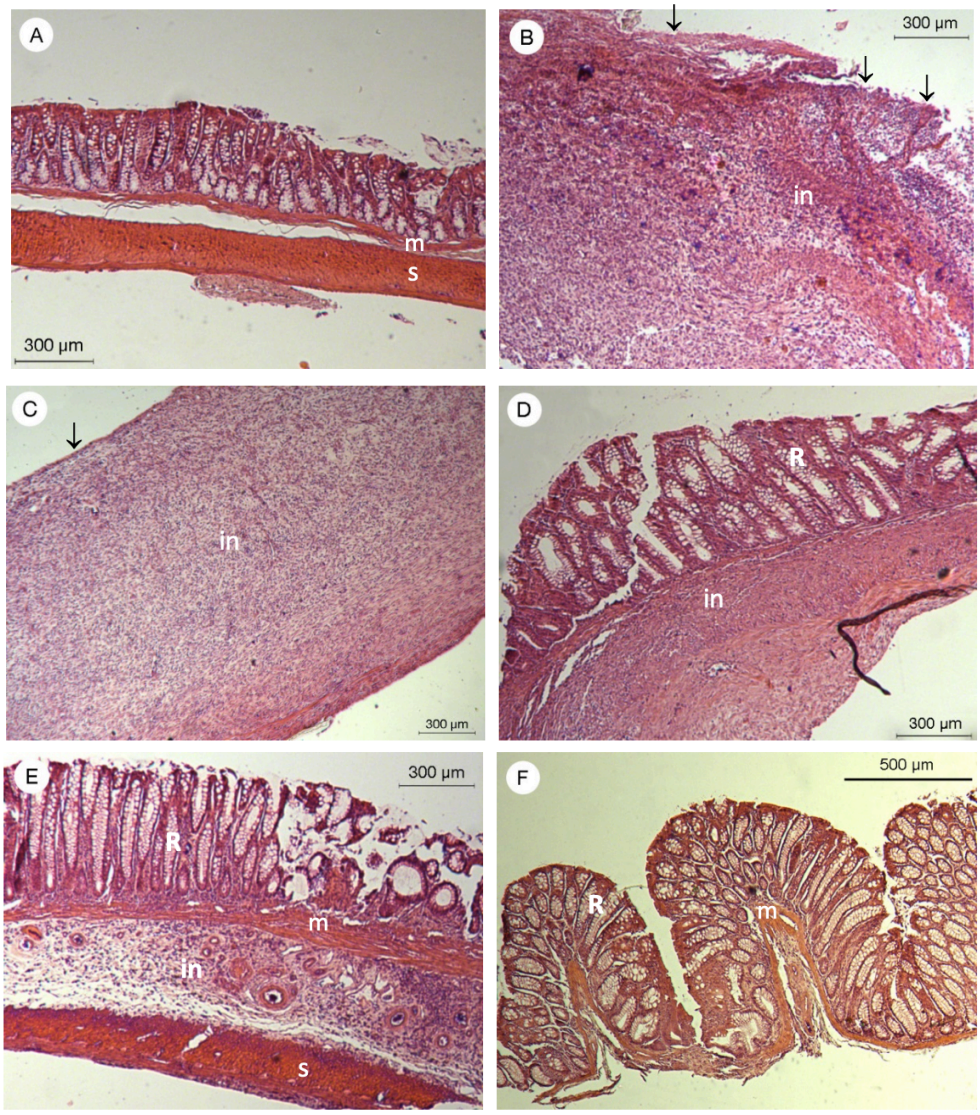

Fig. 11. Histology of a representative colon specimen of A) healthy rat; B) group 1 as positive control (treated with saline solution); C) group 2 (treated with **S0**); D) group 3 (rats administered with hydrocortisone); E) group 4 (subjects treated with a **S2** suspension); F) group 5 (treated with **S2** + magnetic belt). m: muscularis mucosae, s: submucosa, in: infiltration, R: regenerated crypts and mucosal architecture, ↓ absence of surface epithelium.

The results of the histological studies showed that tissues of saline treated TNBS individuals (group 1) presented strong inflammation

accompanied with necrosis and loss of the mucosa. Similar results were obtained for tissues isolated from individuals of group 2 (treated with suspensions of **S0** microparticles). As marked contrast, tissues from rats in groups 4 and 5 (treated with **S2** and **S2** + magnetic belt respectively) showed a decrease in inflammation followed by intensive regeneration and almost normal mucosal structure.

Histological evaluation provided additional information to that obtained by the clinical activity score and colon/body weight ratio observations, thus confirming the usefulness of the **S2** microparticles in the treatment of IBD. **S2** were even more effective if a magnetic field was applied to retain particles in the damaged intestinal areas. The results obtained with **S2** microparticles showed enhanced efficacy with respect of other formulations [42,55] with the added benefit of having no systemic intervention.

4.5 Conclusions

A new oral colon drug delivery device was designed, prepared and its efficacy in the treatment of IBD was evaluated *in vivo* in a TNBS colitis induced rat model. The nanodevices consisted on magnetic mesoporous silica microparticles loaded with safranin O (**S1**) or with hydrocortisone (**S2**) and functionalized in the external surface with a bulky azo derivative covalently grafted through urea bonds. Both materials remained capped at neutral pH whereas a marked payload release was observed in the presence of a reducing agent (such as sodium dithionite). This cargo delivery was ascribed to the reduction of azo bonds in the capping ensemble. Besides, a certain safranin O release was observed at acidic pH mainly related with the partial hydrolysis of the urea bonds that linked the azo derivatives onto the external surface of the loaded scaffold. *In vivo* pharmacokinetic studies carried out with **S1**, evidenced specific safranin O delivery in colon and the absence of safranin O systemic absorption (negligible concentrations of safranin O in plasma). Moreover, improved results (in terms of concentration of dye in colon) were obtained for rats wearing a magnetic belt. Colon/body weight ratio, clinical activity score

systems and histology evaluation showed that rats with a model of chronic inflammation in colon and treated with **S2** microparticles had an improvement in the pathology, being more effective when a magnetic field was externally applied to lengthen the retention time in the areas of interest. **S2** and specially **S2** + magnetic belt improved efficacy of hydrocortisone in the *in vivo* induced colitis model. In conclusion, we demonstrated that our system can be used to specifically deliver drugs or other agents in the last part of intestine while decreasing the systemic absorption; both effects contribute to increase efficacy for the treatment of inflammatory bowel disease and to reduce adverse effects of drugs.

Acknowledgements

We thank the Spanish Government (projects MAT2015-64139-C4-1-R and AGL2015-70235-C2-2-R (MINECO/FEDER)) and the Generalitat Valenciana (project PROMETEOII/2014/047) for support. AHT thanks to the Spanish MEC for his FPU grant. The authors also thank the Electron Microscopy Service at the Universitat Politècnica de València for support. SCSIE (Universitat de València) is also gratefully acknowledged for all the equipment employed. NMR was registered at the U26 facility of ICTS "NANBIOSIS" at the Universitat de València. The authors thanks Dr. L. A. Villaescusa for his helpful discussion about the ^{1}H NMR analysis of the composition of loaded and functionalized supports.

4.6 References

1. A. Kaser, S. Zeissig, R.S. Blumberg, Inflammatory bowel disease, Annu. Rev. Immunol. 28 (2010) 573-621.
2. X.-M. Xu, H.-J. Zhang, miRNAs as new molecular insights into inflammatory bowel disease: crucial regulators in autoimmunity and inflammation, World J. Gastroenterol. 22 (2016) 2206-2218.
3. B.B. Crohn, An historic note on ulcerative colitis, Gastroenterology 42 (1962) 366-367.
4. E.M. DeFilippis, R. Longman, M. Harbus, K. Dannenberg, E.J. Scherl, Crohn's disease: evolution, epigenetics, and the emerging role of microbiome-targeted thera- pies, Curr. Gastroenterol. Rep. 18 (2016) 13.
5. B.B. Crohn, L. Ginzburg, G.D. Oppenheimer, Regional ileitis: a pathologic and clinical entity. 1932, Mt. Sinai, J. Med. 67 (2000) 263-268.

6. Y. Ye, Z. Pang, W. Chen, S. Ju, C. Zhou, The epidemiology and risk factors of inflammatory bowel disease, Int. J. Clin. Exp. Med. 8 (2015) 22529-22542.
7. N.A. Molodecky, I.S. Soon, D.M. Rabi, W.A. Ghali, M. Ferris, G. Chernoff, E.I. Benchimol, R. Panaccione, S. Ghosh, H.W. Barkema, G.G. Kaplan, Increasing incidence and prevalence of the inflammatory bowel diseases with time, based on systematic review, Gastroenterology 142 (2012) 46-54.
8. A.E. M'Koma, Inflammatory bowel disease: an expanding global health problem, Clin. Med. Insights Gastroenterol. 6 (2013) 33–47.
9. M. Fakhoury, R. Negrulj, A. Mooranian, H. Al-Salami, Inflammatory bowel disease: Clinical aspects and treatments, J. Inflamm. Res. 7 (2014) 113–120.
10. C. Mowat, A. Cole, A. Windsor, T. Ahmad, I. Arnott, R. Driscoll, S. Mitton, T. Orchard, M. Rutter, L. Younge, C. Lees, G.-T. Ho, J. Satsangi, S. Bloom, on behalf of the I.S. of the B.S. of IBD Section of the British Society of Gastroenterology, Guidelines for the management of inflammatory bowel disease in adults, Gut. 60 (2011) 571–607.
11. B. Feagan, J. MacDonald, Oral 5-aminosalicylic acid for induction of remission in ulcerative colitis, Cochrane Database Syst. Rev. 17 (2012) CD000543.
12. K. Malik, L. Goswami, P. Kothiyal, S. Mukhopadhyay, A Review on Colon Targeting Drug Delivery System: Novel Approaches, Anatomy and Evaluation, Pharma Innov. J. 1 (2012) 01–12.
13. C. Lautenschläger, C. Schmidt, D. Fischer, A. Stallmach, Drug delivery strategies in the therapy of inflammatory bowel disease, Adv. Drug Deliv. Rev. 71 (2014) 58–76.
14. S. Hua, E. Marks, J.J. Schneider, S. Keely, Advances in oral nano-delivery systems for colon targeted drug delivery in inflammatory bowel disease: selective targeting to diseased versus healthy tissue, Nanomedicine. 11 (2015) 1117–1132.
15. V.R. Sinha, R. Kumria, Microbially triggered drug delivery to the colon, Eur. J. Pharm. Sci. 18 (2003) 3–18.
16. A. Rubinstein, Microbially controlled drug delivery to the colon, Biopharm. Drug Dispos. 11 (1990) 465–475.
17. V. V. Prasanth, R. Jayaprakash, S.T. Mathew, Colon specific drug delivery systems: A review on various pharmaceutical approaches, J. Appl. Pharm. Sci. 2 (2012) 163–169.
18. A.B. Descalzo, R. Martínez-Máñez, F. Sancenón, K. Hoffmann, K. Rurack, The supramolecular chemistry of organic-inorganic hybrid materials, Angew. Chem. Int. Ed. 45 (2006) 5924–5948.
19. E. Aznar, M. Oroval, L. Pascual, J.R. Murguía, R. Martínez-Máñez, F. Sancenón, Gated Materials for On-Command Release of Guest Molecules, Chem. Rev. 116 (2016) 561–718.
20. C. Giménez, C. de la Torre, M. Gorbe, E. Aznar, F. Sancenón, J.R. Murguía, R. Martínez-Máñez, M.D. Marcos, P. Amorós, Gated mesoporous silica nanoparticles for the controlled delivery of drugs in cancer cells, Langmuir. 31 (2015) 3753–3762.
21. A. Stein, Advances in microporous and mesoporous solids - Highlights of recent progress, Adv. Mater. 15 (2003) 763–775.
22. Z. Li, J.C. Barnes, A. Bosoy, J.F. Stoddart, J.I. Zink, Mesoporous silica nanoparticles in biomedical applications, Chem. Soc. Rev. 41 (2012) 2590-2605.
23. T.L. Doane, C. Burda, The unique role of nanoparticles in nanomedicine: imaging, drug delivery and therapy, Chem. Soc. Rev. 41 (2012) 2885-2911.
24. F. Sancenón, L. Pascual, M. Oroval, E. Aznar, R. Martínez-Máñez, Gated Silica Mesoporous Materials in Sensing Applications, ChemistryOpen. 4 (2015) 418– 437.

25. C. Giménez, E. Climent, E. Aznar, R. Martánez-Máñez, F. Sancenón, M.D. Marcos, P. Amorós, K. Rurack, Towards chemical communication between gated nanoparticles, Angew. Chem. Int. Ed. 53 (2014) 12629–12633.
26. A. Llopis-Lorente, P. Díez, A. Sánchez, M.D. Marcos, F. Sancenón, P. Martínez- Ruiz, R. Villalonga, R. Martínez-Máñez, Interactive models of communication at the nanoscale using nanoparticles that talk to one another, Nat. Commun. 8 (2017) 15511.
27. M. Oroval, P. Díez, E. Aznar, C. Coll, M.D. Marcos, F. Sancenón, R. Villalonga, R. Martínez-Máñez, Self-Regulated Glucose-Sensitive Neoglycoenzyme-Capped Mesoporous Silica Nanoparticles for Insulin Delivery, Chem. Eur. J. 23 (2017) 1353–1360.
28. A. García-Fernández, G. García-Laínez, M.L. Ferrándiz, E. Aznar, F. Sancenón, M.J. Alcaraz, J.R. Murguía, M.D. Marcos, R. Martínez-Máñez, A.M. Costero, M. Orzáez, Targeting inflammasome by the inhibition of caspase-1 activity using capped mesoporous silica nanoparticles, J. Control. Release. 248 (2017) 60–70.
29. A. Ultimo, C. Giménez, P. Bartovsky, E. Aznar, F. Sancenón, M.D. Marcos, P. Amorós, A.R. Bernardo, R. Martínez-Máñez, A.M. Jiménez-Lara, J.R. Murguía, Targeting Innate Immunity with dsRNA-Conjugated Mesoporous Silica Nanoparticles Promotes Antitumor Effects on Breast Cancer Cells, Chem. Eur. J. 22 (2016) 1582–1586.
30. E. Aznar, C. Coll, M.D. Marcos, R. Martínez-Máñez, F. Sancenón, J. Soto, P. Amorós, J. Cano, E. Ruiz, Borate-Driven Gatelike Scaffolding Using Mesoporous Materials Functionalised with Saccharides, Chem. Eur. J. 15 (2009) 6877–6888.
31. E. Bringas, O. Koysuren, D. V Quach, M. Mahmoudi, E. Aznar, J.D. Roehling, M.D. Marcos, R. Martinez-Manez, P. Stroeve, Triggered release in lipid bilayer-capped mesoporous silica nanoparticles containing SPION using an alternating magnetic field, Chem. Commun. 48 (2012) 5647–5649.
32. A. Agostini, L. Mondragón, A. Bernardos, R. Martínez-Máñez, M.D. Marcos, F. Sancenón, J. Soto, A. Costero, C. Manguan-García, R. Perona, M. Moreno- Torres, R. Aparicio-Sanchis, J.R. Murguía, Targeted Cargo Delivery in Senescent Cells Using Capped Mesoporous Silica Nanoparticles, Angew. Chem. Int. Ed. 51 (2012) 10556–10560.
33. C. de la Torre, I. Casanova, G. Acosta, C. Coll, M.J. Moreno, F. Albericio, E. Aznar, R. Mangues, M. Royo, F. Sancenón, R. Martínez-Máñez, Gated Mesoporous Silica Nanoparticles Using a Double-Role Circular Peptide for the Controlled and Target-Preferential Release of Doxorubicin in CXCR4-Expresing Lymphoma Cells, Adv. Funct. Mater. 25 (2015) 687–695.
34. L. Polo, N. Gómez-Cerezo, E. Aznar, J.-L. Vivancos, F. Sancenón, D. Arcos, M. Vallet-Regí, R. Martínez-Máñez, Molecular gates in mesoporous bioactive glasses for the treatment of bone tumors and infection, Acta Biomater. 50 (2017) 114–126.
35. C. Navarro, I. González-Álvarez, M. González-Álvarez, M. Manku, V. Merino, V.G. Casabó, M. Bermejo, Influence of polyunsaturated fatty acids on Cortisol transport through MDCK and MDCK-MDR1 cells as blood–brain barrier in vitro model, Eur. J. Pharm. Sci. 42 (2011) 290–299.
36. F. Torres-Molina, J.E. Peris, M.C. Garcia-Carbonell, J.C. Aristorena, L. Granero, J. Chesa-Jimenez, Use of rats chronically cannulated in the jugular vein and the duodenum in pharmacokinetic studies. Effect of ether anesthesia on absorption of amoxicillin, Arzneimittelforschung 46 (1996) 716–719.
37. G.P. Morris, P.L. Beck, M.S. Herridge, W.T. Depew, M.R. Szewczuk, J.L. Wallace, Hapten-induced model of chronic inflammation and ulceration in the rat colon, Gastroenterology 96 (1989) 795–803.

38. W.J. Sandborn, S.B. Hanauer, Systematic review: the pharmacokinetic profiles of oral mesalazine formulations and mesalazine pro-drugs used in the management of ulcerative colitis, Aliment. Pharmacol. Ther. 17 (2003) 29–42.
39. G. Hartmann, C. Bidlingmaier, B. Siegmund, S. Albrich, J. Schulze, K. Tschoep, A. Eigler, H.A. Lehr, S. Endres, Specific type IV phosphodiesterase inhibitor rolipram mitigates experimental colitis in mice, J. Pharmacol. Exp. Ther. 292 (2000) 22–30.
40. A. Lamprecht, N. Ubrich, H. Yamamoto, U. Schafer, H. Takeuchi, P. Maincent, Y. Kawashima, C.M. Lehr, Biodegradable nanoparticles for targeted drug delivery in treatment of inflammatory bowel disease, J. Pharmacol. Exp. Ther. 299 (2001) 775–781.
41. K. Mladenovska, R.S. Raicki, E.I. Janevik, T. Ristoski, M.J. Pavlova, Z. Kavrakovski, M.G. Dodov, K. Goracinova, Colon-specific delivery of 5- aminosalicylic acid from chitosan-Ca-alginate microparticles, Int. J. Pharm. 342 (2007) 124–136.
42. C. Mura, A. Nacher, V. Merino, M. Merino-Sanjuan, C. Carda, A. Ruiz, M. Manconi, G. Loy, A.M. Fadda, O. Diez-Sales, N-Succinyl-chitosan systems for 5-aminosalicylic acid colon delivery: in vivo study with TNBS-induced colitis model in rats, Int. J. Pharm. 416 (2011) 145–154.
43. J. Zhang, X. Li, J.M. Rosenholm, H. Gu, Synthesis and characterization of pore size-tunable magnetic mesoporous silica nanoparticles, J. Colloid Interface Sci. 361 (2011) 16–24.
44. C.T. Kresge, M.E. Leonowicz, W.J. Roth, J.C. Vartuli, J.S. Beck, Ordered mesoporous molecular sieves synthesized by a liquid-crystal template mechanism, Nature. 359 (1992) 710–712.
45. J. El Haskouri, S. Cabrera, M. Caldés, J. Alamo, A. Beltrán-Porter, M.D. Marcos, P. Amorós, D. Beltrán-Porter, Ordered mesoporous materials: Composition and topology control through chemistry, Int. J. Inorg. Mater. (2001) 1157–1163.
46. E.P. Barrett, L.G. Joyner, P.P. Halenda, The Determination of Pore Volume and Area Distributions in Porous Substances. I. Computations from Nitrogen Isotherms, J. Am. Chem. Soc. 73 (1951) 373–380.
47. S. Brunauer, P.H. Emmett, E. Teller, Adsorption of Gases in Multimolecular Layers, J. Am. Chem. Soc. 60 (1938) 309–319.
48. É. Pérez-Esteve, M. Ruiz-Rico, C. De La Torre, L.A. Villaescusa, F. Sancenón, M.D. Marcos, P. Amorós, R. Martínez-Máñez, J.M. Barat, Encapsulation of folic acid in different silica porous supports: A comparative study, Food Chem. 196 (2016) 66–75.
49. S.H. Lee, E. Moroz, B. Castagner, J.-C. Leroux, Activatable cell penetrating peptide-peptide nucleic acid conjugate via reduction of azobenzene PEG chains, J. Am. Chem. Soc. 136 (2014) 12868–12871.
50. Y.-Y. Yang, M. Grammel, A.S. Raghavan, G. Charron, H.C. Hang, Comparative analysis of cleavable azobenzene-based affinity tags for bioorthogonal chemical proteomics, Chem. Biol. 17 (2010) 1212–1222.
51. A.G. Oomen, C.J.M. Rompelberg, M.A. Bruil, C.J.G. Dobbe, D.P.K.H. Pereboom, A.J.A.M. Sips, Development of an in vitro digestion model for estimating the bioaccessibility of soil contaminants, Arch. Environ. Contam. Toxicol. 44 (2003) 281–287.
52. C.H.M. Versantvoort, A.G. Oomen, E. Van de Kamp, C.J.M. Rompelberg, A.J.A.M. Sips, Applicability of an in vitro digestion model in assessing the bioaccessibility of mycotoxins from food, Food Chem. Toxicol. 43 (2005) 31–40.
53. H. Tozaki, T. Fujita, J. Komoike, S.I. Kim, H. Terashima, S. Muranishi, S. Okabe, A. Yamamoto, Colon-specific delivery of budesonide with azopolymer- coated pellets:

therapeutic effects of budesonide with a novel dosage form against 2,4,6-trinitrobenzenesulphonic acid-induced colitis in rats, J. Pharm. Pharmacol. 51 (1999) 257–261.

54. H. Tozaki, T. Odoriba, N. Okada, T. Fujita, A. Terabe, T. Suzuki, S. Okabe, S. Muranishi, A. Yamamoto, Chitosan capsules for colon-specific drug delivery: enhanced localization of 5-aminosalicylic acid in the large intestine accelerates healing of TNBS-induced colitis in rats, J. Control. Release 82 (2002) 51–61.
55. M. Naeem, J. Cao, M. Choi, W.S. Kim, H.R. Moon, B.L. Lee, M.-S. Kim, Y. Jung, J.-W. Yoo, Enhanced therapeutic efficacy of budesonide in experimental colitis with enzyme/pH dual-sensitive polymeric nanoparticles, Int. J. Nanomedicine 10 (2015) 4565–4580.

4.7 Supporting Information

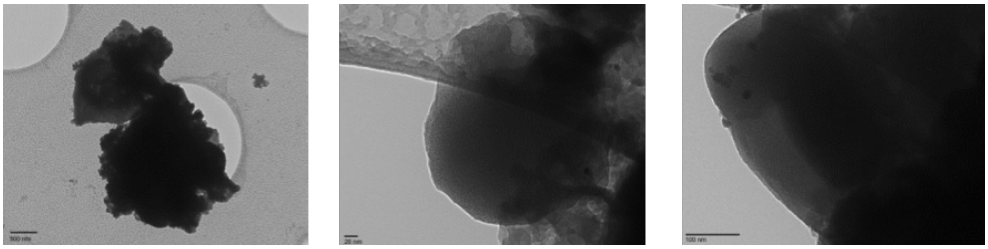

Figure SI-1. TEM images of micrometric magnetic mesoporous silica particles **S2**.

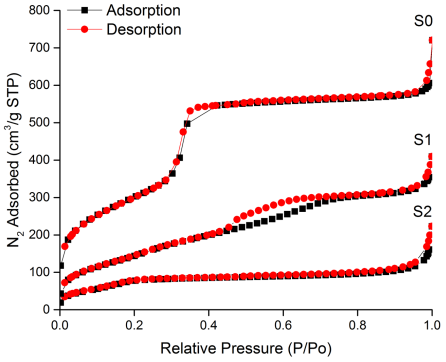

Figure SI-2. N_2 adsorption-desorption isotherms of **S0**, **S1** and **S2** microparticles.

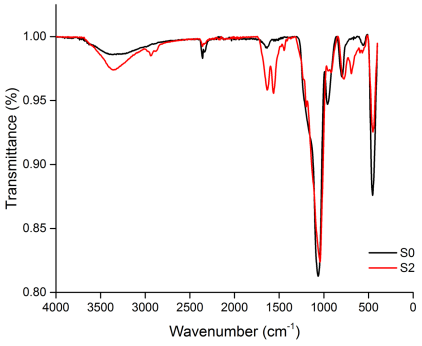

Figure SI-3. FT-IR spectra of **S0** (black) and **S2** (red) microparticles.

Chapter 5

Double Drug Delivery Using Capped Mesoporous Silica Microparticles for the Effective Treatment of Inflammatory Bowel Disease

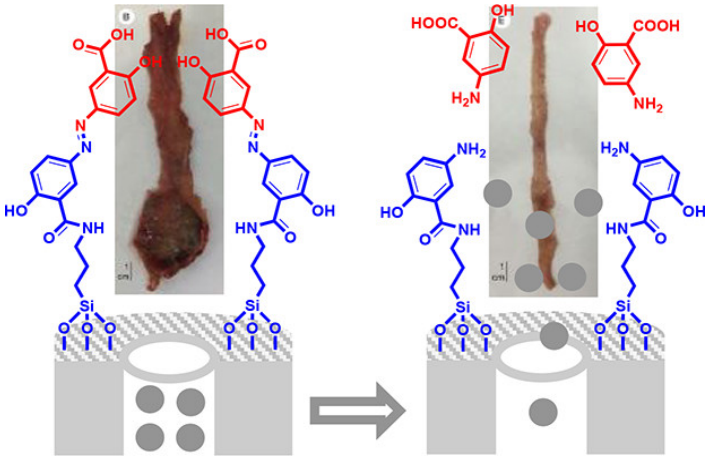

Double Drug Delivery Using Capped Mesoporous Silica Microparticles for the Effective Treatment of Inflammatory Bowel Disease

Adrián H. Teruel [1,2], Édgar Pérez-Esteve [1], Isabel González-Álvarez [3], Marta González-Álvarez [3], Ana M. Costero [1,2,4], Daniel Ferri [1,4], Pablo Gaviña [1,2,4], Virginia Merino [1,5], Ramón Martínez-Máñez [1,2,6,7,*] and Félix Sancenón [1,2,6,7]

[1] Instituto Interuniversitario de Investigación de Reconocimiento Molecular y Desarrollo Tecnológico (IDM), Universitat Politècnica de València, Universitat de València, Spain

[2] CIBER de Bioingeniería, Biomateriales y Nanomedicina (CIBER-BBN), Spain

[3] Departamento de Ingeniería, Sección de Farmacia y Tecnología Farmacéutica, Universidad Miguel Hernandez, Alicante 03550, Spain

[4] Departamento de Química Orgánica, Universitat de València, Doctor Moliner 50, Valencia 46100, Spain

[5] Departamento de Farmacia y Tecnologia Farmacéutica, Universitat de València, Valencia 46100, Spain

[6] Unidad Mixta de Investigación en Nanomedicina y Sensores. Universitat Politècnica de València, Instituto de Investigación Sanitaria La Fe, Valencia, Spain

[7] Unidad Mixta UPV-CIPF de Investigación en Mecanismos de Enfermedades y Nanomedicina, València, Universitat Politècnica de València, Centro de Investigación Príncipe Felipe, Valencia, Spain

Published online: 16 April, 2019

(Reprinted with permission from ***Mol. Pharmaceutics*** **2019, 16, 6, 2418-2429.**

5.1 Abstract

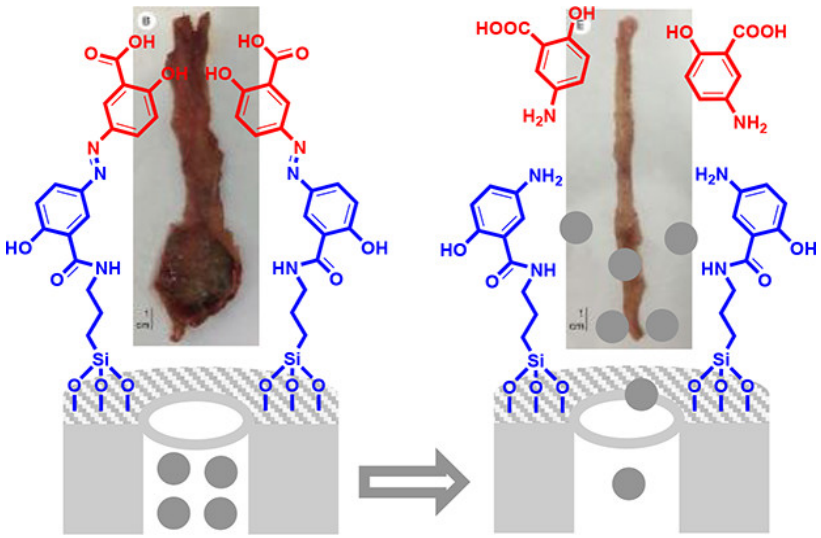

Silica mesoporous microparticles loaded with both rhodamine B fluorophore (**S1**) or hydrocortisone (**S2**), and capped with an olsalazine derivative, are prepared and fully characterized. Suspensions of **S1** and **S2** in water at an acidic and a neutral pH show negligible dye/drug release, yet a notable delivery took place when the reducing agent sodium dithionite is added because of hydrolysis of an azo bond in the capping ensemble. Additionally, olsalazine fragmentation induced 5-aminosalicylic acid (5-ASA) release. *In vitro* digestion models show that **S1** and **S2** solids are suitable systems to specifically release a pharmaceutical agent in the colon. *In vivo* pharmacokinetic studies in rats show a preferential rhodamine B release from **S1** in the colon. Moreover, a model of ulcerative colitis is induced in rats by oral administration of 2,4,6-trinitrobenzenesulfonic acid (TNBS) solutions, which was also used to prove the efficacy of **S2** for colitis treatment. The specific delivery of hydrocortisone and 5-ASA from **S2** material to the colon tissue in injured rats markedly lowers the colon/body weight ratio and the clinical activity score. Histological studies showed a remarkable reduction in inflammation, as well as an intensive regeneration of the affected tissues.

5.2 Introduction

Inflammatory bowel disease (IBD) is an idiopathic autoimmune, inflammatory, and chronic disease. There are essentially two main IBD subtypes: ulcerative colitis (UC) and Crohn's disease (CD). However, this classification is not always obvious because clinical and pathologic features substantially overlap.(1−11) The IBD etiology is still poorly understood, but all the facts indicate a multifactorial origin, where genetics, environmental, and intestinal microbiota are the main factors. Since IBD is a chronic disease with a low mortality, continuous incidence or newly diagnosed patients increase the number of prevalent cases. The comprehensive costs of IBD are quite overwhelming. More than 1 000 000 people are estimated to suffer from IBD (just in the United States), and only the direct medical costs exceeded US$ 6 billion in 2004.(12,13) In Canada over 200 000 people suffer IBD, with more than CDN$ 1.2 billion spent on direct healthcare costs per year.(14) Moreover, over 3 000 000 European patients suffer from IBD, and the direct healthcare expenditures are calculated to be over €5 billion per year.(15) The biggest contributors in these healthcare-related costs are pharmaceuticals, hospitalizations, surgery, and outpatient care.(16) Moreover, nondirect IBD costs (e.g., lost work productivity) exceed even direct costs. In addition, in the last decades, developing countries (in the Middle East, South America, and Asia) have seen an important emergence on IBD incidence and prevalence.(17−21)

Considering together the above-mentioned facts, plus the lack of a definitive solution available on the market, the development of new strategies to treat IBD are of interest. Conventional IBD therapy includes 5-aminosalicylic acid (5-ASA), corticosteroids, and immunosuppressants.(22) Steroids were the cornerstone of ulcerative colitis therapy for several years because of their proven anti-inflammatory efficacy. However, the therapeutic efficacy of steroids in IBD is controversially affected by serious secondary effects. As an alternative, in the past decade, biological agents (especially anti-TNF (tumor necrosis factor) therapies) have been introduced to be used in UC/CD patients who failed conventional therapy.(23,24) As an alternative to these therapies, nano- and

microparticle as drug carriers for oral administration have been tested in experimental colitis models to increase drug efficacy.(25−27) However, among different nano- and microparticles, mesoporous silica particles (MSPs) have still been barely studied as carries for IBD treatment.(28,29) As containers of selected cargo molecules, mesoporous silica nano- or microparticles have been broadly studied in recent decades for their promising characteristics, such as their biocompatibility, large specific surface areas (up to 1200 m^2 g^{-1}), customizable pore size (within the 2–10 nm diameter range), large load capacity, homogeneous porosity, tunable particle, inertness, and good thermal stability. Compared with organic nanocarriers, mesoporous silica materials are generally more resistant to pH, variations in temperature, and mechanical stress, which renders them with improved capability to protect molecules and biomolecules when they come into contact with body fluids. Besides, MSPs can be decorated with selected molecular or supramolecular entities to either enhance selectivity to cells and tissues or control the delivery of certain entrapped cargos at will using specific external stimuli.(30−38)

Considering the urge to find a better solution for the treatment of IBD, we report herein the synthesis and characterization of mesoporous silica microparticles loaded with rhodamine B or hydrocortisone and capped with an olsalazine derivative (see Scheme 1). As a consequence of the grafting of bulky olsalazine groups on the external surface of the loaded inorganic framework, the prepared microparticles are unable to release the entrapped cargo. However, when a reducing agent such as sodium dithionite (which mimic the azoreductase enzyme activity of the colon microbiota) is present, the olsalazine derivative is hydrolyzed and yields 5-aminosalicylic acid (5-ASA). This hydrolysis process induces pore opening and delivery of the entrapped cargo (i.e., rhodamine B or hydrocortisone). As a novelty, one of the prepared mesoporous microparticles is able to deliver two drugs at the same time, that is, hydrocortisone (located in the pores of the inorganic silica scaffold) and 5-ASA (product of the hydrolysis of the gating olsalazine). The effect of the codelivery of both drugs is studied in an *in vivo* IBD rat model. The information obtained by parameters such as the clinical activity score, the colon/body weight ratio, and the histological

evaluation confirms the usefulness of these microparticles system to treat IBD.

Scheme 1. Representation of Rhodamine B (**S1**) or Hydrocortisone (**S2**) Loaded Silica Mesoporous Particles Capped with an Olsalazine Derivative[a].

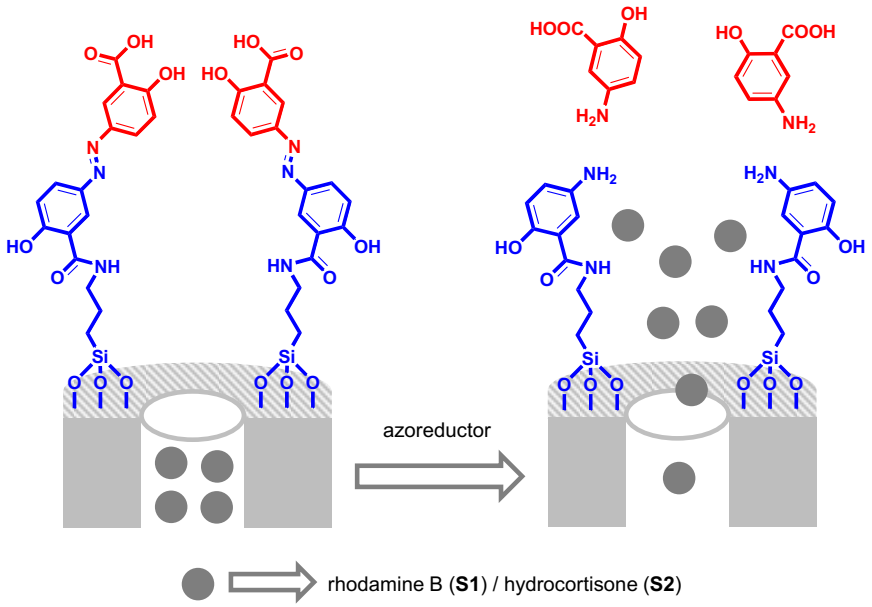

[a]Delivery of both cargos (rhodamine B or hydrocortisone) is induced by an azoreductor.

5.3 Experimental Section

5.3.1. General Techniques

Transmission electron microscopy (TEM), scanning transmission electron microscopy (STEM), thermogravimetric analysis (TGA), N_2 adsorption–desorption isotherms, powder X-ray diffraction (PXRD), Fourier transform infrared spectroscopy (FTIR), nuclear magnetic resonance (NMR), fluorescence spectroscopy, and HPLC techniques were used in order to characterize the prepared materials. The instruments used were the following: JEOL JEM-1010 microscope for TEM images acquisitions. Bruker D8 Advance diffractometer (Cu Kα radiation) for PXRD

measurements. TGA/SDTA 851e Mettler Toledo balance for TGA, using air (80 mL/min) as an oxidant atmosphere with the following heating program: heating ramp of 10 °C/min from 393 to 1273 K, then an isothermal heating step at 1273 K for 30 min. Using the Micromeritics ASAP 2010 automated analyzer for recording of N_2 adsorption–desorption isotherms, samples were degassed at 120 °C in a vacuum overnight. The specific surface areas were calculated from the adsorption data within the low-pressure range using the BET (Brunauer–Emmett–Teller) model. Pore size was determined following the BJH (Barrett–Joyner–Halenda) method. A Bruker AV400 spectrometer was used to measure 1H NMR spectra. A Bruker Tensor 27 instrument was used to record infrared spectra, and PerkinElmer EnSpire Multimode Plate Reader was used for fluorescence measurements. A Hitachi LaChrom Elite HPLC with a UV detector (L-2400) and an autosampler (L-2200) for HPLC analysis, using a Kromaphase 100 C18 column (150 mm × 4.6 mm i.d., 5 μm particle size), were implemented for separations.

5.3.2. Chemicals

The chemicals tetraethylorthosilicate (TEOS), 1-hexadecyltrimethyl-ammonium bromide (CTABr), sodium hydroxide (NaOH), triethanolamine ($TEAH_3$), N-hydroxysuccinimide (NHS), N,N′-dicyclohexylcarbodiimide (DCC), (3-aminopropyl)triethoxysilane, rhodamine B, triethylamine, hydrocortisone, sodium dithionite, and 2,4,6-trinitrobenzenesulfonic acid solution (TNBS) were purchased from Sigma-Aldrich. Sodium acetate anhydrous, potassium chloride, sodium dihydrogen phosphate, potassium dihydrogen phosphate, disodium hydrogen phosphate, hydrochloric acid, and all the solvents were provided by Scharlab. Olsalazine sodium salt (Mordant yellow 5) was purchased from Molekula. The animal facilities supplied isoflurane pentobarbital (dolethal). All the chemicals were used as received.

5.3.3. Synthesis of Mesoporous Silica Microparticles (S0)

We used the “atrane route” to synthesize the microsized mesoporous silica particles.(39) In a typical synthesis, $TEAH_3$ (25.8 g, 0.17 mol) and sodium hydroxide (2 mL, 6 M) were mixed, and the obtained solution was heated to 120 °C and then cooled down to 70 °C. Afterward, TEOS (11 mL, 0.045 mol) was added to the initial solution that was then heated to 120 °C. Next, solution was left to cool down, and the surfactant CTABr (4.7 g, 0.013 mol) was added at 118 °C. At this time, distilled water (80 mL) was slowly added under vigorous stirring at 70 °C. The resultant mixture was aged at 100 °C in an autoclave for 24 h. The obtained powder was filtrated and washed with abundant water. In the last step of the protocol, the solid is dried at 70 °C. To obtain the solid (**S0**), a calcination process at 550 °C is performed in an oxidant atmosphere during 5 h in order to remove the surfactant template from the as-synthesized microparticles.

5.3.4. Synthesis of 1a

Olsalazine sodium salt (0.5 g, 1.65 mmol) was dissolved in an acidic solution of pH ≈ 0 (28.5 mL of distilled water and 1.5 mL 37% HCl solution). The resultant solution was stirred for 5 min at room temperature and then centrifuged. The supernatant was discarded, and the resulting protonated product (**1a**, 0.45 g, 1.49 mmol, 90% yield) was recovered and dried at 70 °C for 24 h. This protocol was repeated 4 times.

5.3.5. Synthesis of 1

DCC (1.04 g, 5 mmol) and NHS (0.59 g, 5 mmol) were dissolved in anhydrous THF (25 mL). Afterward, this mixture was then poured over a solution of compound **1a** (1.53 g, 5 mmol) in anhydrous THF (25 mL). The crude reaction was stirred during 5 h at room temperature in an argon atmosphere. A white-yellowish precipitate of dicyclohexylurea (DCU) was discarded by centrifugation. The supernatant was left stirring for 15 h in an argon atmosphere at room temperature. After 15 h the crude reaction was recentrifuged to remove the newly formed DCU. Then, (3-aminopropyl)triethoxysilane (**1b**, 1.2 mL, 5 mmol) was slowly added to the

crude reaction and was stirred for a further 24 h period (room temperature, argon atmosphere). The solvent was removed using a rotary evaporator to isolate the final product **1** (yellow-orange oil, 2.05 gr, 4.05 mmol, 80% yield). ^{1}H NMR (400 MHz, DMSO–D6): δ = 8.31 (d, 2H), 7.98 (dd, 2H), 7.05 (d, 2H), 3.65 (m, 6H), 3.36 (t, 2H), 1.67 (m, 2H), 1.17 (m, 9H), 0.68 (t, 2H) ppm. HRMS-EI m/z: calcd for $C_{23}H_{31}N_3O_8Si$: 505.1880; found: 436.3410 (M-2(CH_3CH_2OH)+Na) and 391.2828 (M-3(CH_3CH_2OH)+Na).

5.3.6. Synthesis of S1

Solid **S0** (1 g) was suspended in a THF (40 mL) solution containing rhodamine B (400 mg, 0.8 mmol/g of solid) under argon. The suspension was stirred at room temperature overnight. Afterward, compound **1** (2.05 g, 4.05 mmol/g of solid) was dissolved in anhydrous THF (25 mL), and this mixture was added to the solid/rhodamine B suspension and then stirred for 6 h at room temperature in an argon atmosphere. **S1** particles were isolated as a red solid, washed with H_2O and EtOH, and finally dried in a vacuum for 24 h.

5.3.7. Synthesis of S2

Solid **S0** (1 g) was suspended in 40 mL of THF/hydrocortisone solution (296 mg, 0.8 mmol/g of solid) under argon. The suspension was stirred at room temperature overnight. Next, compound **1** (2.05 g, 4.05 mmol/g of solid) was dissolved in anhydrous THF (25 mL) and was then added to the solid/hydrocortisone suspension. The obtained suspension was stirred under argon and at room temperature during 6 h. **S2** particles were isolated as a yellow solid, washed with EtOH and H_2O, and finally dried for 24 h in a vacuum.

5.3.8. Controlled Release Studies

The controlled release behaviors of solids **S1** and **S2** at pH values found along the gastrointestinal tract (GIT) (2.0, 4.5, and 7.4) and in the

presence of a chemical reducing agent (sodium dithionite), to simulate the azo-reductive environment, were assessed. For this purpose, corresponding solid (2 mg) was suspended in 2 mL of the aqueous solution at the selected pH. Aliquots were taken at scheduled times up to 24 h and centrifuged to discard the solid before analyzing. The controlled release performances of both solids were tested under *in vitro* digestion conditions using simulated solutions for GIT fluids including saliva, gastric juice, duodenal juice, bile, and colon (in which azoreductor agent sodium dithionite was added for colon reducing environment simulation). *In vitro* digestion assays were performed with 2 mg of solid **S1** or **S2** at 37 °C (simulating the body temperature in humans) and shaken (100 rpm) to obtain homogeneous suspensions of microparticles. Digestions were started by the addition of 320 µL of simulated saliva fluid (pH = 6.8 ± 0.1) and incubated during 5 min. Next, 630 µL of simulated gastric juice was added, and the mixture was stirred 2 h (total volume of 950 µL and pH = 1.3 ± 0.2). Then, 630 µL of simulated duodenal juice, 320 µL of bile, and 100 µL of a bicarbonate solution (1 M) were added simultaneously (total volume of 2 mL and pH = 6.0 ± 0.5). The resulting solution was stirred during 2 h. Finally, colon fluid was simulated with the addition of 2 mg/mL of sodium dithionite to the last mixture (total volume of 2 mL pH = 6.0 ± 0.5). Aliquots were collected at scheduled times up to 28 h (4 h approximately to reach the colon, plus 24 h of colon residence time), centrifuged, and analyzed. In order to determine the amount of cargo delivered from **S1** microparticles, supernatants were loaded into 96-well plate, and then the rhodamine B emission at 572 nm (upon excitation at 555 nm) was measured. The amount of hydrocortisone released from **S2** microparticles was assessed from the supernatants using an HPLC. The released 5-ASA was also analyzed by HPLC (vide infra).

5.3.9. 5-ASA and Hydrocortisone Quantification

HPLC (with a reverse-phase column) was used for 5-ASA and hydrocortisone determination using the methods described by Lunn(40) and Navarro.(41) The HPLC equipment used was a Hitachi LaChrom Elite

liquid chromatograph connected to an autosampler and a UV detector (L-2200 and L-2400, respectively). For both analytes, a C18 column (Kromaphase 100 of 150 mm × 4.6 mm i.d., 5 μm particle size) was used for separations. For the 5-ASA determinations, mobile phase: (A) 50 mM sodium phosphate/(B) methanol, isocratic program: 90% A/10% B for 15 min. The wavelength of the UV detector was set at 365 nm. For hydrocortisone determinations, mobile phase: (A) water/(B) acetonitrile, isocratic program: 70% A/30% B for 15 min. The UV wavelength of the UV detector was set at 245 nm. Both analytes were quantified using a calibration curve (peak area vs analyte concentration). The used method was validated using a recovery study. In this respect, simulated GIT fluids were spiked with both analytes (5-ASA or hydrocortisone) at five different concentrations. The recovery values were estimated from the determined concentration vs the amounts of 5-ASA or hydrocortisone added. All the recovery values were near to 100%.

5.3.10. *In vivo* studies

These studies followed the Principles of Laboratory Animal Care and were approved by the Institutional Ethics Committee of the University of Valencia (according to RD 1201/2005). For the *in vivo* studies, male Wistar rats (aged 8–12 weeks and with an weight in the 270–330 g interval) were used. Animals were housed in an air-conditioned room (12 h light/dark cycles, 22 ± 3 °C, 55 ± 5% humidity) and were allowed free access to laboratory chow and water during the entire time of the studies.

5.3.11. *In vivo* pharmacokinetic studies

In a first step, male Wistar rats (with an average weight of 300 ± 30 g) were anesthetized to facilitate the cannula implantation 24 h before the experiment. Then, in a second step, a previously reported method for jugular vein permanent cannulation was followed.(42) The implanted cannula allowed blood sampling. The animals were randomly ascribed (n = 8–10) to different groups: Group 1: 1 mL of rhodamine B solution (750

μg/mL in saline solution) was given orally. Group 2: 1.75 mL of a **S1** suspension (containing 30 mg of solid which should deliver about 750 μg of rhodamine B) was given orally. Blood samples (0.6–0.7 mL) were drawn with heparinized syringes and replaced by heparinized saline (10 IU/mL), at previously established sampling time (up to 4 h). Plasma samples were centrifuged (10 000 rpm, 10 min), and supernatant was stored at −20 °C until analyzed by HPLC. A fluorescence detector, with excitation and emission wavelength fixed at 225 and 535 nm, respectively, was used. The solvent delivery system (Alliance System, Waters 2695) was used to provide a mobile phase 70:30 v/v of trifluoroacetic acid aqueous solution (pH 3)-acetonitrile. The stationary phase was a Waters model Nova Pak C-18 (150 mm length, 3.9 mm in diameter and particle size of 4 μm) column preceded by a Teknocroma TCR–C130-B precolumn. Flow rate was set at 1 mL/min, and the injection volume was 90 μL for *in vivo* samples. Retention time of rhodamine B was 2.5 min. Analytical method was validated in terms of selectivity, specificity, precision, linearity, and accuracy. After 4 h, rat subjects were euthanized, and the cecum, colon tissues, and feces were extracted and treated in order to determine rhodamine B amount. The analyzed rhodamine B corresponded to that released from **S1** particles in the GIT of subjects (**S1** release was not forced *in vitro*).

5.3.12. *In vivo* efficacy studies. Inducing colonic inflammation

Several slight modifications were introduced in the method described by Mura et al. to induce the chronic inflammation model in the colon of rats.(43) For this purpose, rats were indistinctly separated in different treatment groups (having free access to water) and were then anaesthetized with isoflurane. TNBS solution in 50% v/v ethanol (0.6 mL, 78 mg/kg body weight) was instilled into the lumen of the colon using a graduated rubber cannula inserted rectally into the colon (taking into account that the tip was 8 cm proximal to the anus). After the induction procedure, the development of inflammation was monitored daily for the next 10 days for the entire duration of the assays. Rats were sacrificed

using an overdose of isoflurane at the end of the 10th day (after induction with TNBS). Inflammation development was evaluated through determination of the clinical activity score, colon/body weight ratio, and also studying changes in tissue histology.

5.3.13. Treatment study design

Rats were distributed into four groups: group 1 (positive control group, 3 rats) with saline solution as treatment; group 2 (8 rats) treated with a suspension of **S0** (empty mesoporous silica microparticles); group 3 (8 rats) treated with hydrocortisone solution; group 4 (8 rats) treated with an aqueous suspension of **S2** microparticles. The hydrocortisone dose that groups 3 and 4 received (5.58 mg/kg/day) was calculated from the dose normally used for humans.(44) All the treatments were carried out using an oral gavage once a day during 3 days in the most intensive inflammation period (days 3, 4, and 5 after TNBS administration). Groups and treatments are summarized in Table 1.

Table 1. Treatment Groups

group 1	group 2	group 3	group 4
saline solution (1.5 mL)	60 mg of **S0** in 1.5 mL	1.5 mg of hydrocortisone in 1.5 mL	30 mg of **S2** in 1.5 mL

5.3.14. Clinical Activity Score System

A clinical score that assessed weight loss, stool consistency, and rectal bleeding (see Table 2) was used to quantify colitis activity.(27,45).

Table 2. Clinical Activity Score System

control	range	score
% weight loss	<1%	0
	1−5%	1
	5−10%	2
	10−20%	3
	>20%	4
stool consistency	well-formed pellets	0
	pasty and semiformed stools	2
	liquid stools or absence	4
bleeding	no blood	0
	positive finding	2
	gross bleeding	4

The sum of these scores resulted in the clinical activity which ranged from 0 (healthy animal) to 12 (higher colitis activity). An activity score of 12 was assigned to rats that died or had to be sacrificed before day 10.

5.3.15. Assessing Colonic Injury and Inflammation

Rats were monitored during the 10 day period of the assay, and lastly, the clinical activity score of colitis was evaluated. On day 10 after administering TNBS, rats were sacrificed with isoflurane to obtain the distal colon for subsequent processing and analyzing. The samples from inflamed tissue were excised to calculate C/B ratio, with C being the distal colon weight and B the body weight. Besides, an histological evaluation was also carried out.

5.3.16. Determining the Colon/Body Weight Ratio

After the animal was sacrificed, the distal colon was extracted and longitudinally opened along the mesenteric edge. Then, colon was washed with a 0.9% (w/v) saline solution, weighed, and placed on a glass plate with the mucosal surface lying upward.(46) The 8 cm segment distal colon weight ratio was calculated as an index of colonic tissue edema.

5.3.17. Histological Evaluation

A 3 cm sample from the distal colon (and a similar portion from proximal part) was excised from each subject and maintained in 4% (v/v) p-formaldehyde for 24 h. Afterward, the samples were changed to a 0.4% (v/v) p-formaldehyde medium in order to perform the microscopic studies. These colonic tissue samples were routinely processed and then embedded in paraffin. Then, longitudinal sections of 5 μm were stained with hematoxylin and eosin. Microscopic assessment by a light microscope was performed blind on coded slices.

5.3.18. Statistical analysis

Nonparametric Mann–Whitney U and Kruskal–Wallis tests were performed to assess the differences among groups using SPSS v.22.0 (SPSS Inc., U.S.A.) on Windows.

5.4 Results and discussion

5.4.1. Synthesis of Mesoporous Silica Microparticles Functionalized with Molecular Gates

The mesoporous silica carrier was synthesized following previously reported procedures with minor adjustments.(39) In this synthetic protocol, tetraethylorthosilicate (TEOS) was employed as the source of silica and 1-

hexadecyltrimethylammonium bromide (CTABr) as a structure-directing agent. The resulting white powder was rinsed and then calcined (in order to remove the CTABr template). This protocol yielded the mesoporous silica microparticles **S0**. Pores in **S0** were loaded with a selected dye (rhodamine B) or hydrocortisone, and then the external surface of both microparticles was functionalized with the olsalazine derivative **1**. This procedure yielded the final solids **S1** (loaded with rhodamine B) and **S2** (containing hydrocortisone) as depicted in Scheme 1. The pores of **S1** and **S2** were expected to be capped due to the presence of bulky azoderivative **1** anchored to the external surface of microparticles. Additionally, rhodamine B or hydrocortisone release should be observed in the presence of azoreductor agents such as azoreductase enzymes, produced by colon bacteria, or chemical-reducing species.

The synthesis of azo derivative containing trialkoxysilane moieties (**1**) was carried out using a two-step sequence (see Scheme 2). First olsalazine sodium salt was protonated to yield the free acid (**1a**), which was then reacted with (3-aminopropyl) triethoxysilane (**1b**). The final azo compound containing alkoxysilane groups (**1**) was fully characterized using ^{1}H and ^{13}C NMR and HRMS.

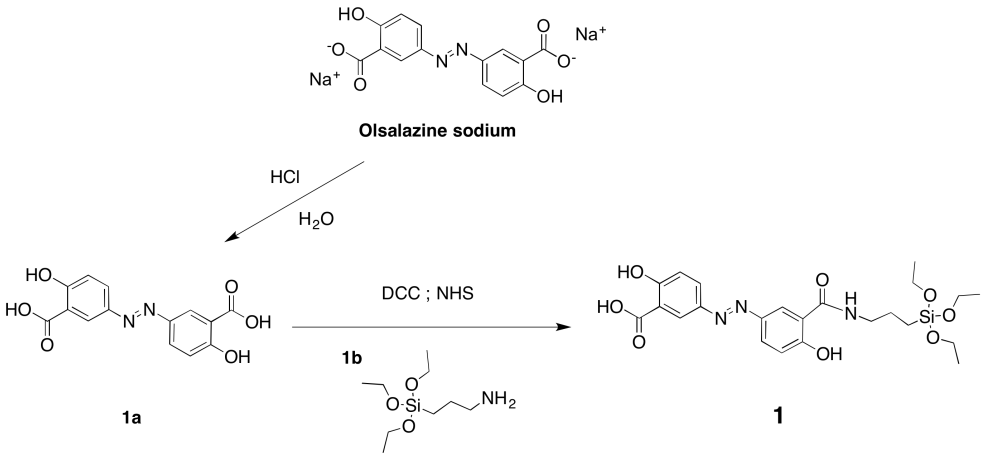

Scheme 2. Synthetic Route Used To Prepare **1**

5.4.2. Characterization of the Final Materials

Solids **S0**, **S1**, and **S2** were characterized using powder X-ray diffraction (PXRD), transmission electron microscopy (TEM), thermogravimetric measurements (TGA), and N_2 adsorption–desorption isotherms. The PXRD pattern of the as-synthesized microparticles showed four reflections indexed as (100), (110), (200), and (210) Bragg peaks typical of a mesoporous material with a hexagonal order. A marked shift of the (100) reflection in calcined material S0 was observed. This shift was ascribed to silanol groups condensation during the calcination step. Moreover, the preservation of the (100) reflection in the PXRD patterns of **S1** and **S2** microparticles showed that the mesoporous structure was preserved during the loading process and functionalization with **1**. TEM images of **S0** and **S2** also showed the typical porosity of mesoporous silica materials, which confirmed that there was no framework modification (data not shown).

The N_2 adsorption–desorption measurements on the calcined solid (**S0**) showed a type IV isotherm, typical of the mesoporous silica materials. This isotherm presented an adsorption step at intermediate P/P_0 values (0.2–0.4). From the adsorption branch of the isotherm, the values of pore volume (0.98 $cm^3\ g^{-1}$) and pore diameter (2.55 nm) were calculated. Besides, the pore diameter estimated from the TEM images agreed with this calculated value. The total specific surface of **S0** microparticles (1193 $m^2\ g^{-1}$) was evaluated using the Brunauer–Emmett–Teller (BET) model. On the other hand, the N_2 adsorption–desorption isotherms of **S1** and **S2** microparticles were typical of mesoporous systems with partially filled mesopores. When compared with **S0**, both, the specific surface area and adsorbed N_2 volume were clearly reduced (see Table 3). The loading of pores with rhodamine B (for **S1**) or hydrocortisone (for **S2**), and the grafting of olsalazine derivative **1** onto the external surface accounted for the reduction in the BET surface observed for both solids.

Table 3. Structural Parameters for **S0**, **S1**, and **S2** Microparticles

	S_{BET} (m^2 g^{-1})	pore volume[a] (cm^3 g^{-1})	pore size[a,b] (nm)
S0	1193	0.98	2.55
S1	200	0.06	-
S2	770	0.35	-

[a]Total pore volume estimated using the BJH model. [b]Pore size according to the BJH model applied to the adsorption branch of the isotherm (for $P/P_0 < 0.6$) which can be assigned to the mesopores generated by the surfactant.

Thermogravimetric analysis and ^{1}H NMR measurements were employed to assess the organic content in **S1** and **S2** (see Table 4). The amount of total organic matter was larger in **S1** than in **S2**, which agrees with the larger specific surface found for **S2** (see Table 3), indicating that the loading of the mesoporous support with rhodamine B in **S1** was more efficient than for hydrocortisone in **S2**. The amounts of olsalazine derivative grafted onto the outer surface of **S1** and **S2** were determined by ^{1}H NMR measurements. For this purpose, the corresponding solid was dissolved in NaOD/D_2O using $(CH_3CH_2)_4NBr$ as internal standard. Moreover, HPLC was used to quantify the amount of 5-ASA released. In the presence of a reducing agent (vide infra), **S1** and **S2** were able to deliver 107 μg/mg and 93 μg/mg of 5-ASA, respectively. FT-IR analysis on **S2** revealed the presence of typical amide signals at 1633 cm^{-1} (carbonyl), 1594 cm^{-1} (N–H torsion), and 1486 cm^{-1} (C–N stretching), and azo signal at 1558 cm^{-1} (data not shown).

Table 4. Total Organic Matter (in g) Content per Gram of SiO_2, Olsalazine Derivative **1** (in g) Content per Gram of SiO_2, Dye or Drug (Hydrocortisone: HC) Released (in μg) per mg of Solid and Drug (5-ASA) Released per mg of Solid for **S1** and **S2**

solid	organic content (g/g SiO_2)	**1** (g/g SiO_2)	dye/HC release (μg/mg solid)	5-ASA release (μg/mg solid)
S1	0.24	0.16	21.50	107
S2	0.19	0.11	24.36	93

5.4.3. Payload Delivery from S1 and S2

The cargo release (rhodamine B or hydrocortisone) from solids **S1** and **S2** was evaluated at acidic pH (2.0 and 4.5) and at neutral pH (7.4) in the absence or in the presence of sodium dithionite (an azoreductor agent). These pH values were selected bearing in mind typical pH values for gastric juices (pH 2.0), transition from stomach to the intestine (pH 4.5), and intestine (pH 7.4). Cargo release profiles for **S1** and **S2** microparticles are shown in Figure 1a,b, respectively. Aqueous suspensions of **S1** and **S2** showed poor rhodamine B (**S1**) or hydrocortisone (**S2**) release at acidic and neutral pHs. However, a marked delivery of the entrapped payload (rhodamine B from **S1** and hydrocortisone from **S2**) was seen at pH 7.4 when sodium dithionite was present, which showed a sustained release profile that reached ca. 90% (for **S1**) and 80% (for **S2**) of the maximum dye/drug delivered after 6 h. The observed cargo release was ascribed to the presence of the azoreductor agent (sodium dithionite), which is able to reduce the azo groups in the capping molecule **1**. This azo group reduction resulted in pore opening and rhodamine B (**S1**) or hydrocortisone (**S2**) release. The maximum rhodamine B release from **S1** was ca. 21.50 μg/mg solid, in the presence of an azoreductor (pH = 7.4). Under the same experimental conditions, the maximum hydrocortisone release from **S2** was ca. 24.36 μg/mg solid. The release of 5-ASA in the absence of the azoreductor agent was negligible (at pH of 2.0, 4.5 and 7.4), although a clear cargo release was attained after 1 h for **S1** and **S2**, respectively, when sodium dithionite was present. To conclude, both pharmaceutical active compounds (i.e., hydrocortisone and 5-ASA) were released at a neutral pH when the reducing agent sodium dithionite was present, mimicking the colon environment.

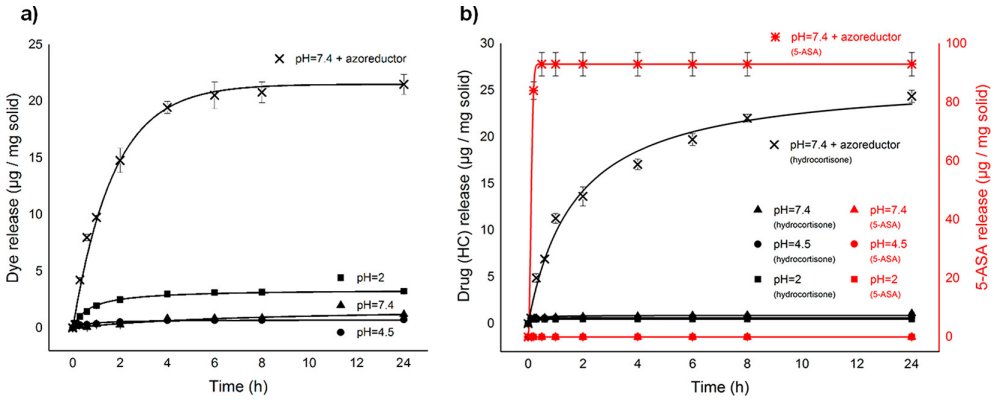

Figure 1. (a) Release profiles of rhodamine B from **S1** microparticles in water at pH ≈ 2 (square), pH ≈ 4.5 (circle), pH ≈ 7.4 (triangle), and pH ≈ 7.4 in the presence of sodium dithionite (2 mg/mL) (cross). (b) Release kinetics of hydrocortisone (black) and 5-ASA (red) from **S2** microparticles in water at pH ≈ 2 (square), pH ≈ 4.5 (circle), pH ≈ 7.4 (triangle), and pH ≈ 7.4 in the presence of sodium dithionite (2 mg/mL) (cross: hydrocortisone, star: 5-ASA).

5.4.4. *In vitro* Digestion Model Assay

In a further step, the delivery of olsalazine and 5-ASA from **S2** was thoroughly evaluated in a digestion model using simulated solutions. The used model was inspired in that reported by Oomen and consisted of a procedure of three steps simulating the digestive process (from the mouth, through the stomach, and to the small intestine).(47,48) Moreover, we added an additional step after the small intestine, in order to simulate digestion in the colon. In a typical experiment, **S2** (2 mg) was suspended for 5 min in the simulated saliva at 37.5 °C, and afterward simulated gastric juice (stomach) was added and the suspension was stirred during 2 h. Next, the simulated small intestine fluid (duodenal simulated juice, bile, and bicarbonate solution) was added, and the mixture was stirred for 2 h. Finally, addition of sodium dithionite simulated the azoreductor colon environment. This final suspension was left for 24 h. The release of hydrocortisone and 5-ASA from **S2** was quantified by HPLC under the conditions described above. Figure 2 shows the obtained results.

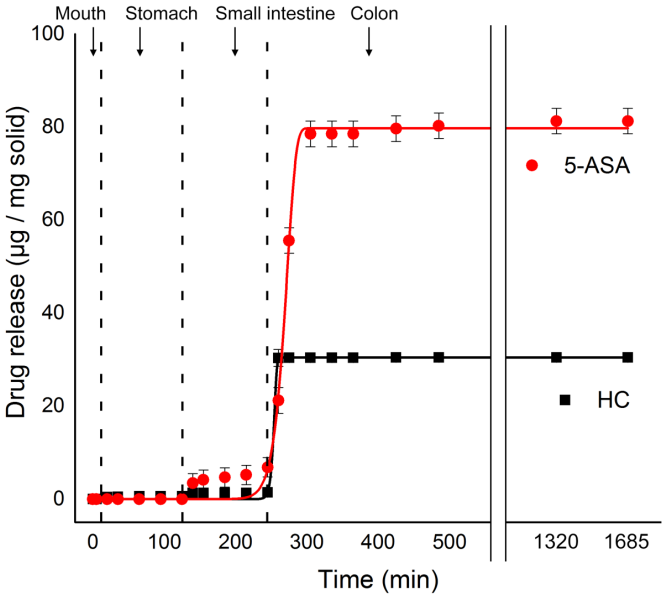

Figure 2. Release kinetics of the hydrocortisone (HC) and 5-ASA from **S2** in simulated GIT fluids.

As seen in Figure 2, the released hydrocortisone or 5-ASA from **S2** was less than 5% in the simulated mouth, stomach, and small intestine juices, which indicates that acidic media over a period shorter than 2 h does not induce hydrocortisone or 5-ASA delivery. In contrast, a clear release of both drugs (maximum delivery was 30.44 and 81.25 µg/mg solid for hydrocortisone and 5-ASA respectively) was observed when **S2** came into contact with the simulated colon juice because of the reduction of the azo linkages in the gated material.

5.4.5. *In vivo* Pharmacokinetics Studies

To test both the specific colon release and systemic absorption prevention, *in vivo* pharmacokinetic studies with **S1** microparticles were performed. Rats in group 1, which were administered with a rhodamine B solution, showed plasma levels of rhodamine B with a maximum of 0.45 µg/mL 1 h after administration (Figure 3). Group 2, which received

formulation **S1**, showed negligible rhodamine B systemic absorption, and no rhodamine B was found in plasma (Figure 3). The presence of rhodamine B in the cecum, colon, and feces was also evaluated. Figure 4 shows significant larger presence of rhodamine B in the colon and cecum in rats fed with **S1** (group 2) compared with those treated with rhodamine B (group 1). These results evidence the specific dye/drug delivery to the colon from the systems designed in this work and also demonstrated that systemic absorption was avoided when rhodamine B was encapsulated in **S1**. Besides, C_{max} and T_{max} values for rats in groups 1 (administered with rhodamine B solution) and 2 (treated with **S1**) are shown in Table 5.

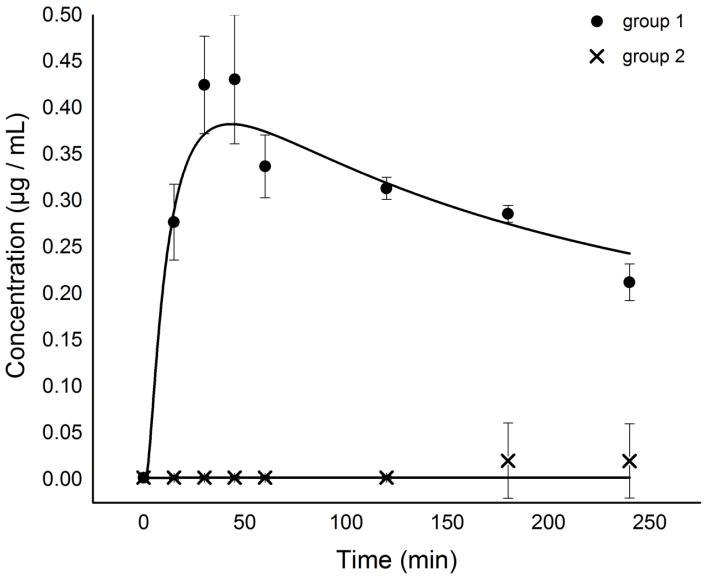

Figure 3. Rhodamine B concentration (µg/mL) in plasma. For the subjects which received rhodamine B solution (group 1) and those which receiving suspension **S1** (group 2).

Table 5. C_{max} and T_{max} of Both Formulations Assayed (n = 4)[a]

	AUC t_0–t_∞/dose (mL^{-1} h^{-1})	C_{max} ($\mu g/mL$)	T_{max} (min)
group 1	56.92	0.45*	50*
group 2	9.21	0.02	250

[a]Note: * statistically significant differences ($p < 0.05$) between group 1 and group 2 C_{max} (maximal drug concentration), T_{max} (time to reach C_{max}) of rhodamine B plasma profiles were calculated and compared to determine if the prepared suspension modify the dye solution parameters. Presented results are the average of four animals per group.

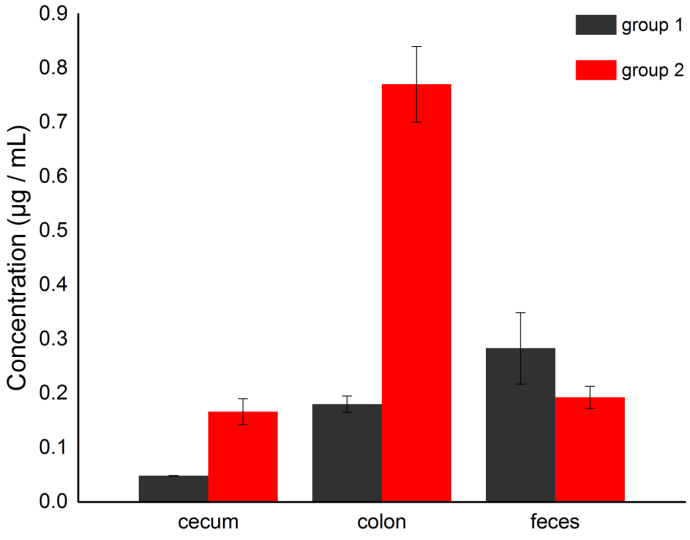

Figure 4. Rhodamine B concentration (µg/mL) in the cecum, colon, and feces. For the subjects that received rhodamine B solution (group 1) and those administered **S1** suspension (group 2).

5.4.6. *In vivo* Efficacy Studies. Inducing Colonic Inflammation

TNBS was used to induce the IBD model in rats. In this model, enema administration of TNBS (50% v/v in ethanol) induced IBD-like injuries. The reproducibility, simplicity, dose- and time-related development of inflammation are the most remarkable advantages of this model.(49,50) Inflammation development was monitored daily. During the period of study, individuals suffered weight loss and diarrhea but no rectal bleeding.

Figure 5A shows the typical appearance of a healthy colon of rats. Figure 5B shows the opened colon of the rats that received saline serum (placebo treatment, group 1), whereas Figure 5C–E show the opened colons of rats after inducing colitis with TNBS and treated with **S0**, hydrocortisone, and **S2**, groups 2, 3, and 4 respectively. All rats were sacrificed 10 days after treatment with TNBS. Colons from groups 1 (Figure 5B) and 2 (Figure 5C) were strikingly similar, and both presented a thick rigid bowel and showed necrotic tissue. In colons from individuals treated with hydrocortisone (group 3, Figure 5D) some tissue started to heal, but although thickened tissue and necrotic zone had reduced, they were still present. In contrast, colons of rats from group 4 treated with **S2** (Figure 5E) generally appeared healthy, and only a few presented very small mild injuries. In addition, after the administration of **S2**, subjects from group 4 gained some weight and presented normal stools, similar to some subjects of group 3 (which received hydrocortisone solution). On the other hand, after the administration of saline solution or **S0**, rats from groups 1 and 2 had diarrhea and lost weight throughout the experiment. Figures 6 and 7 showed the effects after oral administration of the different formulations on the colon/body weight ratio and clinical activity score, respectively.

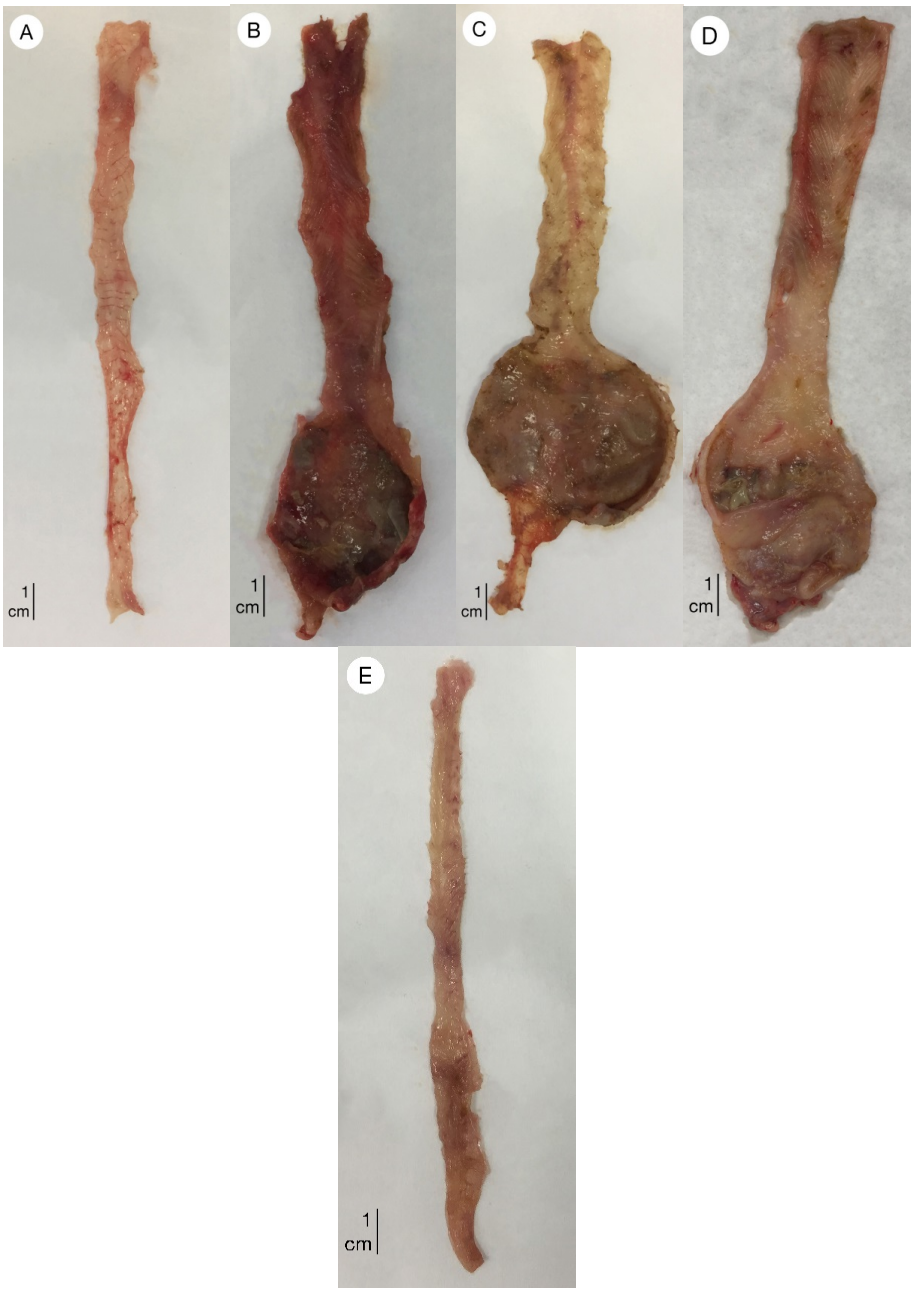

Figure 5. Pictures of rat colon 10 days after inducing colitis with TNBS: A healthy control (without TNBS administration), B positive control (group 1, treated with saline serum), C (group 2, treated with **S0**), D (group 3, administered with hydrocortisone), and E (group 4, administered with **S2**).

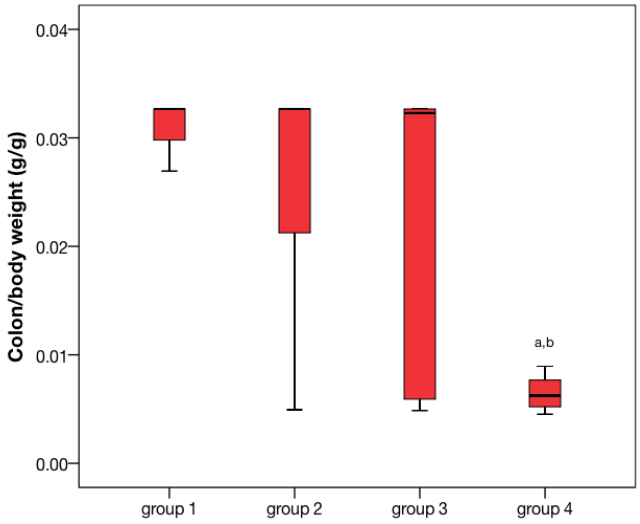

Figure 6. Colon/body weight ratio of rats with TNBS-induced colitis after receiving subsequent treatments: saline solution (group 1, positive control), **S0** (group 2), hydrocortisone (group 3) and **S2** (group 4). Each box represents the median value, the 25% and 75% percentiles, the minimal and maximal values ([a,b] statistical significant difference ($P < 0.05$) compared with the saline and **S0** solid, respectively).

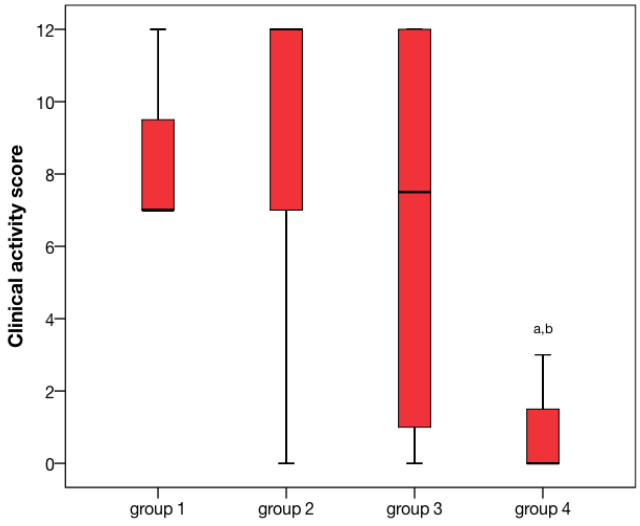

Figure 7. Clinical activity score of rats with TNBS-induced colitis after receiving subsequent treatments: saline solution (group 1, positive control), **S0** (group 2), hydrocortisone (group 3) and **S2** (group 4). Each box represents the median value, the 25% and 75% percentiles, the minimal and maximal values ([a,b] statistical significant difference ($P < 0.05$) compared with the saline and **S0** solid, respectively).

The colon/body weight ratio decreased considerably in rats of group 4 (treated with **S2**) compared with the control, which received saline solution (group 1). In contrast, no accentuated effect was observed on the colon/body weight ratio for subjects treated with **S0** particles (group 2). Rats in group 3 (treated with the hydrocortisone solution) had a wide variability, with several cases of improvement and several cases without improvement at all (Figure 6). Similar results (i.e., wide variability) were found for group 3 in the clinical activity score (Figure 7). This large variation observed for group 3 can be due to one of the following reasons: (a) orally taken hydrocortisone is almost absorbed completely before reaching its site of action; (b) the dose of an administered drug in not enough to allow recovery. In contrast, the **S2** formulation allowed the release of two drugs, that is, hydrocortisone (carried inside the mesoporous silica microparticles) and 5-ASA (externally anchored to the surface of microparticles), which results in a high concentration of both active ingredients in the injured area having a remarkable therapeutic effect.

5.4.7. Histological Evaluation

Histological tissue examinations in healthy control rats and in rats treated with TNBS of different groups: that is, 1 (saline solution, positive control group); 2 (**S0**); 3 (hydrocortisone solution); 4 (**S2** formulation) were carried out. Samples were always taken from the sacrificed subjects on day 10 after TNBS treatment. The healthy control showed a usual colon structure: that is, connective tissue and goblet cells (lamina propria, Figure 8A), healthy mucosa with enterocytes, muscularis mucosae, normal submucosa, and muscularis externa. On the other hand, tissues from rats of groups 1 and 2 showed loss of necrotic mucosa and substitution for granulation tissue (see Figure 8B,C). Besides, a strong inflammatory process was present in the lamina propria, submucosa, and muscularis extern in the individuals of both groups. Figure 8B,C also show the ulceration process with the fibrinoid necrosis of the mucosal surface and granulation tissue below necrotic tissue. Rats of group 3 (treated with hydrocortisone) only showed superficial erosion, thinning mucosa

(complemented by a thickening of muscularis mucosae), and a chronic inflammatory process which affected the mucosa and submucosa with an early development of lymphoid follicle. Besides, Figure 8D also shows a small number of parts with a normal mucosa structure. However, the presence of strong follicular hyperplasia (in the muscularis externa and parts with necrosis), loss of mucosa and substitution for granulation tissue, and the inflammation process is also observed in Figure 8D. The individuals treated with **S2** microparticles (group 4) showed a normal mucosal structure with the presence of minor chronic inflammation in muscularis propria (see Figure 8E).

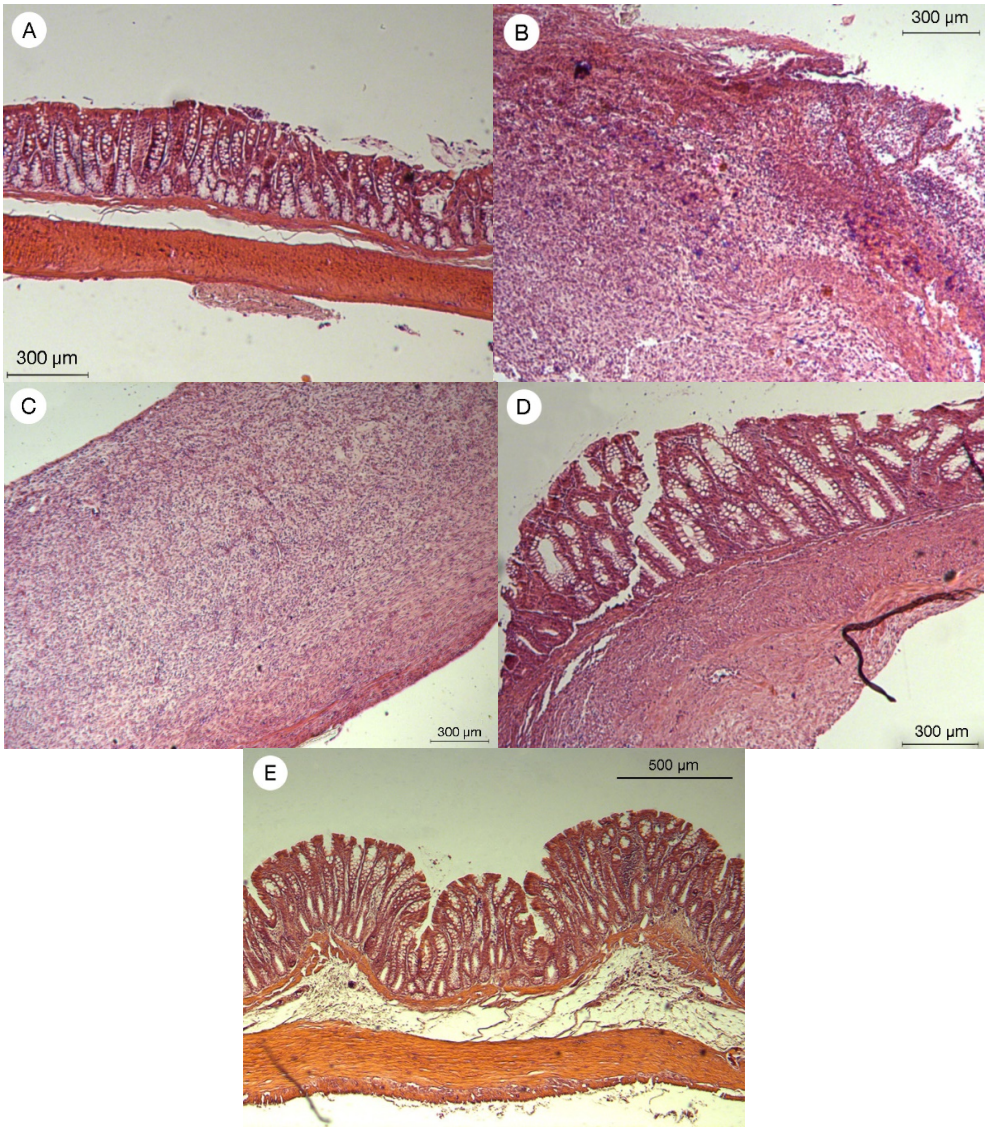

Figure 8. Histology of a representative colon specimen of healthy rats (A) and rats after inducing colitis with TNBS, treated and sacrificed on day 10: (B) administered with saline solution (positive control, group 1), (C) treated with **S0** (group 2), (D) administered with hydrocortisone (group 3), and (E) treated with **S2** (group 4).

The histological findings indicated that group 1 individuals (the saline-treated TNBS group) showed necrosis, strong inflammation, and mucosa loss. Similar results were observed with the rats treated with microparticles

S0 (group 2). In contrast, the histological findings of the rats treated with **S2** (group 4) showed an intensive regeneration, softer inflammation, and an almost normal mucosal structure. The information obtained by the colon/body weight ratio, the clinical activity score, and the histological evaluation, confirming the usefulness of **S2** system to treat IBD. Moreover, it can be stated that our formulation improved the results reported in previous studies by Mura et al., Naeem et al., or Teruel et al., with the added benefit of not involving any systemic intervention.(29,43,51).

5.5 Conclusions

A novel oral colon drug delivery system is designed and prepared, and its efficiency to treat IBD was evaluated *in vivo* in a TNBS-induced colitis rat model. The prepared system consists of mesoporous silica microparticles loaded with either, rhodamine B (**S1**) or hydrocortisone (**S2**), and decorated on the external surface with an olsalazine derivative. This olsalazine derivative is a bulky azo compound, covalently grafted onto the external surface of the loaded support through amide linkages, which yielded drug 5-ASA upon hydrolysis of the azo bonds. Both materials (i.e., **S1** and **S2**) remained capped at neutral and acidic pH, yet a remarkable payload delivery is evident when sodium dithionite (a reducing agent that mimics the azo-reductase enzymes present in colon) was present. Cargo release is a consequence of the sodium dithionite-induced reduction of azo bonds in the bulky capping ensemble, whereas 5-ASA is also delivered from both microdevices upon the hydrolysis of the olsalazine derivative. *In vivo* pharmacokinetic studies performed with **S1** showed specific rhodamine B delivery at colonic area. The clinical activity score, the colon/body weight ratio, and the histological colon tissue evaluation evidenced that rats with chronic colon inflammation and treated with microparticles **S2** show an improvement in the pathology due to the simultaneous hydrocortisone and 5-ASA release. In conclusion, we demonstrate that microparticles reported here can be used to release drugs specifically in the last part of the intestine, while diminishing systemic absorption. Specifically, **S2** is a

formulation able to treat IBD due to the double drug delivery (i.e., hydrocortisone and 5-ASA release) at the colon.

Acknowledgements

We thank the Generalitat Valenciana (Project PROMETEO2018/024) and the Spanish Government (Projects AGL2015-70235-C2-2-R and MAT2015-64139-C4-1-R (MINECO/FEDER)) for support. A.H.T. thanks the Spanish MEC for his FPU fellowship. The authors also thank the support of the Electron Microscopy Service at the UPV. The SCSIE (of the Universitat de València) is also gratefully acknowledged for all the equipment used. NMR spectra were measured at the U26 facility of ICTS "NANBIOSIS" at the Universitat de València.

5.6 References

1. Baumgart, D.; Sandborn, W. Crohn's Disease. Lancet 2012, 380, 1590– 1605, DOI: 10.1016/S0140-6736(12)60026-9 [Crossref], [PubMed], [CAS]
2. Liu, T.-C.; Stappenbeck, T. S. Genetics and Pathogenesis of Inflammatory Bowel Disease. Annu. Rev. Pathol.: Mech. Dis. 2016, 11, 127– 148, DOI: 10.1146/annurev-pathol-012615-044152 [Crossref], [PubMed], [CAS]
3. Pierik, M.; Yang, H.; Barmada, M. M.; Cavanaugh, J. A.; Annese, V.; Brant, S. R.; Cho, J. H.; Duerr, R. H.; Hugot, J. P.; McGovern, D. P.; Paavola-Sakki, P.; Radford-Smith, G. L.; Pavli, P.; Silverberg, M. S.; Schreiber, S.; Taylor, K. D.; Vlietinck, R. The IBD International Genetics Consortium Provides Further Evidence for Linkage to IBD4 and Shows Gene-Environment Interaction. Inflamm. Bowel Dis. 2005, 11, 1– 7, DOI: 10.1097/00054725-200501000-00001 [Crossref], [PubMed], [CAS]
4. Loftus, E. V. Clinical Epidemiology of Inflammatory Bowel Disease: Incidence, Prevalence, and Environmental Influences. Gastroenterology 2004, 126, 1504– 1517, DOI: 10.1053/j.gastro.2004.01.063 [Crossref], [PubMed], [CAS]
5. Ye, Y.; Pang, Z.; Chen, W.; Ju, S.; Zhou, C. The Epidemiology and Risk Factors of Inflammatory Bowel Disease. Int. J. Clin. Exp. Med. 2015, 8, 22529– 22542[PubMed], [CAS]
6. Lupp, C.; Robertson, M. L.; Wickham, M. E.; Sekirov, I.; Champion, O. L.; Gaynor, E. C.; Finlay, B. B. Host-Mediated Inflammation Disrupts the Intestinal Microbiota and Promotes the Overgrowth of Enterobacteriaceae. Cell Host Microbe 2007, 2, 119– 129, DOI: 10.1016/j.chom.2007.06.010 [Crossref], [PubMed], [CAS]
7. Takaishi, H.; Matsuki, T.; Nakazawa, A.; Takada, T.; Kado, S.; Asahara, T.; Kamada, N.; Sakuraba, A.; Yajima, T.; Higuchi, H.; Inoue, N.; Ogata, H.; Iwao, Y.; Nomoto, K.; Tanaka, R.; Hibi, T. Imbalance in Intestinal Microflora Constitution Could Be Involved in

the Pathogenesis of Inflammatory Bowel Disease. Int. J. Med. Microbiol. 2008, 298, 463– 472, DOI: 10.1016/j.ijmm.2007.07.016 [Crossref], [PubMed], [CAS]
8. Sokol, H.; Seksik, P.; Furet, J. P.; Firmesse, O.; Nion-Larmurier, I.; Beaugerie, L.; Cosnes, J.; Corthier, G.; Marteau, P.; Doré, J. Low Counts of Faecalibacterium Prausnitzii in Colitis Microbiota. Inflamm. Bowel Dis. 2009, 15, 1183– 1189, DOI: 10.1002/ibd.20903 [Crossref], [PubMed], [CAS]
9. Friswell, M.; Campbell, B.; Rhodes, J. The Role of Bacteria in the Pathogenesis of Inflammatory Bowel Disease. Gut Liver 2010, 4, 295– 306, DOI: 10.5009/gnl.2010.4.3.295 [Crossref], [PubMed], [CAS]
10. Qiu, X.; Zhang, M.; Yang, X.; Hong, N.; Yu, C. Faecalibacterium Prausnitzii Upregulates Regulatory T Cells and Anti-Inflammatory Cytokines in Treating TNBS-Induced Colitis. J. Crohn's Colitis 2013, 7, e558– e568, DOI: 10.1016/j.crohns.2013.04.002 [Crossref], [PubMed]
11. Yu, C. G.; Huang, Q. Recent Progress on the Role of Gut Microbiota in the Pathogenesis of Inflammatory Bowel Disease. J. Dig. Dis. 2013, 14, 513– 517, DOI: 10.1111/1751-2980.12087 [Crossref], [PubMed], [CAS]
12. Kappelman, M. D.; Rifas-Shiman, S. L.; Porter, C. Q.; Ollendorf, D. A.; Sandler, R. S.; Galanko, J. A.; Finkelstein, J. A. Direct Health Care Costs of Crohn's Disease and Ulcerative Colitis in US Children and Adults. Gastroenterology 2008, 135, 1907– 1913, DOI: 10.1053/j.gastro.2008.09.012 [Crossref], [PubMed], [CAS]
13. Kappelman, M. D.; Rifas-Shiman, S. L.; Porter, C. Q.; Ollendorf, D. A.; Sandler, R. S.; Galanko, J. A.; Finkelstein, J. A. Direct Health Care Costs of Crohn's Disease and Ulcerative Colitis in US Children and Adults. Gastroenterology 2008, 135, 1907– 1913, DOI: 10.1053/j.gastro.2008.09.012 [Crossref], [PubMed], [CAS]
14. Rocchi, A.; Benchimol, E. I.; Bernstein, C. N.; Bitton, A.; Feagan, B.; Panaccione, R.; Glasgow, K. W.; Fernandes, A.; Ghosh, S. Inflammatory Bowel Disease: A Canadian Burden of Illness Review. Can. J. Gastroenterol. 2012, 26, 811– 817, DOI: 10.1155/2012/984575 [Crossref], [PubMed], [CAS]
15. Burisch, J.; Jess, T.; Martinato, M.; Lakatos, P. L. The Burden of Inflammatory Bowel Disease in Europe. J. Crohn's Colitis. 2013, 7, 322– 337, DOI: 10.1016/j.crohns.2013.01.010 [Crossref], [PubMed], [CAS]
16. Marchetti, M.; Liberato, N. L. Biological Therapies in Crohn's Disease: Are They Cost-Effective? A Critical Appraisal of Model-Based Analyses. Expert Rev. Pharmacoecon. Outcomes Res. 2014, 14, 815– 824, DOI: 10.1586/14737167.2014.957682 [Crossref], [PubMed], [CAS]
17. Park, S. J.; Kim, W. H.; Cheon, J. H. Clinical Characteristics and Treatment of Inflammatory Bowel Disease: A Comparison of Eastern and Western Perspectives. World J. Gastroenterol. 2014, 20, 11525– 11537, DOI: 10.3748/wjg.v20.i33.11525 [Crossref], [PubMed], [CAS]
18. Ng, S. C.; Tang, W.; Ching, J. Y.; Wong, M.; Chow, C. M.; Hui, A. J.; Wong, T. C.; Leung, V. K.; Tsang, S. W.; Yu, H. H.; Li, M. F.; Ng, K. K.; Kamm, M. A.; Studd, C.; Bell, S.; Leong, R.; de Silva, H. J.; Kasturiratne, A.; Mufeena, M. N. F.; Ling, K. L.; Ooi, C. J.; Tan, P. S.; Ong, D.; Goh, K. L.; Hilmi, I.; Pisespongsa, P.; Manatsathit, S.; Rerknimitr, R.; Aniwan, S.; Wang, Y. F.; Ouyang, Q.; Zeng, Z.; Zhu, Z.; Chen, M. H.; Hu, P. J.; Wu, K.; Wang, X.; Simadibrata, M.; Abdullah, M.; Wu, J. C.; Sung, J. J. Y.; Chan, F. K. L. Incidence and Phenotype of Inflammatory Bowel Disease Based on Results from the Asia-Pacific Crohn's and Colitis Epidemiology Study. Gastroenterology 2013, 145, 158– 165, DOI: 10.1053/j.gastro.2013.04.007 [Crossref], [PubMed], [CAS]

19. Sood, A.; Midha, V.; Sood, N.; Bhatia, A. S.; Avasthi, G. Incidence and Prevalence of Ulcerative Colitis in Punjab, North India. Gut 2003, 52, 1587– 1590, DOI: 10.1136/gut.52.11.1587 [Crossref], [PubMed], [CAS]
20. Tozun, N.; Atug, O.; Imeryuz, N.; Hamzaoglu, H. O.; Tiftikci, A.; Parlak, E.; Dagli, U.; Ulker, A.; Hulagu, S.; Akpinar, H.; Tuncer, C.; Suleymanlar, I.; Ovunc, O.; Hilmioglu, F.; Aslan, S.; Turkdogan, K.; Bahcecioglu, H. I.; Yurdaydin, C. Clinical Characteristics of Inflammatory Bowel Disease in Turkey: A Multicenter Epidemiologic Survey. J. Clin. Gastroenterol. 2009, 43, 51– 57, DOI: 10.1097/MCG.0b013e3181574636 [Crossref], [PubMed], [CAS]
21. Victoria, C. R.; Sassak, L. Y.; Nunes, H. R. de C. Incidence and Prevalence Rates of Inflammatory Bowel Diseases, in Midwestern of São Paulo State, Brazil. Arq. Gastroenterol. 2009, 46, 20– 25, DOI: 10.1590/S0004-28032009000100009 [Crossref], [PubMed], [CAS]
22. Fakhoury, M.; Negrulj, R.; Mooranian, A.; Al-Salami, H. Inflammatory Bowel Disease: Clinical Aspects and Treatments. J. Inflammation Res. 2014, 113– 120, DOI: 10.2147/JIR.S65979 [Crossref], [PubMed], [CAS]
23. Mowat, C.; Cole, A.; Windsor, A.; Ahmad, T.; Arnott, I.; Driscoll, R.; Mitton, S.; Orchard, T.; Rutter, M.; Younge, L.; Lees, C.; Ho, G. T.; Satsangi, J.; Bloom, S. Guidelines for the Management of Inflammatory Bowel Disease in Adults. Gut 2011, 60, 571– 607, DOI: 10.1136/gut.2010.224154 [Crossref], [PubMed], [CAS]
24. Di Sario, A.; Bendia, E.; Schiadà, L.; Sassaroli, P.; Benedetti, A. Biologic Drugs in Crohn's Disease and Ulcerative Colitis: Safety Profile. Curr. Drug Saf. 2016, 11, 55– 61, DOI: 10.2174/1574886311011602121717 57 [Crossref], [PubMed], [CAS]
25. Collnot, E.-M.; Ali, H.; Lehr, C.-M. Nano- and Microparticulate Drug Carriers for Targeting of the Inflamed Intestinal Mucosa. J. Controlled Release 2012, 161, 235– 246, DOI: 10.1016/j.jconrel.2012.01.028 [Crossref], [PubMed], [CAS]
26. Lamprecht, A.; Rodero Torres, H.; Schafer, U.; Lehr, C. M. Biodegradable Microparticles as a Two-Drug Controlled Release Formulation: A Potential Treatment of Inflammatory Bowel Disease. J. Controlled Release 2000, 69, 445– 454, DOI: 10.1016/S0168-3659(00)00331-X [Crossref], [PubMed], [CAS]
27. Lamprecht, A.; Ubrich, N.; Yamamoto, H.; Schafer, U.; Takeuchi, H.; Maincent, P.; Kawashima, Y.; Lehr, C. M. Biodegradable Nanoparticles for Targeted Drug Delivery in Treatment of Inflammatory Bowel Disease. J. Pharmacol. Exp. Ther. 2001, 299, 775– 781[PubMed], [CAS]
28. Teruel, A. H.; Coll, C.; Costero, A.; Ferri, D.; Parra, M.; Gaviña, P.; González-Álvarez, M.; Merino, V.; Marcos, M.; Martínez-Máñez, R.; Sancenón, F. Functional Magnetic Mesoporous Silica Microparticles Capped with an Azo-Derivative: A Promising Colon Drug Delivery Device. Molecules 2018, 23, 375, DOI: 10.3390/molecules23020375 [Crossref], [CAS]
29. Teruel, A. H.; Pérez-Esteve, É.; González-Álvarez, I.; González-Álvarez, M.; Costero, A. M.; Ferri, D.; Parra, M.; Gaviña, P.; Merino, V.; Martínez-Mañez, R.; Sancenón, F. Smart Gated Magnetic Silica Mesoporous Particles for Targeted Colon Drug Delivery: New Approaches for Inflammatory Bowel Diseases Treatment. J. Controlled Release 2018, 281, 58– 69, DOI: 10.1016/j.jconrel.2018.05.007 [Crossref], [PubMed], [CAS]
30. Sancenón, F.; Pascual, Ll; Oroval, M.; Aznar, E.; Martínez-Máñez, R. Gated Silica Mesoporous Materials in Sensing Applications. ChemistryOpen 2015, 4, 418– 437, DOI: 10.1002/open.201500053 [Crossref], [PubMed], [CAS]
31. Aznar, E.; Oroval, M.; Pascual, Ll; Murguía, J. R.; Martínez-Máñez, R.; Sancenón, F. Gated Materials for On-Command Release of Guest Molecules. Chem. Rev. 2016,

116, 561– 718, DOI: 10.1021/acs.chemrev.5b00456 [ACS Full Text ACS Full Text], [CAS]
32. Llopis-Lorente, A.; Díez, P.; Sánchez, A.; Marcos, M. D.; Sancenón, F.; Martínez-Ruiz, P.; Villalonga, R.; Martínez-Máñez, R. Interactive Models of Communication at the Nanoscale Using Nanoparticles that Talk to One Another. Nat. Commun. 2017, 8, 15511, DOI: 10.1038/ncomms15511 [Crossref], [PubMed], [CAS]
33. de la Torre, C.; Domínguez-Berrocal, L.; Murguía, J. R.; Marcos, M. D.; Martínez-Máñez, R.; Bravo, J.; Sancenón, F. ε-Polylysine-Capped Mesoporous Silica Nanoparticles as Carrier of the C9h Peptide to Induce Apoptosis in Cancer Cells. Chem. - Eur. J. 2018, 24, 1890– 1897, DOI: 10.1002/chem.201704161 [Crossref], [PubMed], [CAS]
34. Oroval, M.; Díez, P.; Aznar, E.; Coll, C.; Marcos, M. D.; Sancenón, F.; Villalonga, R.; Martínez-Máñez, R. Self-Regulated Glucose-Sensitive Neoglycoenzyme-Capped Mesoporous Silica Nanoparticles for Insulin Delivery. Chem. - Eur. J. 2017, 23, 1353– 1360, DOI: 10.1002/chem.201604104 [Crossref], [PubMed], [CAS]
35. de la Torre, C.; Casanova, I.; Acosta, G.; Coll, C.; Moreno, M. J.; Albericio, F.; Aznar, E.; Mangues, R.; Royo, M.; Sancenón, F.; Martínez-Máñez, R. Gated Mesoporous Silica Nanoparticles Using a Double-Role Circular Peptide for the Controlled and Targeted-Preferential Release of Doxorubicin in CXCR4-Expressin Lymphoma Cells. Adv. Funct. Mater. 2015, 25, 687– 695, DOI: 10.1002/adfm.201403822 [Crossref], [CAS]
36. Giménez, C.; Climent, E.; Aznar, E.; Martínez-Máñez, R.; Sancenón, F.; Marcos, M. D.; Amorós, P.; Rurack, K. Towards Chemical Communication between Gated Nanoparticles. Angew. Chem., Int. Ed. 2014, 53, 12629– 12633, DOI: 10.1002/anie.201405580 [Crossref], [PubMed], [CAS]
37. García-Fernández, A.; García-Laínez, G.; Ferrándiz, M. L.; Aznar, E.; Sancenón, F.; Alcaraz, M. J.; Murguía, J. R.; Marcos, M. D.; Martínez-Máñez, R.; Costero, A. M.; Orzáez, M. Targeting Inflammasome by the Inhibition of Caspase-1 Activity Using Capped Mesoporous Silica Nanoparticles. J. Controlled Release 2017, 248, 60– 70, DOI: 10.1016/j.jconrel.2017.01.002 [Crossref], [PubMed], [CAS]
38. Llopis-Lorente, A.; Lozano-Torres, B.; Bernardos, A.; Martínez-Máñez, R.; Sancenón, F. Mesoporous Silica Materials for Controlled Delivery Based-on Enzymes. J. Mater. Chem. B 2017, 5, 3069– 3083, DOI: 10.1039/C7TB00348J [Crossref], [CAS]
39. Cabrera, S.; El Haskouri, J.; Guillem, C.; Latorre, J.; Beltrán-Porter, A.; Beltrán-Porter, D.; Marcos, M. D.; Amorós, P. Generalised Syntheses of Ordered Mesoporous Oxides: The Atrane Route. Solid State Sci. 2000, 2, 405– 420, DOI: 10.1016/S1293-2558(00)00152-7 [Crossref], [CAS]
40. Lunn, G. HPLC Methods for Recently Approved Pharmaceuticals; John Wiley & Sons, Inc.: Hoboken, New Jersey, 2005.[Crossref]
41. Navarro, C.; González-Álvarez, I.; González-Álvarez, M.; Manku, M.; Merino, V.; Casabó, V. G.; Bermejo, M. Influence of Polyunsaturated Fatty Acids on Cortisol Transport through MDCK and MDCK-MDR1 Cells as Blood–Brain Barrier in Vitro Model. Eur. J. Pharm. Sci. 2011, 42, 290– 299, DOI: 10.1016/j.ejps.2010.12.005 [Crossref], [PubMed], [CAS]
42. Torres-Molina, F.; Peris, J. E.; García-Carbonell, M. C.; Aristorena, J. C.; Granero, L.; Chesa-Jiménez, J. Use of rats cronically cannulated in the jugular vein and the duodenum in pharmacokinetic studies. Effect of ether anestesia on absorption of amoxicillin. Arzneimittelforschung 1996, 46, 716– 719[PubMed], [CAS]

43. Mura, C.; Nacher, A.; Merino, V.; Merino-Sanjuan, M.; Carda, C.; Ruiz, A.; Manconi, M.; Loy, G.; Fadda, A. M.; Diez-Sales, O. N-Succinyl-Chitosan Systems for 5-Aminosalicylic Acid Colon Delivery: In Vivo Study with TNBS-Induced Colitis Model in Rats. Int. J. Pharm. 2011, 416, 145– 154, DOI: 10.1016/j.ijpharm.2011.06.025 [Crossref], [PubMed], [CAS]
44. Sandborn, W. J.; Hanauer, S. B. Systematic Review: The Pharmacokinetic Profiles of Oral Mesalazine Formulations and Mesalazine pro-Drugs Used in the Management of Ulcerative Colitis. Aliment. Pharmacol. Ther. 2003, 17, 29– 42, DOI: 10.1046/j.1365-2036.2003.01408.x [Crossref], [PubMed], [CAS]
45. Hartmann, G.; Bidlingmaier, C.; Siegmund, B.; Albrich, S.; Schulze, J.; Tschoep, K.; Eigler, A.; Lehr, H. A.; Endres, S. Specific Type IV Phosphodiesterase Inhibitor Rolipram Mitigates Experimental Colitis in Mice. J. Pharmacol. Exp. Ther. 2000, 292, 22– 30[PubMed], [CAS]
46. Mladenovska, K.; Raicki, R. S.; Janevik, E. I.; Ristoski, T.; Pavlova, M. J.; Kavrakovski, Z.; Dodov, M. G.; Goracinova, K. Colon-Specific Delivery of 5-Aminosalicylic Acid from Chitosan-Ca-Alginate Microparticles. Int. J. Pharm. 2007, 342, 124– 136, DOI: 10.1016/j.ijpharm.2007.05.028 [Crossref], [PubMed], [CAS]
47. Oomen, A. G.; Rompelberg, C. J. M.; Bruil, M. A.; Dobbe, C. J. G.; Pereboom, D. P. K. H.; Sips, A. J. A. M. Development of an in Vitro Digestion Model for Estimating the Bioaccessibility of Soil Contaminants. Arch. Environ. Contam. Toxicol. 2003, 44, 281– 287, DOI: 10.1007/s00244-002-1278-0 [Crossref], [PubMed], [CAS]
48. Versantvoort, C. H. M.; Oomen, A. G.; Van de Kamp, E.; Rompelberg, C. J. M.; Sips, A. J. A. M. Applicability of an in Vitro Digestion Model in Assessing the Bioaccessibility of Mycotoxins from Food. Food Chem. Toxicol. 2005, 43, 31– 40, DOI: 10.1016/j.fct.2004.08.007 [Crossref], [PubMed], [CAS]
49. Tozaki, H.; Fujita, T.; Komoike, J.; Kim, S. I.; Terashima, H.; Muranishi, S.; Okabe, S.; Yamamoto, A. Colon-Specific Delivery of Budesonide with Azopolymer-Coated Pellets: Therapeutic Effects of Budesonide with a Novel Dosage Form against 2,4,6-Trinitrobenzenesulphonic Acid-Induced Colitis in Rats. J. Pharm. Pharmacol. 1999, 51, 257– 261, DOI: 10.1211/0022357991772420 [Crossref], [PubMed], [CAS]
50. Tozaki, H.; Odoriba, T.; Okada, N.; Fujita, T.; Terabe, A.; Suzuki, T.; Okabe, S.; Muranishi, S.; Yamamoto, A. Chitosan Capsules for Colon-Specific Drug Delivery: Enhanced Localization of 5-Aminosalicylic Acid in the Large Intestine Accelerates Healing of TNBS-Induced Colitis in Rats. J. Controlled Release 2002, 82, 51– 61, DOI: 10.1016/S0168-3659(02)00084-6 [Crossref], [PubMed], [CAS]
51. Naeem, M.; Cao, J.; Choi, M.; Kim, W. S.; Moon, H. R.; Lee, B. L.; Kim, M.-S.; Jung, Y.; Yoo, J.-W. Enhanced Therapeutic Efficacy of Budesonide in Experimental Colitis with Enzyme/PH Dual-Sensitive Polymeric Nanoparticles. Int. J. Nanomed. 2015, 10, 4565– 4580, DOI: 10.2147/IJN.S87816 [Crossref], [PubMed], [CAS]

Chapter 6

Conclusions

- Magnetic mesoporous silica microparticles loaded with safranin O and capped with bulky azo derivative bearing pH-hydrolysable moieties (carbamate group) have been developed (1).
    - At neutral pH, the capped material showed a negligible safranin O release, whereas the addition of a reducing agent such as sodium dithionite (mimicking azoreductase enzyme) to the neutral pH solution, induced a marked safranin O release. The observed delivery was ascribed to a reduction of the azo bonds.
    - A partial payload release was also observed at acidic pH, maybe by a partial hydrolysis of carbamate groups.
    - Delivery studies in a digestion model indicated an important part of the payload was released in colon.
    - The inclusion of magnetic nanoparticles into mesoporous silica scaffolds was set up to potentially apply magnetic fields to enhance the retention time of the solids in colon, in future *in vivo* studies.

- A new oral colon drug delivery device was designed, prepared and its efficacy in the treatment of IBD was evaluated *in vivo* in a TNBS colitis induced rat model. The nanodevice consisted of magnetic mesoporous silica microparticles loaded with safranin O or with hydrocortisone and

functionalized in the external surface with a bulky azo derivative covalently grafted through urea bonds (2).

- Both materials (safranin O loaded and hydrocortisone loaded) remained capped at neutral pH, yet a marked payload release was observed in the presence of a reducing agent (such as sodium dithionite). Cargo delivery was ascribed to the reduction of azo bonds in the capping ensemble.
- Certain safranin O release was observed at acidic pH due to the partial hydrolysis of the urea bonds that linked the azo derivatives onto the external surface of the loaded scaffold.
- *In vivo* pharmacokinetic studies evidenced specific safranin O delivery in colon and the absence of safranin O systemic absorption (negligible concentrations of safranin O in plasma).
- The usefulness of including magnetic properties in this hybrid system was evaluated *in vivo*. Improved results (in terms of concentration of dye in colon) were obtained for rats wearing a magnetic belt.
- Colon/body weight ratio, clinical activity score systems and histology evaluation in a rat model of chronic inflammation in colon and treated with (2) microparticles loaded with hydrocortisone showed an improvement in the pathology.
- The results were enhanced when a magnetic field was externally applied to lengthen the retention time of the particles in colon.
- We demonstrated that our system can be used to specifically deliver drugs or other agents in the last part of intestine while decreasing the systemic absorption; both effects contribute to increase efficacy for the treatment of inflammatory bowel disease and to reduce adverse effects of drugs.

- A novel oral colon drug delivery system is designed and prepared, and its efficiency to treat IBD was evaluated *in vivo* in a TNBS-induced colitis rat model. The prepared system consists of mesoporous silica microparticles loaded with either, rhodamine B or hydrocortisone, and

decorated on the external surface with an olsalazine derivative. This olsalazine derivative is a bulky azo compound, covalently grafted onto the external surface of the loaded support through amide linkages, which yielded drug 5-ASA upon hydrolysis of the azo bonds (3).

- Both materials (i.e., rhodamine B loaded and hydrocortisone loaded) remained capped at neutral and acidic pH, whereas remarkable payload delivery is evident when the reducing agent sodium dithionite was present at neutral pH.
- Cargo release is a consequence of the sodium dithionite-induced reduction of azo bonds in the bulky capping ensemble, whereas 5-ASA is also delivered upon the hydrolysis of the olsalazine derivative.
- *In vivo* pharmacokinetic studies performed showed specific rhodamine B delivery at colonic area.
- The clinical activity score, the colon/body weight ratio, and the histological colon tissue evaluation evidenced that rats with chronic colon inflammation and treated with microparticles loaded with hydrocortisone show an improvement in the pathology due to the simultaneous hydrocortisone and 5-ASA release.
- These studies demonstrated that the capped microparticles can be used to release drugs specifically in the last part of the intestine. Specifically, the hydrocortisone loaded formulation is able to treat IBD due to a targeted double drug delivery (i.e., hydrocortisone and 5-ASA release) at the colon.

Gracias al Ministerio de Educación y Ciencia del Gobierno de España
por concederme el contrato pre-doctoral FPU.